TECHNISCHE UNIVERSITÄT WIEN
Vienna University of Technology

DIPLOMARBEIT

PEM Fuel Cell Operation and Applications Using BioH_2

ausgeführt zum Zwecke der Erlangung des akademischen Grades eines Diplom-Ingenieurs unter der Leitung von

Univ. Prof. Dipl.-Ing. Dr. techn. Hermann Hofbauer
und der Mitbetreuung von
Dipl.-Ing. Dr. techn. Nicolas Felipe Diaz Perez
Dipl.-Ing. Dipl.-Ing.(FH) Silvester Fail
E166
Institut für Verfahrenstechnik, Umwelttechnik und Technische Biowissenschaften

eingereicht an der Technischen Universität Wien
Fakultät für Maschinenwesen und Betriebswissenschaften

von

Michael Kraussler
Matrikelnummer 0825858

Wien, 10. Juni 2014

Michael Kraussler

Contents

List of Figures

List of Tables

Abstract

Today, hydrogen is mostly produced from fossil fuels like methane and coal. In order to decrease the world's carbon dioxide emissions several sustainable ways of hydrogen generation exist. One of them is electrolysis of water. If it is powered by renewable electricity like solar, hydro or eolic energy it can depict an environmentally friendly and carbon dioxide emission poor way to produce hydrogen with a high purity.

Another possibility for sustainable hydrogen production is from biomass. Especially, wood gasification with further gas processing seems to be a promising technology which could be realized with the current and proven technology (water gas shift, absorption, membrane separation and adsorption). For gasification, the already industrially applied dual fluidized bed technology has shown advantages which still has room for improvement by means of sorption enhanced reforming (SER).

Fuel cells are devices which are able to convert hydrogen directly into electricity and heat without the limits of the Carnot cycle. Several fuel cell technologies exist with its own advantages and disadvantages.

A proton exchange membrane (PEM) fuel cell, Mobixane^{TM}, was tested in experiments with Alphagaz 1^{TM} H_2 hydrogen (pure hydrogen from a gas cylinder), from Air Liquide^{TM}, and $BioH_2$ acquired from wood gas from biomass gasification. The wood gas from the biomass gasification plant was subsequently processed in a water gas shift unit, in a RME gas scrubbing unit and in a pressure swing adsorption unit in order to achieve high purity $BioH_2$. The experimental results showed that the operation with those two different hydrogen sources made no differences regarding the performance of the PEM fuel cell. A flawless fuel cell operation with $BioH_2$ was possible. The experimental approach with detailed information is part of two papers which can be reviewed in Appendix C of this work. Past experiments using a process chain employing a RME scrubbing unit, a membrane separation unit and a pressure swing adsorption unit showed that a more than 100 hours lasting flawless operation of a PEM fuel cell with hydrogen generated from wood gas was possible.

Today hydrogen is needed for several applications. Therefore storage of hydrogen is an important aspect, especially in context with Power to Gas concepts. Different possibilities exist like storage in pressure vessels, storage as liquid and in metal hydrids. A future project for hydrogen is the addition to the natural gas grid in order to reduce dependence of energy

imports. This could be realized without issues because the Wobbe index of natural gas and hydrogen is quite similar. If the materials for hydrogen applications are chosen properly no significant damages or risks are expected.

Several car manufacturers see fuel cells fed by hydrogen as possible future for locomotion being an alternative to combustion engines which could also be powered by hydrogen. Another possible hydrogen application is the utilization in households by fuel cells for satisfying heat and electricity demands which would enhance fuel use efficiency. This seems to be especially the case if several fuel cells are interconnected to a "Virtual Power Plant" which is assumed to be able to replace large centralized power plants. Furthermore, hydrogen is an substance which is also needed in very high amounts in refineries, metal and chemical industry.

Kurzfassung

Wasserstoff wird heute in vielen Fällen aus fossilen Brennstoffen wie Methan und Kohle gewonnen. Um den weltweiten CO_2 Ausstoß zu reduzieren, existieren jedoch noch andere, nachhaltige Methoden, um Wasserstoff zu produzieren. Eine dieser Möglichkeiten ist die Wasserelektrolyse. Wird der Elektrolyseur von einer erneuerbaren Stromquelle betrieben, z.B. Solar oder Wind, dann ist dies eine umweltfreundliche Methode, um hochreinen Wasserstoff zu gewinnen. Eine weitere Möglichkeit ist die Wasserstoffherstellung aus Biomasse. Besonders die Holzvergasungstechnologie mit anschließenden Gasreinigungs- und Aufbereitungsschritten (Wasser Gas Shift Reaktion, Absorbtion, Membranverfahren und Adsorption) scheint eine vielversprechende Lösung zu sein, die ohne größere Probleme mit heutiger Technologie zu realisieren wäre. Für die Holzvergasung bietet sich die bereits kommerziell genutze DFB Technologie an, die viele Vorteile aufweist und durch die SER Technologie noch verbessert werden könnte.

Mit Brennstoffzellen ist es möglich den produzierten Wasserstoff direkt in elektrischen Strom und Wärme ohne die Limitierung durch den Carnot-Prozess umzuwandeln. Dazu wurden mehrere Brennstoffzellentechnologien mit spezifischen Vor - und Nachteilen entwickelt.

Holzgas aus dem Biomassekraftwerk Oberwart (siehe Abschnitt 4.1) wurde in einer Prozesskette, bestehend aus einer Wasser-Gas-Shift Einheit, Gaswäschereinheit und einer Druckwechseladsorption aufbereitet, um hochreinen $BioH_2$ herzustellen. Eine PEM Brennstoffzelle (Mobixane^{TM}) wurde im Verlauf des Experiments mit Alphagaz 1^{TM} H_2 Wasserstoff von Air Liquide^{TM} und $BioH_2$ betrieben. Während des Experiments konnte kein Leistungsunterschied bzgl. des Betriebs mit beiden Wasserstoffquellen festgestellt werden. Ein Betrieb der Brennstoffzelle mit $BioH_2$ war problemlos möglich. Mehr Informationen dazu finden sich in den beiden Artikeln in Anhang C dieser Arbeit. In der Vergangenheit wurden innerhalb der Arbeitsgruppe ähnliche Experimente mit einer Prozesskette durchgeführt, die aus einem Gaswäscher, einer Membrantrennstufe und einer Druckwechseladsorption bestand. Diese Experimente haben gezeigt, dass ein problemloser Betrieb einer PEM Brennstoffzelle mit $BioH_2$ für mehr als 100 Stunden möglich ist.

Wasserstoff wird heutzutage in vielen Bereichen benötigt. Um eine problemlose Versorgung zu gewährleisten, ist die Speicherung von Wasserstoff ein wichtiger Faktor, ganz

besonders im Zusammenhang mit Power to Gas Konzepten. Wasserstoff kann in Druckspeichern, als Flüssigkeit und in Metallhydriden gespeichert werden. Abseits der Speicherung von Wasserstoff ist das Beimischen von diesem in das bestehende Erdgasnetz eine Möglichkeit, um die Abhängigkeit von Gasimporten zu verringern. Dies könnte ohne Probleme realisiert werden, da Wasserstoff und Erdgas einen ähnlichen Wobbe-Index aufweisen. Wenn auf Materialverträglichkeiten geachtet wird, sollten hierbei keine Schäden oder Gefahren zu erwarten sein.

Mehrere Autohersteller sehen die Brennstoffzelle mit Wasserstoff als Brennstoff als eine der zukünftigen Möglichkeiten für Mobilität und als Alternative zu Verbrennungskraftmaschinen, die ebenfalls mit Wasserstoff betrieben werden könnten. Als weitere Anwendung für Wasserstoff und Brennstoffzellen bietet sich die Wärme - und Elektrizitätsbereitstellung in Haushalten an, was wiederrum die Brennstoffausnutzung verbessern würde. Besonders im Fall sogenannter "Virtueller Kraftwerke", bei denen mehrere kleinere Brennstoffzellenanlagen verbunden werden und so die Möglichkeit haben, ein großes zentralisiertes Kraftwerk zu ersetzen. Weitere Anwendungsmöglichkeiten finden sich in Raffinerien, in der Metall- und chemischen Industrie, wo Wasserstoff in großen Mengen benötigt wird.

Chapter 1

Introduction

World's energy demand is increasing every year. Thereby, in 2001, 85.5 % of it was provided by fossil fuels. The remaining percentage was covered by nuclear power (6.5 %) and other energy sources (8 %) [7]. From the beginning of the industrial revolution the fossil fuels carried the advance. They bare the disadvantage of strong environmental impact and are non-renewable. Starting with coal at the beginning of the industrial revolution the carbon-to-hydrogen ratio in the fuels decreased over time. The usage of coal was surpassed by oil in the 20th century. In the last decades natural gas has been the preferred fuel with a carbon to hydrogen ratio of 1/4 which would decrease the emission CO_2 compared to other fossil fuels with a higher carbon to hydrogen ratio. Though the emissions per unit of fuel decreased due to the use of natural gas, the demand for fuel and energy increased rapidly. As a result the world has to face increasing greenhouse gas emissions. Consequently, utilization of hydrogen as a fuel which is produced by renewable energy sources would be a solution for the problem of increasing greenhouse gas emissions due to its carbon to hydrogen ratio of 0 [7].

Today, the most common production process for hydrogen is steam reforming of hydrocarbons, especially methane and gasification of coal. A description of these processes is given in Section 1.2. Steam reforming of biomass is a CO_2 neutral way for hydrogen production. Another possibility is electrolysis of water. If it is powered by renewable electricity, it is an environmental friendly and sustainable approach for hydrogen production. Both concepts are going to be explained in Chapter 2 of this work.

Fuel cells are electrochemical devices which are a promising technology for utilization of hydrogen in order to produce heat and electricity. Therefore, Chapter 3 gives an overview about different fuel cell types and their advantages and disadvantages.

Experimental work was carried out in order to produce hydrogen from a biomass feedstock. Biomass was gasified and the resulting wood gas subsequently treated in a process chain for the generation of hydrogen which is referred to as $BioH_2$. Furthermore, the $BioH_2$ was fed into a PEM fuel cell to proof its quality. These experiments are presented in Chapters 4 and 5.

Chapter 6 deals with possible applications of hydrogen and fuel cells. In this context, hydrogen storage technology and material compatibility of hydrogen is discussed aswell.

1.1 H_2 Properties

About 15 % of all components on the lithosphere are hydrogen atoms ligated with other atoms. The main hydrogen source on the earth's surface is water. The H_2 molecule is non polar with weak intermolecular bindings. This fact results in a low boiling point and a low melting point. Its solubility in water is very low. Hydrogen is the smallest molecule and has therefore a high diffusion coefficient and at the same time a high heat conductivity [40, p. 378] . Table 1.1 gives an overview of some hydrogen properties.

Table 1.1: Properties of hydrogen [34, p. 6] [40, p. 378]

Property	Unit	Value
Boiling point	°C	-252.7
Melting point	°C	-259.1
Critical temperature	°C	-240
Critical pressure	kPa	1310
LHV	MJ/kg	120
HHV	MJ/kg	142
Density at 0 °C and 1.013 bar	kg/m^3	0.09

1.2 State of the Art H_2 Production

Today hydrogen is mainly produced from fossil fuels. Its production capacity is distributed among the following sources [49]:

- Reforming of natural gas (48 %)
- Off gases recovery in refineries or chemical industry (30 %)
- Coal gasification (18 %)
- By product of the chlorine-alkali electrolysis (2 %)
- Water electrolysis (2 %)

In the above mentioned processes hydrogen purification plays an important role because, apart from electrolysis, hydrogen is always acquired as a compound in a mixture of gases containing CO, CO_2, and CH_4 and other hydrocarbons as the main impurities. The reforming of natural gas as well as coal gasification for hydrogen production are described in the following sections. Processes for further gas conditioning and cleaning are reviewed in Chapter 2 of this work. [18], [21, p. 59-91] and [36] give a more detailed overview of the different technologies for hydrogen production and processing.

1.2.1 Steam Reforming of Natural Gas

The general formulation of the steam reforming reaction of hydrocarbons can be seen in Equation 1.1.

$$C_xH_y + x\ H_2O \leftrightharpoons \left(x + \frac{y}{2}\right) H_2 + x\ CO \tag{1.1}$$

This equation shows the ideal case if hydrogen and carbon monoxide are the only products.

Natural gas mainly consists of methane which reacts with steam in presence of a nickel catalyst to a mixture of CO, CO_2 and H_2 according to Equations 1.2 and 1.3.

$$CH_4 + H_2O \leftrightharpoons CO + 3H_2 \quad \Delta H_R^0 = +206\ \frac{\text{kJ}}{\text{mol}} \tag{1.2}$$

$$CH_4 + 2H_2O \leftrightharpoons CO_2 + 4H_2 \quad \Delta H_R^0 = +415\ \frac{\text{kJ}}{\text{mol}} \tag{1.3}$$

Before being fed into the reformer the natural gas is desulfurized in order to protect the catalyst. The endothermic reacions take place at about 850 °C and at a pressure level between 2.5 MPa and 5.0 MPa. After heat recovery the H_2 enrichment and purification processes start. The reformed gas enters a water gas shift (WGS) reactor in order to decrease the CO content and at the same time to increase the H_2 content of the gas according to Equation 1.4.

$$CO + H_2O \leftrightharpoons CO_2 + H_2 \quad \Delta H_R^0 = -41.1\ \frac{\text{kJ}}{\text{mol}} \tag{1.4}$$

Then the hydrogen is usually purified by means of pressure swing adsorption. Sometimes, gas scrubbing is applied before the PSA in order to reduce the CO_2 content in the feed. A simplified process chain is shown in Figure 1.1.

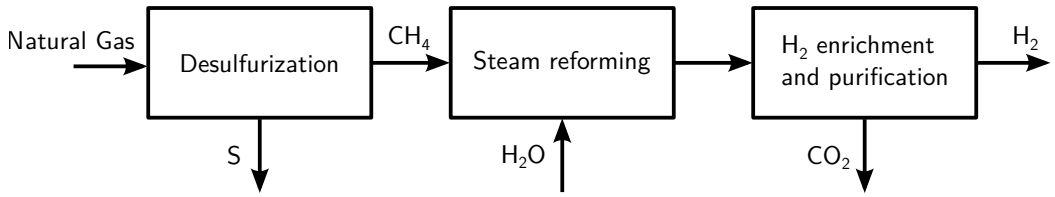

Figure 1.1: Principle of steam reforming of CH_4 for hydrogen production from natural gas

1.2.2 Coal Gasification

Coal gasification is a well known technology for converting coal into a syngas, which generally consists of CO, H_2, CO_2, CH_4, and impurities like H_2S and NH_3. If oxygen is used as a gasification agent the following main reactions can take place during the gasification process:

$$C + O_2 \rightarrow CO_2 \quad \Delta H_R^0 = -393.5 \ \frac{\text{kJ}}{\text{mol}} \tag{1.5}$$

$$2C + O_2 \rightarrow 2CO \quad \Delta H_R^0 = -221 \ \frac{\text{kJ}}{\text{mol}} \tag{1.6}$$

$$2CO + O_2 \rightarrow 2CO_2 \quad \Delta H_R^0 = -566 \ \frac{\text{kJ}}{\text{mol}} \tag{1.7}$$

Reactions 1.5 to 1.7 are highly exothermic providing heat for the subsequent endothermic gasification reactions. If steam is used as a gasification medium different reactions can take place. Gasification with steam increases the amount of hydrogen in the resulting synthesis gas.

$$C + H_2O \leftrightharpoons CO + H_2 \quad \Delta H_R^0 = +118 \ \frac{\text{kJ}}{\text{mol}} \tag{1.8}$$

$$C + 2H_2O \leftrightharpoons CO_2 + 2H_2 \quad \Delta H_R^0 = +178.2 \ \frac{\text{kJ}}{\text{mol}} \tag{1.9}$$

Due to the endothermic behaviour of 1.8 and 1.9 the reaction rate slows down as the reactions proceed since the temperature decreases with the extent of the reactions. Another set of reactions are the methanation reactions which would result in a higher CH_4 content in the syngas. However, these reactions are very slow at atmospheric pressure and in absence of a proper catalyst. Another reaction which takes also place during coal gasification is the reverse Boudouard reaction according Equation 1.10.

$$C + CO_2 \leftrightharpoons 2CO \quad \Delta H_R^0 = +159.9 \ \frac{\text{kJ}}{\text{mol}} \tag{1.10}$$

The reaction is endothermic and its reaction rate is several magnitudes lower than the rates of 1.5 and 1.6 at the same temperatures and in absence of a proper catalyst. After gasification the resulting syngas is processed by means of hydrogen enrichment and purification [36]. Figure 1.2 shows a simplified process chain for hydrogen production using coal as feedstock.

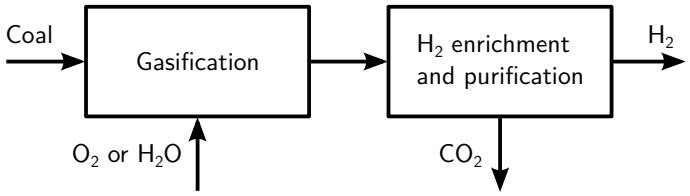

Figure 1.2: Principle of coal gasification for hydrogen production

Hydrogen production is not the only available option for utilization of synthesis gas acquired by steam reforming or coal gasification. The production of alcohols or different liquid fuels like gasoline or diesel in a Fischer-Tropsch process chain is also possible [31, p. 656-662].

1.3 Aim of this Work

The aims of this work are

1. Literature overview of different possibilities for sustainable hydrogen production,
2. Literature overview of state of the art fuel cell technology,
3. Experiments with a PEM fuel cell fed with high purity hydrogen (Alphagaz 1^{TM} H_2),
4. Experiments with a PEM fuel cell fed with $BioH_2$ from a process chain which uses biomass as feedstock,
5. Review of PEM fuel cell poisoning components which are contained in the process chains feedstock,
6. Review of applications for hydrogen especially in context with household heating via fuel cells.

In order to achieve point 1 and 2, a literature study was performed. To achieve point 3 and 4, a process chain for $BioH_2$ production at the commercial biomass power plant in Oberwart, Austria, was used. $BioH_2$ was generated and fed into a PEM fuel cell (Mobixane^{TM}), manufactured by AXANE^{TM}. Furthermore, for the high purity experiments, Alphagaz 1^{TM} H_2 gas cylinders were used. The performance of the $BioH_2$ and Alphagaz 1^{TM} H_2 fuel cell operation was compared. Point 5 was achieved via a literature study of several articles which covered PEM fuel cell poisoning experiments. Point 6 was covered by a literature review as well as by the review of different pilot projects which use hydrogen as a feedstock. In this context, hydrogen material compatibility and storage technologies are addressed as well.

Chapter 2

Renewable H_2 Production

This chapter provides an overview of different methods for sustainable hydrogen production. First, electrolysis powered by renewable energy sources is reviewed and second biomass gasification with further gas conditioning possibilities is addressed.

2.1 Electrolysis Based on Renewable Energies

Today electrolysis is a well known technology for producing very pure hydrogen from water. An overview of today's technology and key data is given in [29] [52].

Water electrolysis is basically the splitting of water into hydrogen and oxygen, as a useful byproduct, with electrical current. If renewable energy sources like water, wind and solar energy are used, no air pollution occurs during the operation of the electrolysis process [14].

This concept for the generation of hydrogen is used in industrial scale since 1890. Today, there are three main technologies, which are the alkaline electrolysis, the PEM (proton exchange membrane) electrolysis and the solid oxide electrolysis. All of them use water as feedstock and need an electrolyte which ensures high conductivity [14].

Water electrolysis takes up relatively little space and can use the existing electricity and water infrastructure. The major drawback of this technology is the environmental impact if no renewable power sources like water, wind or solar energy are used. Hydrogen generation powered by renewable sources may utilize "off peak" power and reduce therefore the costs. Also nuclear power plants are thought of as facilities which are able to produce CO_2 emission free hydrogen. If research and development makes further progress high temperature electrolyzers would reduce the costs even more due to their higher performance and higher efficiencies [14].

The law of Faraday in Equation 2.1, enables the calculation of the theoretical amount of electricity for water electrolysis.

$$n = \frac{Q}{F \cdot z} \tag{2.1}$$

For hydrogen production, a theoretical electrical energy of about 3 $\frac{\text{kWh}}{\text{Nm}^3}$ would be needed.

2.1.1 Alkaline Electrolysis

Plants for alkaline electrolysis are composed of an electrolyte with 30 wt.% KOH or NaOH for improving the conductivity. The cathode consists of nickel with platinum coating and the anode is built of nickel or copper, coated with metal oxides. During operation the liquid electrolyte needs to be replenished. They operate in a temperature range between 50 and 100 °C, they reach a degree of efficiency up to 73 % according to

$$\eta_E = \frac{\dot{Q}_{H_2}}{P_{el}}. \tag{2.2}$$

Large plants operate at megawatt scale and can produce hydrogen in an amount up to 200 $\frac{\mathrm{Nm}^3}{\mathrm{h}}$. In general, operation at higher temperatures and pressures increases the performance [23]. The principle of the alkaline electrolysis can be seen in Figure 2.1.

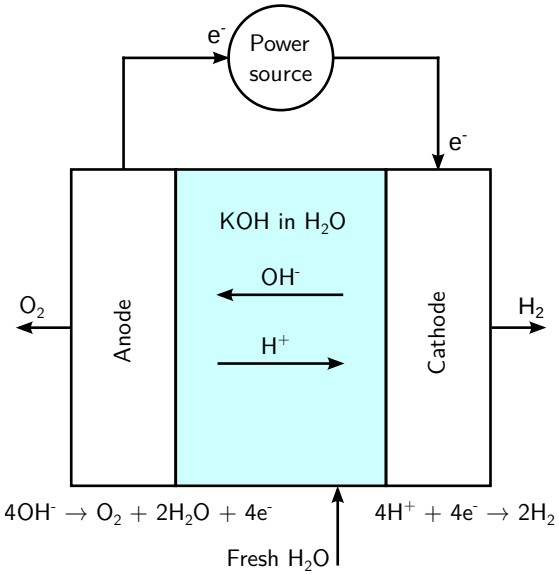

Figure 2.1: Alkaline electrolysis principle

2.1.2 PEM Electrolysis

PEM electrolysis (see Figure 2.2) can be designed for pressures up to several hundred bars and for stationary as well as mobile applications. It uses a proton exchange membrane (PEM) as electrolyte instead of KOH which results in a more simple design and higher safety. Its operating temperature is between 70 and 90 °C. The main drawback is the limited lifetime of the membrane. Due to this disadvantage PEM electrolyzers are currently not as mature as alkaline electrolyzers [48].

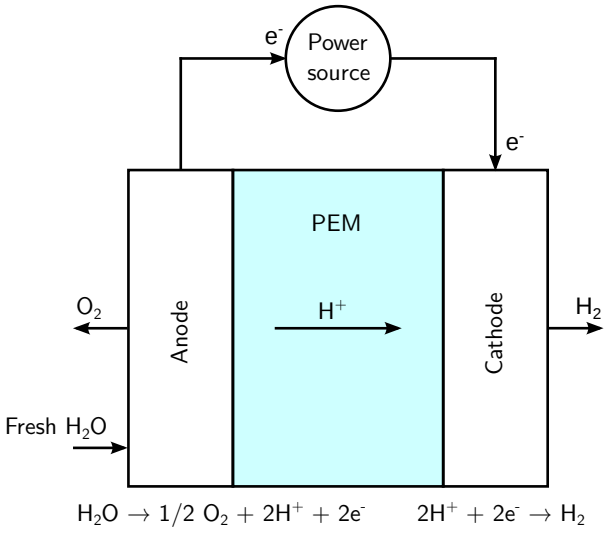

Figure 2.2: PEM electrolysis principle

2.1.3 High Temperature Electrolysis

The electrical energy demand for splitting water at 1000 °C is considerably lower than at 100 °C. This means that an electrolyzer operated at high temperatures can achieve higher performance and in addition a higher degree of efficiency. A typical technology is the solid oxide electrolyzer cell (SOEC). As electrolyte a ceramic is used. The device operates between 700 and 1000 °C. At these temperatures the electrode reactions are much faster. For providing the necessary heat geothermal, solar or other sources can be used. Similar to the PEM electrolyzers research and development regarding the material issues needs to be done [25] [48]. The principle can be seen in Figure 2.3.

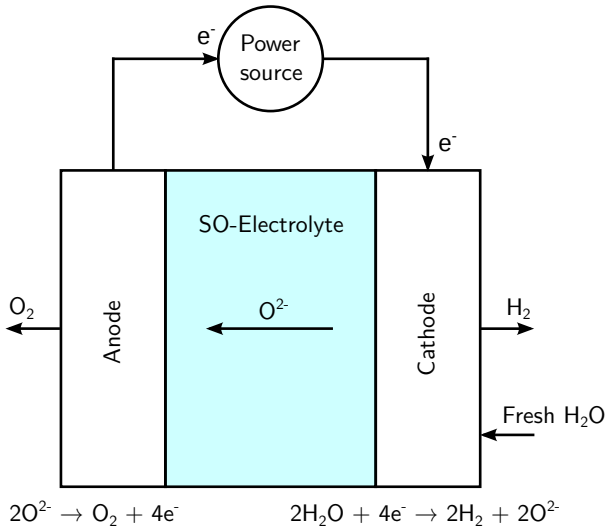

Figure 2.3: Solid oxide electrolyzer principle

2.2 Biomass Gasification and Gas Conditioning Steps

Biomass gasification and subsequent gas processing can be used for hydrogen production. Different biomass gasification technologies exist but the well approved and reliable method of dual fluidized bed (DFB) gasification seems to be one of the most promising today, because the generated wood gas has negligible amounts of nitrogen and offers a high hydrogen content (see Table 2.1). The technology was developed at Vienna University of Technology.

This section shows the principles of this gasification technology as well as possible operations which are required for generating a high quality $BioH_2$.

2.2.1 Dual Fluidized Bed (DFB) Gasification and Sorption Enhanced Reforming (SER)

The aim of producing wood gas suitable for further processes in order to produce hydrogen brings the dual fluidized bed steam gasification of biomass into focus. It consists of two distinct fluidized chambers. One bed is used for the endothermic gasification process, the other bed is used for combustion in order to provide the heat for the gasification. Heat is exchanged through a bed material which circulates between the fluidized beds. The process of providing the necessary heat for gasification via an external medium is referred to as allothermic. Figure 2.4 shows the principle of the wood gasification process.

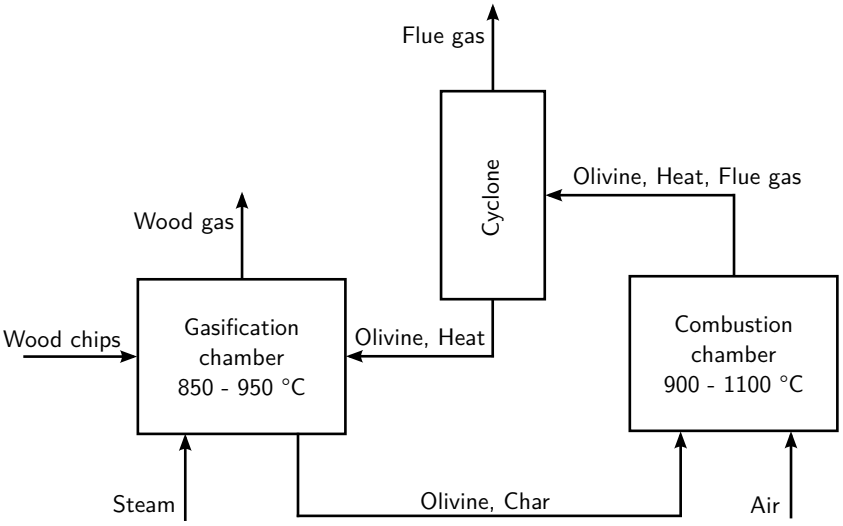

Figure 2.4: Principle of Dual Fluidized Bed Gasification (DFB)

Biomass is fed into the gasifier and processed with steam as a gasification agent at temperatures between 850 to 950 °C. The produced wood gas is practically free of nitrogen. The heat is generated in the corresponding combustion chamber and exchanged between the two fluidized beds by means of a solid bed material. The combustion chamber usually works at a

50 to 150 °C higher temperature level than the gasification chamber. Air with the containing oxygen is used as oxidant and fluidizing agent for the combustion. The bed material is separated of the flue gas in a cyclone which can be used for further processes which require heat (e.g. district heat). The resulting wood gas is a medium calorific gas with a high hydrogen amount (see Table 2.1).

Olivine is a suitable bed material because of its ability for catalytic reduction of the tar content. At the same time it is mechanically stable in the environment of the dual fluidized bed process [28].

This process is already utilized in several biomass gasification plants, e.g. Güssing and Oberwart, Austria.

Table 2.1: Dry composition and lower heating value of wood gas after DFB gasification [31, p. 621]

Parameter	Unit	Value
H_2	vol.%	35 - 40
CO	vol.%	22 - 25
CO_2	vol.%	20 - 25
CH_4	vol.%	9 - 11
N_2	vol.%	< 1
LHV	$\frac{MJ}{m^3}$	12 - 14

In order to further increase the hydrogen content in the wood gas, Sorption Enhanced Reforming (SER) is considered as an effective approach. Higher amounts of hydrogen are reached with limestone (CaO) as bed material instead of olivine. At the same time limestone is also able to decrease the tar content in the wood gas through higher catalytic activity compared with olivine. Figure 2.5 illustrates the main principle of the Sorption Enhanced Reforming process.

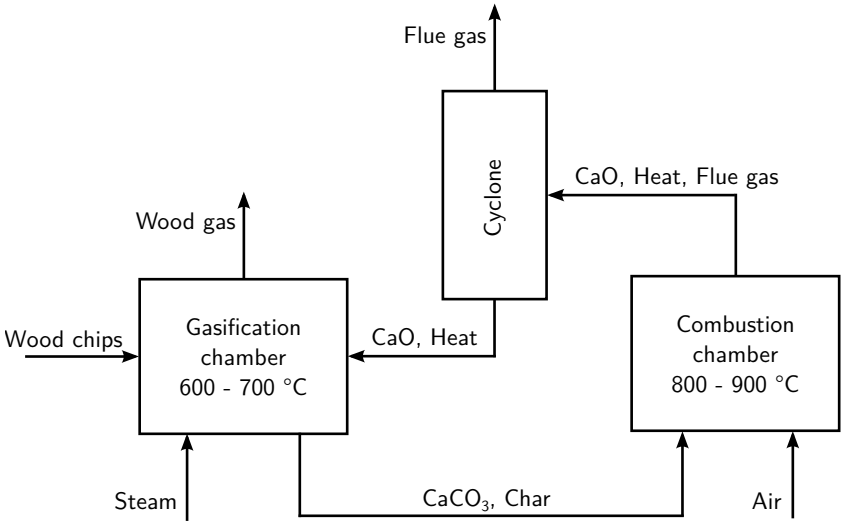

Figure 2.5: Principle of Sorption Enhanced Reforming (SER)

The whole process is very similar to the dual fluidized bed process mentioned above. The most important difference is the use of limestone (CaO) as bed material which replaces the olivine. The gasifier is operated at 600 to 700 °C in order to enhance the formation of $CaCO_3$ according to Equation 2.3.

$$CaO + CO_2 \rightarrow CaCO_3 \quad \Delta H_R^0 = -181.4 \ \frac{\text{kJ}}{\text{mol}} \tag{2.3}$$

$$CaCO_3 \rightarrow CaO + CO_2 \quad \Delta H_R^0 = +181.4 \ \frac{\text{kJ}}{\text{mol}} \tag{2.4}$$

The lower temperature can be applied due to the higher catalytic effect of limestone compared to olivine. The low temperature also increases the cold gas efficiency of the process. Due to the removal of CO_2 the amount of hydrogen is increased according to the equilibrium law of WGS reaction (see Equation 1.4). At the same time, due to the catalytic activity of limestone tar content is decreased as well. The calcination (Equation 2.4), in order to recover the CaO, takes place in the combustion chamber at temperatures between 800 and 900 °C beside the combustion. The resulting wood gas composition can be seen in Table 2.2 [18] [42] [47].

Table 2.2: Dry composition of the wood gas after SER gasification at the DFB gasifier in Güssing, Austria [42]

Parameter	Unit	Value
H_2	vol.%	50
CO	vol.%	12
CO_2	vol.%	17
CH_4	vol.%	13
Non condensable C_xH_y	vol.%	6
Other components	vol.%	2

The results in Table 2.2 were gathered at Vienna University of Technology and at the gasification plant in Güssing, Austria, [32] [42] [46].

This section shows that it is possible to generate a synthesis gas, or in this context wood gas, which can be processed in subsequent steps in order to produce hydrogen. The conventional dual fluidized bed gasification technology is well established and already in use for several thousand hours in different biomass gasification plants. In these plants, wood gas is used in a combined heat and power (CHP) concept for parallel generation of electricity and district heat.

2.2.2 Water Gas Shift Technology

The exothermic water gas shift (WGS) reaction is a reversible reaction which forms hydrogen from carbon monoxide and steam (see Equations 1.4 and 2.5).

$$CO + H_2O \leftrightharpoons H_2 + CO_2 \quad \Delta H_R^0 = -41.1 \frac{\text{kJ}}{\text{mol}} \tag{2.5}$$

The reaction is typically catalyzed and used industrially for hydrogen production after the steam reforming and coal gasification process described in Chapter 1.2. It is applied in processes which require a high amount of hydrogen, e.g. Haber-Bosch synthesis. WGS reaction is a proper approach in order to increase the hydrogen amount and to decrease the carbon monoxide amount at the same time. The equilibrium constant

$$K_{WGS} = \frac{[H_2] \cdot [CO_2]}{[CO] \cdot [H_2O]} \tag{2.6}$$

is a function of temperature. It is about 10 at 415 °C, 100 at about 240 °C and 330 at 180 °C. This would mean that more hydrogen is formed at lower temperatures. Despite this fact typical WGS units are operated at higher temperatures than 200 °C because at low temperature levels the reaction becomes kinetically controlled and therefore too slow for proper conversion. The pressure influence to the equilibrium is negligible due to reaction's mole ratios of one. WGS units are usually designed in a two step process (see Figure 2.6).

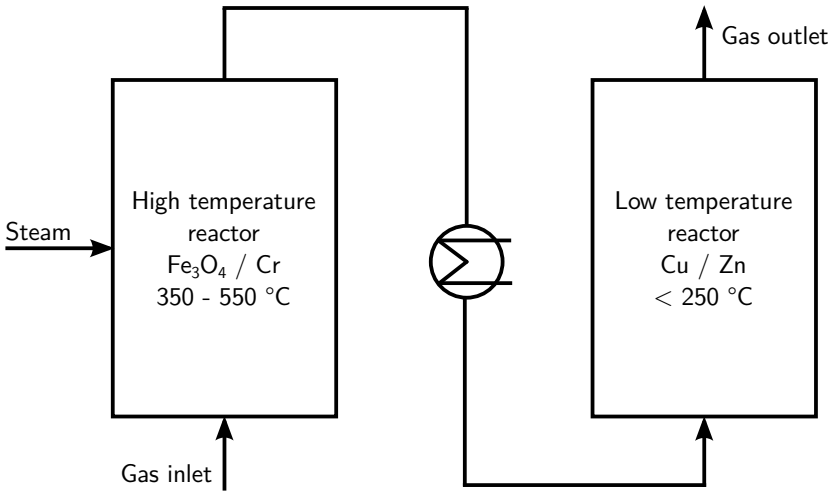

Figure 2.6: Simplified principle of a commercial water gas shift unit

The first step, the high temperature WGS, operates adiabatic with a temperature level of 350 to 550 °C, depending on feed composition. The pressure is chosen according to the process requirements. An iron-chromium (Fe/Cr) catalyst is used in order to accelerate the reaction. Gas hourly space velocities of 400 to 1200 h^{-1} are applied. The result is a decrease

of CO content down to 2 % dry basis. The second process step takes place at temperature levels below 250 °C and takes therefore advantage of the favourable equilibrium in order to reduce the CO content down to 0.2 to 0.4 % dry basis in the presence of a Cu/ZnO catalyst which shows a higher activity at low temperatures compared to the Fe/Cr catalyst. In this step the condensation of water needs to be avoided because otherwise the catalyst would be destroyed. A steam to dry gas ratio of 0.4 and a GHSV of about 3600 h^{-1} is applied [36, p. 311-315].

2.2.3 Absorption

Absorption or scrubbing is the dissolution of vapors or gases in liquids. With this technique gas or vapor mixtures can be separated. The absorption equilibrium between a component i in the liquid and the gaseous phase can be described by the law of Henry

$$x_i = \frac{p_i}{H_{ij}}. \tag{2.7}$$

The molar fraction of component i in the solvent is proportional to the partial pressure of component i in the gaseous phase. The Henry coefficient depends on the solvent j and the component i. It increases very strongly with rising temperatures which results in a higher demand for solvent at low pressures and high temperatures. As a side effect of the operation at preferable low temperatures water which is maybe contained in the gas stream is condensed and therefore removed [39, p. 296-297].

Gases dissolve depending on their interaction with the solvent. This is called a physical absorption. For example noble gases, hydrogen, nitrogen, oxygen, carbon monoxide and lower hydrocarbons show low solubility in water. Chemical absorption involves a chemical reaction which enables the separation. An example for a chemical absorption is the removal of dihydrogen sulfide contained in natural gas. As a solvent a solution of ethanolamines in water is used. Due to the basic behaviour of the solvent the sour dihydrogen sulfide is bound as ammonia salt. Under certain conditions this reaction is reversible and the dihydrogen sulfide can be processed in further steps, for example for the generation of elementary sulfur [5, p. 95-96].

In wood gas processing, rapeseed methyl ester (RME) is a suitable solvent in order to clean the gas from different impurities. It shows a very good compromise between tar solubility and pressure drop compared to other solvents [27].

Figure 2.7 shows the basic scheme of a gas scrubbing process. Gas inlet is at the bottom of a packed or plate column. During its way up to the top of the column it is contacted in counter current flow with the solvent. Depending on the solvent certain unwanted compounds are reduced. Then it flows into a reservoir where the used solvent is periodically replaced with fresh solvent. Another possibility for regeneration of the solvent is to increase the temperature which is referred to as stripping.

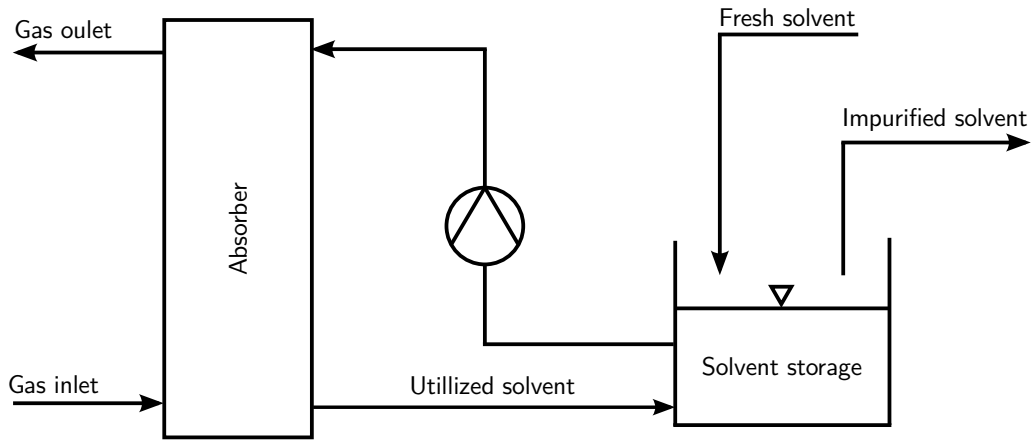

Figure 2.7: Basic scheme of a gas scrubbing process

2.2.4 Pressure Swing Adsorption

Pressure swing adsorption (PSA) has become a state of the art technology regarding the separation of high purity hydrogen. Over 85 % of current global hydrogen production uses the PSA process [36, p. 414]. The physical background is very simple. Impurities which are contained in a H_2 rich feed gas are selectively adsorbed on a solid adsorbent (zeolites, activated carbon, silica, etc.). The process uses high pressures in order to load the adsorbent with impurities. After the adsorbent has reached its maximum capacity of impurities, lowering of the column pressure leads to desorption of the gathered components. With these steps the reuse of the solid adsorbent is possible. The process needs a multi-column design for continuous operation which makes it very complex [36, p. 414-418].

Separation takes place because different components are adsorbed differently on the adsorbent. This behaviour is described by the so called sorption isotherms (see Figure 2.8) which vary according to the gas component and the solid adsorbent phase.

Figure 2.8 presents different curves which show the adsorbed amount of the component (n_i) over the partial pressure (p_i). The higher the partial pressure of a component the more it is adsorbed on the solid phase. If the pressure is lowered during desorption the amount of a specific component on the solid phase is reduced. Brunauer and coworkers classify between five types of isotherms for physical adsorption (Type I to V). Curves that are concave downward throughout (Type I) have been designated as favourable for adsorption technology. Those which are concave upward throughout (Type III) are unfavourable. Types II, IV and V are somewhere in between Type I and III with one or more points of inflection. A favourable isotherm for uptake is unfavourable for the desorption. This is very important where a favourable isotherm may be too favourable for regeneration to occur effectively [45, p. 16/11-12]. Type I isotherms usually describe adsorption of organic or inorganic gases

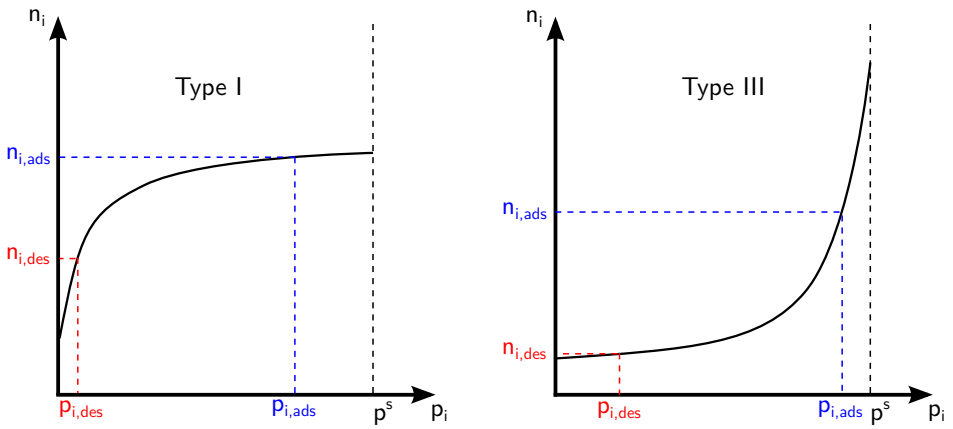

Figure 2.8: Different types of sorption isotherms [45, p. 16/12]

and vapors on solids like activated carbon or zeolites [39, p. 70]. Therefore, Type I is also well suited for gases present in wood gas. Type III is very rare and can be observed at water adsorption on a hydrophobic solid [15].

Figure 2.9 and 2.10 show a simplified PSA system. The feed is split up into the raffinate, which is the purified gas stream and the adsorbate which contains the unwanted impurities. If adsorber 1 is adsorbing gas from the feed, valves V1, V2, V3, V6 and V7 need to be open and the other one is closed in order to clean the feed gas. At the same time adsorber 2 is desorbed from impurities. After the solid adsorbent in adsorber 1 is saturated with impurities the adsorber tasks are switched which means that adsorber 1 is now desorbing and therefore producing impurity rich adsorbate and adsorber 2 takes over the adsorption part for producing clean raffinate from the feed. Therefore vales V1, V3, V4, V5 and V8 need to be open.

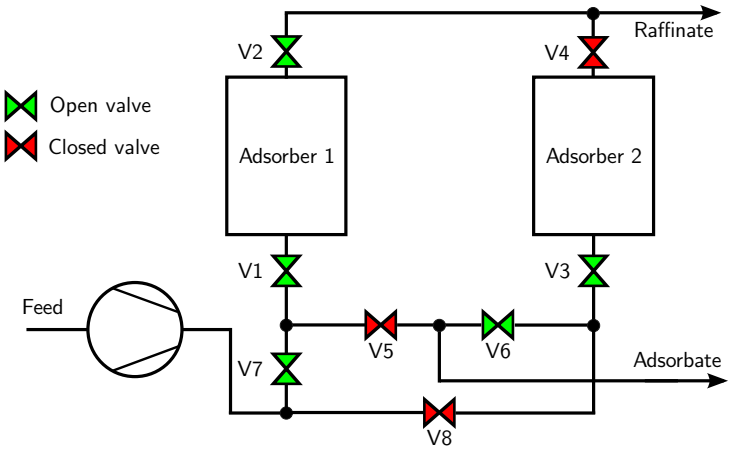

Figure 2.9: Adsorption process where adsorber 1 is adsorbing and adsorber 2 is desorbing.

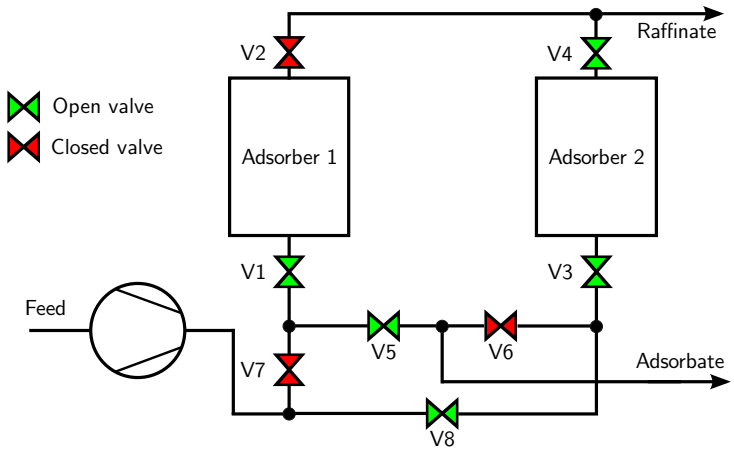

Figure 2.10: Adsorption process where adsorber 2 is adsorbing and adsorber 1 is desorbing.

2.2.5 Membrane Process for Hydrogen Enrichment

Membranes are structures which are more permeable to specific components and less permeable to other components. This effect allows the separation of a feed in two fractions with different compositions (permeate and retentate). In the past years membrane systems prevailed in water treatment and many other different fields in chemistry and medicine. They are used, for example, for blood cleaning, sea water desalination and air separation in low scale [38, p. 1-3].

The wide field of applications of membranes requires different membrane processes. For example pervaporation, reverse osmosis, ultra and nano filtration, electrodialysis and gas permeation. In theory, all of them have low energy consumption and can perform separation at low costs. Different mechanisms depending on the membrane process provide unique strengths and weaknesses like in some cases unusual sharpness of separation. This is a result of the selectivity of membranes which means that some components pass through faster than others but no one is rejected completely. It is a kinetic, not an equilibrium process. Substances move through membranes by several mechanisms. For porous membranes, such as are used in microfiltration, viscous flow dominates the process. For electrodialytic membranes, the mass transfer is caused by an electrical potential resulting in ionic conduction [45, p. 22/37-38].

For gas separation, gas permeation is the approach which is based on Fick's diffusion. All other membrane processes also involve the Fick's diffusion but in case of gas permeation it is the main driving force for separation [45, p. 22/61]. Figure 2.11 shows the principle of gas permeation.

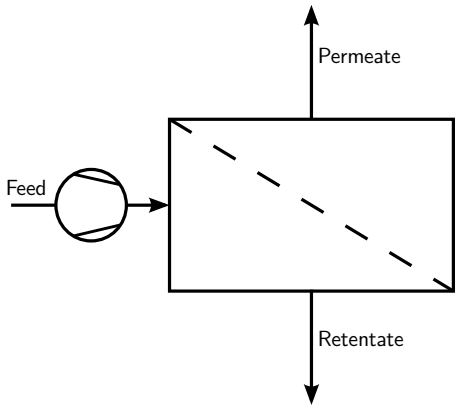

Figure 2.11: Gas permeation principle

If the simplified law of Fick

$$J_i = D_{ij} \cdot \frac{\Delta x_i}{\Delta x} \tag{2.8}$$

is applied together with Henry's law in Equation 2.7 the result is

$$J_i = \frac{D_{ij}}{H_{ij}} \cdot \frac{\Delta p_i}{\Delta x}. \tag{2.9}$$

Equation 2.9 shows that, in case of gas permeation, the driving force for the specific mass transfer J_i by area of component i is the partial pressure in the feed and in the permeate. Due to the selectivity of a membrane there is always a trade-off between purity and product recovery [45, p. 22/38-39].

For separation of hydrogen, different possible types of membranes are discussed. Polymer-based membranes are the cheapest and easiest processed materials and have a huge flexibility in their compositions therefore they can be tailored as the knowledge and performance base grows. Disadvantages are the limited lifetime of polymeric membranes and the lack of sufficient selectivity and flux capacities. Membranes, especially made from palladium and zeolites, provide the highest selectivities and flux capacities of all membrane classes for separation of hydrogen. The typically higher operating temperature range is parasitic energy costs which must be considered over lifetime of these kinds of membranes. Another disadvantage is the potential phase transitions and hydride embrittlement experienced by many pure metals and alloys offering a substantial obstacle for a permanent membrane solution [44].

Practice has shown that PSA processes for gas separation are more economic in higher scales than membrane units. In lower scales it might be different. Membranes are usually also easier to control because they are operated continuously compared to multibed PSA processes which are operated cyclic. If high purity hydrogen is valued, dense metal membranes are an option over polymeric membranes. The same purity and recovery as polymeric membranes can be achieved in a multi step membrane system, metal membranes are able to achieve the same target in only one step [36, p. 357-358].

Chapter 3

State of the Art Fuel Cell Technologies

This part of the work gives an overview of the fundamentals as well as of the state of the art technology of today's types of fuel cells. The focus lies on the PEM fuel cell because it is the type which was chosen for proving the high quality of the generated BioH_2. For this reason it is also described how different gas components which are usually present in wood gas affect the performance of a PEM fuel cell.

3.1 Fundamentals and Performance

Fuel cells are electrochemical devices which are able to convert chemical energy directly into electrical energy and excess heat as a by-product. In contrast to thermal processes, e.g. Rankine process powering a generator, they do not have to convert the chemical energy into thermal energy, convert the thermal energy into mechanical energy and further into electrical energy. Because of this fact fuel cells are not limited by the Carnot factor which means that in theory higher degrees of efficiency are possible. As combustion is avoided fuel cells generate power with minimal emissions. Though, fuel cells could use a wide variety of fuels, which have to enable a redox reaction with negative Gibbs energy ($\Delta G < 0$), most fuel cells use hydrogen and oxygen as feed [20, p. 1/1].

A typical fuel cell system consists of the unit cells, which are built together to a stack and components for thermal- and water management as well as control systems. A unit cell consists of two electrodes and an electrolyte. The reaction takes place at the three phase interface between the electrode, the electrolyte and the fuel. According to the electrochemical series a certain voltage is achieved. In case of the H_2 - O_2 fuel cell the voltage would be 1.23 V. This is just a theoretical value and it is only reached if there is no current flow, furthermore, no load. In reality there are several effects which cause that the achieved voltage will be much lower than the voltage according to the electrochemical series. In order to reach

higher voltages and, furthermore, higher power several unit cells are combined to a fuel cell stack. Typically, fuel (hydrogen) is fed continuously to the anode, where the oxidation takes place and the oxidant is fed continuously to the cathode where the reduction takes place. The electrochemical reaction produces electrical current which can work on the load, charge equalization takes place through the electrolyte [20, p. 1/2].

The maximum electrical work a fuel cell can achieve is described by the Gibbs energy

$$\Delta G = -z \cdot F \cdot E_0. \tag{3.1}$$

With z as the number of charge carriers participating in the reaction, F as the Faraday constant (96485 $\mathrm{C \cdot mol^{-1}}$) and E_0 as the cell potential according to the electrochemical series. The negative prefix of z is necessary because of the negative Gibbs energy. The overall energy which is stored in the fuel can be described by the standard formation enthalpy of the reaction ΔH_f^0 or, if the standard conditions are considered, the HHV (Higher Heating Value) of hydrogen. With these values a theoretical degree of efficiency of the fuel cell can be calculated according to

$$\eta_{FC_{H_2}} = \frac{\Delta G}{\mathrm{HHV}_{H_2}}. \tag{3.2}$$

The result is a theoretical electrical degree of efficiency of 83 %. Because of the temperature dependence of the Gibbs energy according to

$$\Delta G = \Delta H - T \cdot \Delta S, \tag{3.3}$$

the degree of efficiency of a fuel cell decreases with higher temperatures. Contrary to ohmic conduction the resistance of an electrolyte decreases with rising temperature. As mentioned before there are several effects which make the achievement of the theoretical potential of a fuel cell difficult. Figure 3.1 helps to understand these effects.

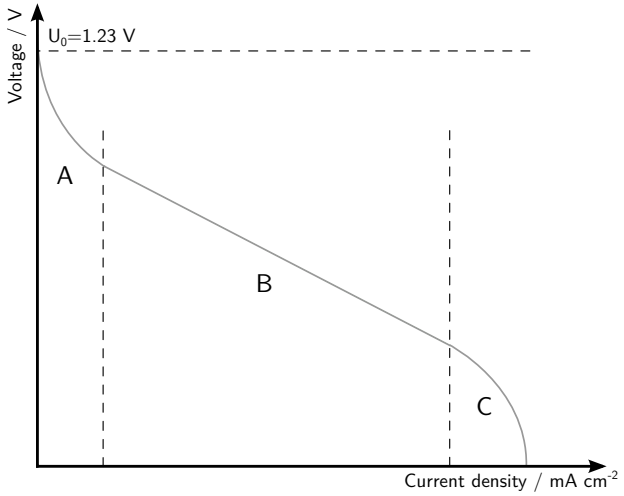

Figure 3.1: Cell voltage over current density of a fuel cell

The characteristic line can be split in three areas (A, B and C). One can see that if there is no load connected to the fuel cell and so no current flows the theoretical voltage of 1.23 V is reached. But once there is a load and current flows the voltage of the fuel cell is decreasing according to the increasing current density. This effect occurs in every electrical power source if connected to a load. In area A the decrease in voltage is caused by activation effects in order to start the reaction. In area B the voltage drop is due to losses according to the ohmic law, which causes the linear character of the curve in this area. In area C the mass transport of hydrogen to the three phase interface is the limiting factor. The transport of hydrogen is too slow for the amount which would be needed for the load [34, p. 28].

In order to consider this behaviour the definition of the degree of efficiency in Equation 3.2 can be rewritten to

$$\eta_{FC_{H_2},Load} = \frac{\Delta G}{\mathrm{HHV}_{H_2}} \cdot \frac{E_{Load}}{E_0} \tag{3.4}$$

with E_{Load} as the actual cell potential. The behaviour described above is reffered to as overpotential. As a result the overpotential causes a drop in degree of efficiency and subsequently that a fuel cell has its highest efficiency at medium current flows or medium powers. This makes them very interesting for partial load operations [17, p. 259-263] [34, p. 24-26].

There are several different types of fuel cells, which have different electrodes and electrolytes, but the main principle is always the same. A review of the different types of fuel cells are part of the following sections with the main focus on the PEM fuel cell.

3.2 Proton Exchange Membrane Fuel Cell - PEMFC

There are currently two types of PEM fuel cells under development. On the one hand the low temperature PEM fuel cell (LT-PEMFC) which works around temperatures about 60 to 80 °C and on the other hand the high temperature PEM fuel cell (HT-PEMFC) which works at temperatures up to 180 °C. In most cases the LT-PEMFC uses Nafion^{TM} as an proton exchange membrane which serves as electrolyte. Platinum is used as electrode material. This makes a low operating temperature possible which means it can be started very fast when its power is needed. The actual units have an electrical degree of efficiency of about 50-68 % [34, p. 79]. A complex part of the LT-PEMFC is the water management which takes care of the humidity of the membrane in order to keep the conductivity at an optimum level. Today LT-PEMFC have a wide application range. They are used in fuel cell cars, for household heating, in space ships and in submarines as power units. Research activities are carried out in order to decrease the ageing of the membrane, which causes a creeping performance loss over time and for replacing the platinum electrodes in order to lower the price [20, p. 3/1-3/25] [34, 77-95].

Figure 3.2 shows the principle of a PEM fuel cell.

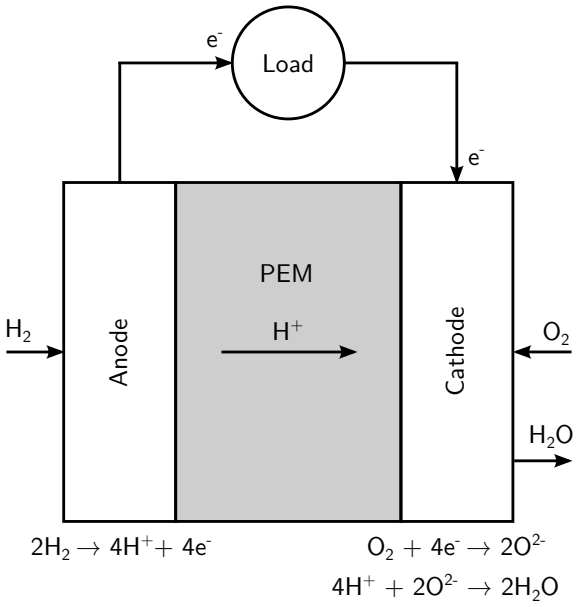

Figure 3.2: Principle of proton exchange membrane fuel cell

The HT-PEMFC is based on the same principle as the LT-PEMFC. The only difference is the electrolyte. Instead of a Nafion^{TM} membrane which needs a certain water content and subsequently a complex water management to achieve a high conductivity for protons it uses a polybenzimidazole membrane (PBI). This membrane is soaked in phosphoric acid (H_3PO_4) and ensures proton conductivity without complex water management. Because of the higher temperature the overall degree of efficiency is higher due to the usage of more excess heat. Another advantage is the higher CO tolerance. At 120 °C the HT-PEMFC tolerates up to 500 ppm CO and at 180 °C even up to 5000 ppm (0.5 %). Disadvantages are the necessity of temperature and acid resistant materials for compressors, sealing, valves, etc. The formation of liquid water needs to be avoided in order to prevent dilution of the phosphoric acid with water which would cause a conductivity loss [21, p. 234-235].

3.2.1 Toxic Components and Dilution Affecting PEM Fuel Cells

There are several components which can have negative influence on the performance of a PEM fuel cell. The main source of wood gas is the reforming process of biomass. Wood gas contains unavoidable components like CO, CO_2, sulfur compounds (H_2S), and sulfur organics (COS, thiophene) and ammonia which need to be removed before feeding hydrogen into the fuel cell. Another possible source for contamination is air, which is fed on the cathode side into the PEM fuel cell. It can also contain the compounds mentioned above but many other mostly due to exhaust gases, e.g. benzene, NO_x, SO_x. Other sources of contamination can be in the fuel cell itself, for example components of seals or compressor oils. Most influences of these compounds seem to decrease the catalyst layer activity of the PEM fuel cell [16].

The main impurities of the produced BioH$_2$ and their effects on PEM fuel cell performance, especially on the platinum electrodes, are described below.

Carbon monoxide (CO) CO is the most crucial compound affecting the PEM fuel cell because its high amount in the wood gas and the performance issues it can cause. It has very strong influence on PEM fuel cell performance due to dilution effects according to the Nernst equation (see Equation 3.5) but mostly because of poisoning of the platinum catalyst. The effects depend on concentration, pressure, operating temperature and current densities of the fuel cell [16].

$$E = E_0 - \frac{R \cdot T}{F \cdot z} \cdot \ln\left(\frac{a(H^+)}{\sqrt{p(H_2)}}\right) \tag{3.5}$$

Carbon monoxide is adsorbed on the active surface of the catalyst and reduces the available area for hydrogen oxidation. A significant performance decreasing effect could be observed at a concentration of 50 ppm [6]. But even smaller amounts of CO, e.g. concentrations from 4.5 to 0.5 ppm, cause a certain voltage drop of the fuel cell which is direct proportional to the CO concentration [9]. At these small amounts the voltage drop stays constant after a few hours of operation. This is because CO is converted to CO_2 if a certain overpotential is reached. Then there is an equilibrium of CO converting and CO_2 desorption and CO adsorption on the catalyst. CO_2 itself is not a poison for the platinum catalyst, it is just dilution for the anode gas [9].

If the fuel cell is operated with higher CO content in the anode gas, the voltage drop does not reach a steady state and keeps decreasing. This is because CO is adsorbed faster than CO_2 can be formed. CO poisoning is reversible if the fuel cell is operated with pure hydrogen afterwards. However, the regeneration of the catalyst needs more time than its poisoning [9].

Carbon dioxide (CO_2) The performance loss due to dilution with CO_2 is assumed to be higher than that from N_2. Reason for this seems to be the formation of CO, either through the reverse water gas shift reaction (WGSR) or an electrochemical reduction reaction. Both of them occur at CO_2 concentrations of about 20 % [9]. Especially at higher current densities the effects of CO_2 have to be taken into account [16].

Methane (CH_4) During an experiment at operating conditions which have been similar to the conditions of the experiment described in this thesis, it was discovered that even high amounts, up to 92 %, of methane in the anode feed do not cause poisoning or degradation effects neither of the catalyst layer of the anode nor of the proton exchange membrane. The performance is just limited to the Nernst Equation and so to the partial pressure of hydrogen. Actually an efficient method for separating H_2 and CH_4 was established [10].

Hydrogen sulfide (H_2S) Hydrogen sulfide is adsorbed on the catalyst's surface and reduces the area for hydrogen oxidation. This mechanism is observed even at small concentration of about 0.25 ppm. It seems to be very similar to the effect of CO. A problem of hydrogen sulfide poisoning is that it seems to be not reversible as it is the case for CO poisoning [9]. In addition, COS is also reported to reduce the active surface of the catalyst [34].

Ammonia (NH_3) Poisoning with ammonia is severe and happens very slowly, for example it takes up to 24 h to reach a steady state at one certain ammonia concentration [24]. Ammonia affects the performance in two different ways. After short exposure times, NH_4^+ ions replace the H^+ ions leading to a reduction in anode conductivity. After long exposure times, NH_4^+ ions migrate into the proton exchange membrane and compete with H^+ ions, also resulting in a lower conductivity. These effects were only observed at ammonia concentrations above 1 ppm (from 1 to 50 ppm). Below 1 ppm none of these effects take place. Regeneration of the catalyst with hydrogen seems possible but much slower than the poisoning itself [9].

Nitrogen (N_2) Nitrogen seems to have just a dilution effect due to the Nernst Equation through lowering the partial pressure of H_2 [9].

Oxygen (O_2) The oxygen content in the feed gas of the anode needs to be as low as possible in order to avoid direct formation of water [9].

As described above, several components can have different contamination effects on a PEM fuel cell. Therefore, a careful fuel pretreatment is necessary in order to avoid performance loss and long term stability issues.

3.3 Direct Methanol Fuel Cell - DMFC

The DMFC uses methanol (CH_3OH) as a fuel instead of hydrogen. Methanol has the highest electrochemical activity of all hydrocarbons. Overall the DMFC shows lower power characteristics than the PEMFC but the buildup is not that complex because no reforming of the fuel or complicated water management is needed. Figure 3.3 shows the basic principle of a DMFC.

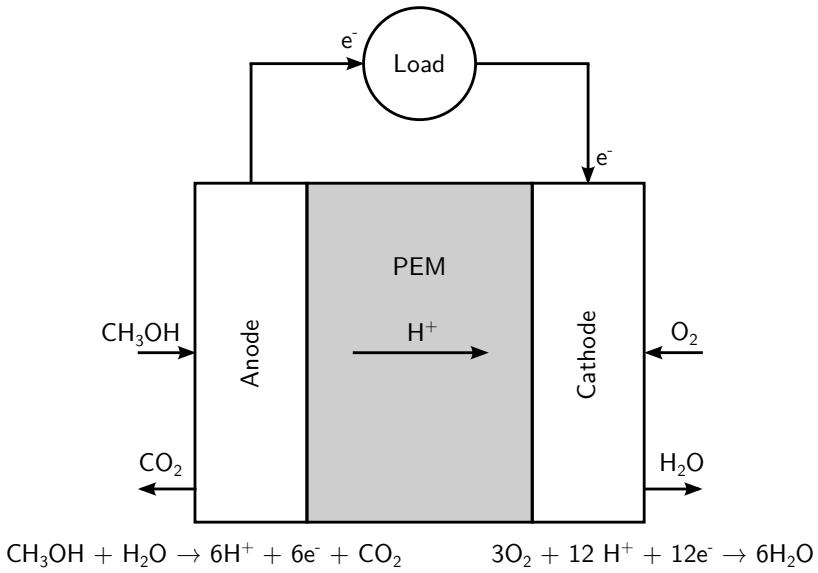

Figure 3.3: Principle of direct methanol fuel cell

A PEM (proton exchange membrane) is used as an electrolyte. Oxidation agent is oxygen gathered from air. Platinum covered carbon is used as electrode material on the anode side as well on the cathode side of the unit. Intermediate formation of CO, aldehyde, carbon acids and other intermediate products during the oxidation can cause poisoning of the catalyst. According to the electrochemical series a DMFC unit should reach a cell voltage of 1.186 V. Because of overpotential effects only about 0.5 V are reached in practice. The operation temperature of a DMFC is between 60 and 130 °C. The higher temperature is necessary due to the otherwise much lower power density. The electrical degree of efficiency is between 20 and 30 % with the highest values in partial load operation. In order to decrease this effect a certain CH_3OH to H_2O ratio (1 to 2 molar) is used as a fuel so the methanol concentration diffusing through the membrane is lowered [34, p. 126].

Anode overpotential is assumed to be caused by adsorption of partial decomposition products of methanol (e.g. CO). The cathode overpotential is assumed to be due to poisoning of the electro-catalyst by cross over methanol and its decomposition products [20, p. 3/19].

A possible application of direct methanol fuel cells lies in portable usage as an alternative to accumulators. Stationary systems with a power of 5 kW exist but for overall stationary or mobile applications in cars the power densities of the DMFC are considered too low [34, p. 138-139].

3.4 Alkaline Fuel Cell - AFC

The AFC uses a 30 % potassium hydroxide (KOH) aqueous solution as an electrolyte. The fuel and oxidant, in this case hydrogen respectively oxygen, need to be pure gases with as less as contamination as possible. CO_2 as impurity leads to the formation of potassium carbonate according to Equation 3.6.

$$2KOH + CO_2 \rightarrow K_2CO_3 + H_2O \quad \Delta H_R^0 = -194.1 \frac{\text{kJ}}{\text{mol}} \tag{3.6}$$

Potassium carbonate causes blinding of the electrodes and, therefore, a performance loss of the unit. The electrodes consist of nickel or platinum depending on operating conditions. On the one hand the usage of nickel, which is less sensitive for CO or H_2S, makes the fuel cell unit cheaper but on the other hand the application of nickel lowers the performance. At operation with pure gases the AFC has the highest electrical degree of efficiency compared to all other types of fuel cells but its low operating temperature between 20 and 90 °C makes the application of excess heat very difficult. Another problem is the limited life cycle of the electrodes because of corrosion problems [34, p. 54-55]. The AFC working principle can be seen in Figure 3.4.

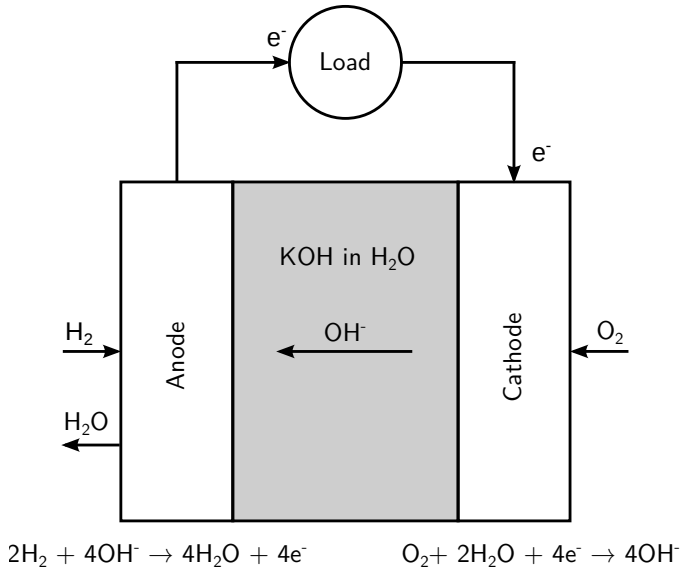

Figure 3.4: Principle of alkaline fuel cell

The alkaline fuel cell (AFC) was the most important fuel cell type in the past. The moon program of NASA would not have been possible without the AFC. It powered the Apollo spaceships on their way to the moon and was providing the astronauts with water. Later NASA used this type in the space shuttles where they proved as reliable energy source [20, p. 4/1-4/5].

3.5 Phosphoric Acid Fuel Cell - PAFC

Experiments for using gasoline as a fuel for fuel cells led to the development of the phosphoric acid fuel cell (PAFC). Concentrated phosphoric acid (H_3PO_4) is used as electrolyte which has a higher electrical resistance than sulfuric acid but the removal of water which is formed according to the cell reactions in Figure 3.5 is simplified. As an oxidant, oxygen acquired from air can be used. The electrodes are composed of platinum which serves as a catalyst and the operating temperature is between 160 and 220 °C. Higher operating pressure than atmospheric pressure increases the fuel cell performance but causes corrosion problems because of H_3PO_4 vapor. An electrical degree of efficiency up to 55 % is reached [34, p. 143-149].

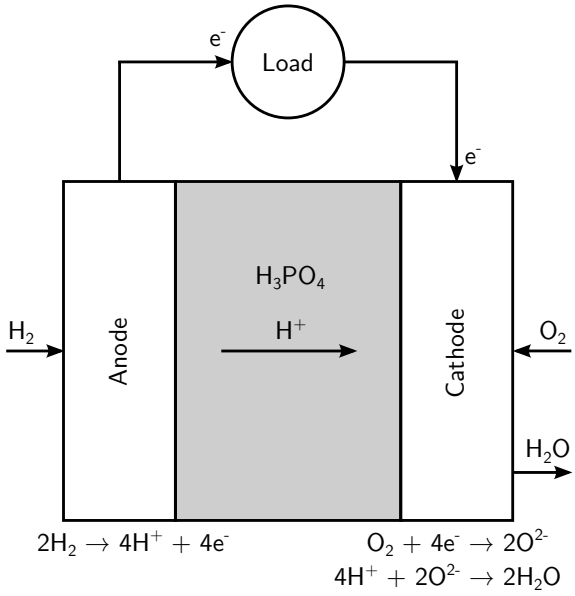

Figure 3.5: Principle of phosphoric acid fuel cell

These qualities make the PAFC very attractive. In countries like the USA or Japan several commercial block heating stations are in operatong using PAFC technology with powers up to 500 kW for one system. Systems which are still under development can provide electrical power up to 5 MW [34, p. 150-156].

3.6 Molten Carbonate Fuel Cell - MCFC

The MCFC is a representative of medium temperature fuel cells due to its operation temperature of 620 to 650 °C. At this temperature level overpotential is irrelevant so Ni electrodes can be used instead of expensive noble metals in order to achieve high reaction kinetics. Alkali carbonate casts are used as electrolytes, e.g. Li_2CO_3-K_2CO_3 mixtures or Na_2CO_3 in a heat prove matrix ($LiAlO_2$). CO_3^{2-} ions serve as charge carriers as Figure 3.6 illustrates.

Oxidant is an O_2/CO_2 mixture and, therefore, CO_2, which is formed on the anode side of the fuel cell unit is recycled to the cathode side. This leads to slow start up and shut down phases. Electrical degrees of efficiency between 55 to 65 % are reached by such a fuel cell system [34, p. 159-161].

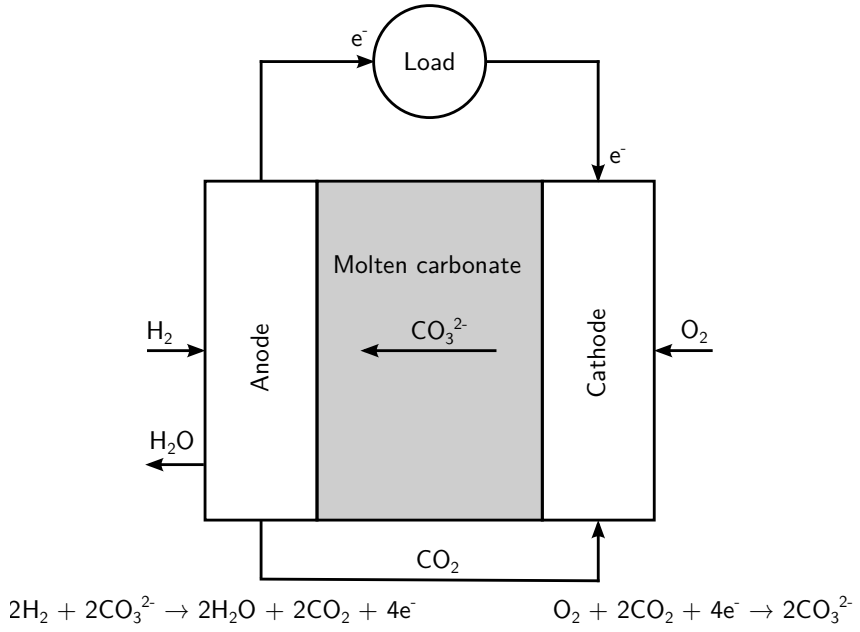

Figure 3.6: Principle of molten carbonate fuel cell

Hydrogen or reformed natural gas can be used as a fuel. Therefore CO is tolerated without any performance losses. Even contamination with sulfur up to 1 ppm is reversible. Sulfur compounds like H_2S, COS, CS_2 and C_4H_4S cause overpotential and form SO_2 in the electrolyte which leads to irreversible performance loss of the MCFC unit. NH_3, HCN and N_2 react with the molten carbonate electrolyte and cause problems. Long term contamination of the electrodes with hydrocarbons leads to coking and to a subsequent performance loss [34, p. 163-166].

There are combined systems of MCFC units, excess heat application and steam turbines in application which can reach an overall degree of efficiency of 85 % [34, p. 170].

3.7 Solid Oxide Fuel Cell - SOFC

The SOFC is a high temperature fuel cell and, therefore, no noble metals as anode catalysts are needed. Instead, the anode consists of nickel which makes the SOFC resistant against CO. The cathode is made of so called perovskites with dispersed platinum or palladium which serves as a catalyst for reduction of the oxygen which can be acquired directly from

air. Yttrium stabilized zirconium (YSZ) is applied as electrolyte which enables O^{2-} as charge carrier. A typical SOFC unit can be seen in Figure 3.7.

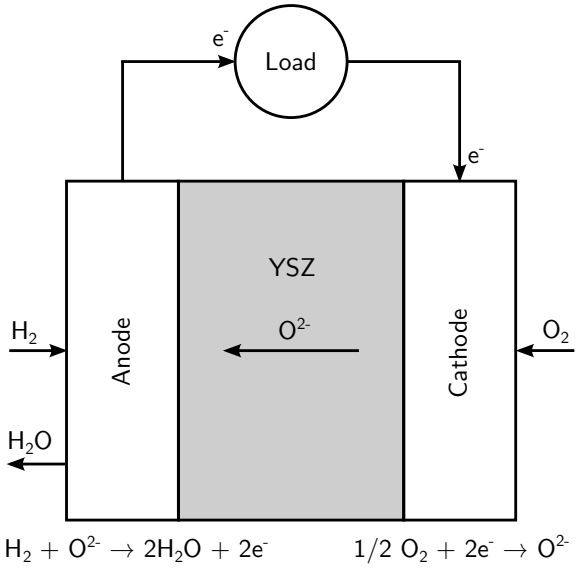

Figure 3.7: Principle of solid oxide fuel cell

Due to the high operation temperature between 800 and 1000 °C, reformed hydrocarbons or reformed biomass can be used as a fuel. Today's prototypes reach a power up to 250 kW and an electrical degree of efficiency of 60 to 65 % [34, p. 176].

SOFCs can be combined with excess heat utilization and a gas respectively a steam turbine in order to increase the fuel utilization as well as the overall degree of efficiency [34, p. 189].

Problems can be caused by the heat resistance of sealings and other parts of the fuel cell unit as well as by the thermal tensions during start up and shut down periods. If reformed hydrocarbons or reformed biomass is used as a fuel different components present in the fuel gas can have performance decreasing effects. For example, depending on the applied perovskite on the cathode, H_2S is tolerated up to 200 ppm if cobalt cermet[1] is used. 50 ppm of H_2S in the fuel gas showed a voltage drop of about 5 % but is assumed to be reversible. Furthermore, NH_3 concentrations up to 5000 ppm seem to have no performance decreasing effects [20, p. 7/9-7/13] [34, p. 181].

[1] cermet = ceramic and metal

Chapter 4

Experimental Setup of $BioH_2$ Production and Fuel Cell Testing

This chapter overviews the process which was operated in order to produce $BioH_2$. The $BioH_2$ was fed into a PEM fuel cell to evaluate its performance. Furthermore, the performance of the operation with $BioH_2$ and the operation with Alphagaz 1^{TM} H_2 under same conditions was compared. Detailed information can be found in the papers in Chapter C.

4.1 Setup for $BioH_2$ Production

The process for $BioH_2$ production consisted of a biomass steam gasification plant where wood gas was generated. Subsequently, the wood gas was fed into a process chain consisting of a water gas shift (WGS) unit, a rapeseed methyl ester (RME) and glycol gas scrubber and a pressure swing adsorption (PSA) unit.

4.1.1 Biomass Gasification Plant Oberwart, Austria

The feed of the process chain for the production of $BioH_2$ was wood gas from a commercial biomass steam gasification plant.

The plant is located in Oberwart, Austria and operated by Energie Burgenland AG. It is a combined heat and power (CHP) plant, which means that district heat and electricity are generated. It is quite similar to the well documented biomass gasification plant in Güssing, Austria [28]. The three main differences compared to the plant in Güssing are a biomass dryer, an ORC process for additional electricity production and two gas engines instead of one. A detailed description can be found in [11]. A flow sheet of the CHP Oberwart can be seen in Figure 4.1.

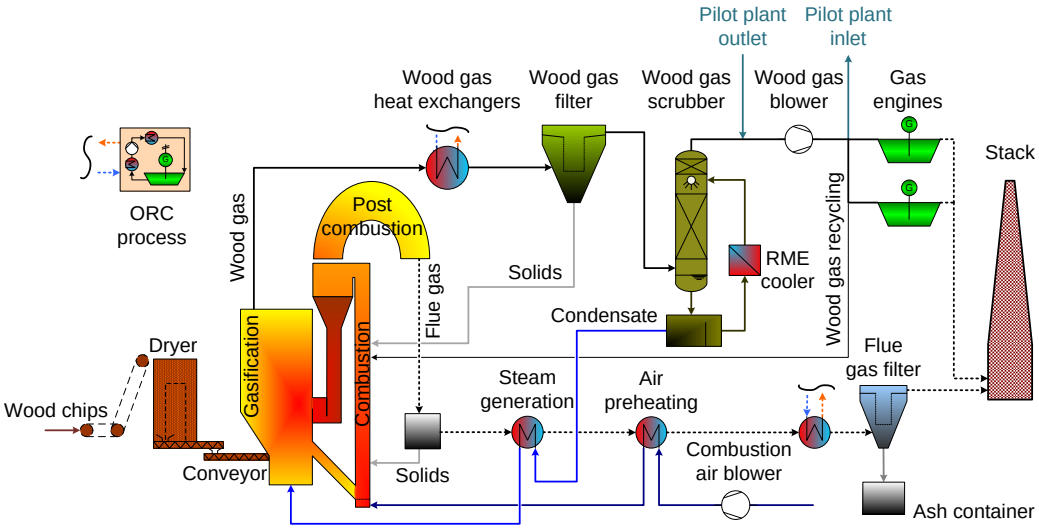

Figure 4.1: Flowchart of the biomass steam gasification plant Oberwart, Austria

The gasification is based on DFB technology which is described in Section 2.2.1. Biomass, in this case wood chips, is transported to the dryer. After drying, which is realized with low temperature heat which can't be used for district heat supply or the ORC cycle, the wood chips enter the gasifier. After the gasification reactions, wood gas leaves the gasifier, is cooled in heat exchangers, enters a bag house filter where particles are separated and flows through a RME gas scrubber where higher hydrocarbons (tar) and water is removed whereas the wood gas is cooled to about 40 °C. RME, which is saturated with tar, is fed into the combustion chamber. After the cleaning step in the RME scrubber a fraction of wood gas is recycled to the riser as fuel. The main amount of wood gas is fed into the gas engines by means of a blower for generating electricity. The water which is condensed in the RME gas scrubber is recycled into the gasifier. There it is used as a gasification agent.

Flue gas leaves the riser and is fed into a gravitational chamber where abrasive particles and the bed material (olivine) is separated. It enters several heat exchangers, where the gas is cooled. The heat is used for steam generation and for combustion air preheating, the remaining heat is used for district heat extraction as well as the ORC process. The flue gas enters the flue gas filter, conducted as bag house filter, and is finally led into the stack [18]. Key data of the biomass gasification plant in Oberwart can be seen in Table 4.1.

Table 4.1: Key data CHP Oberwart [18]

Parameter	Unit	Value
Fuel power	MW_h	8.7
Thermal output for district heat	MW_{th}	4.0
Electrical power of gas engines	MW_{el}	2.4
Electrical power of ORC	MW_{el}	0.4
Electrical efficiency	%	32
Thermal efficiency	%	46
Total energy utilization	%	78

4.1.2 Process Chain for BioH$_2$ Production

The applied process for BioH$_2$ production consisted of the following operation units: sulfur tolerant catalysis of the water gas shift (WGS) reaction, gas cleaning in a rapeseed methyl ester (RME) and glycol scrubber and pressure swing adsorption (PSA) for the final hydrogen purification.

The extraction of the wood gas which was used for BioH$_2$ production and feedback points can be seen in Figure 4.1. For BioH$_2$ production the wood gas was extracted after the RME scrubber of the power plant. It was fed into the WGS unit where, according to Equation 1.4, the hydrogen amount was increased.

In the next step, the gas was led into the RME and glycol scrubbing unit in order to remove impurities as well as to reduce the water content of the gas before it was fed into the PSA unit.

In the PSA unit, the gas stream was separated into the BioH$_2$ and the adsorbate, which contained the impurities. The BioH$_2$ was fed into the PEM fuel cell (Mobixane^{TM}) and the adsorbate was fed back to the gas engines of the power plant.

The process chain for BioH$_2$ production (see Figure 4.2) is well described in the papers in the appendix of this work.

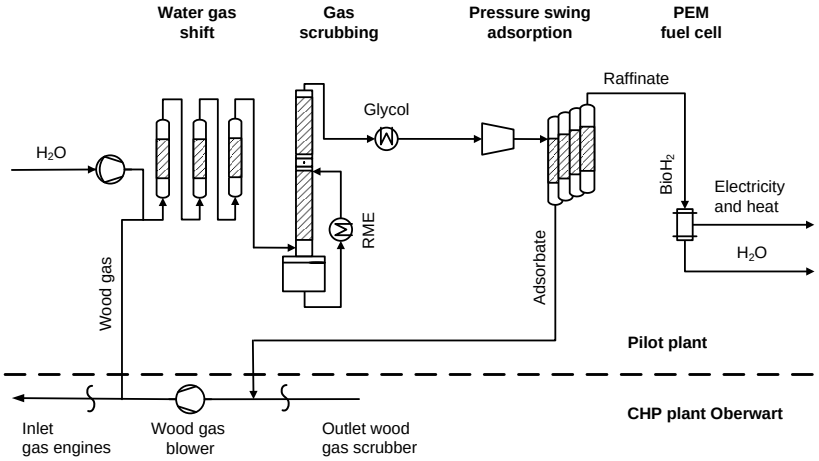

Figure 4.2: Flowchart of the pilot plant for BioH$_2$ production

4.2 Experimental Setup for the PEM Fuel Cell (Mobixane^{TM})

Axane^{TM}, a subsidiary of Air Liquide^{TM} Group, provided the PEM fuel cell (Mobixane^{TM}) for quality demonstrations of the generated BioH$_2$. Its operation parameters (e.g. H$_2$ flowrate, voltage, current, power, operation time, etc.) were recorded by a LabVIEW^{TM} program over a serial port. The key data of the PEM fuel cell are shown in Table 4.2.

Table 4.2: Key data of Mobixane^{TM} PEM fuel cell unit

Parameter	Unit	Value
Nominal voltage DC	V	48
Nominal voltage AC	V	230
Minimum power	W	500
Maximum power	W	2500
H$_2$ quality (ISO 14687)	vol.%	99.99
H$_2$ operating pressure	mbarg	250 ± 30
H$_2$ consumption at max power	NL · min^{-1}	35.1
H$_2$ flushing peak flow rate	NL · min^{-1}	60

The fuel cell integration into the process chain for BioH$_2$ production can be seen in Figure 4.2. A heating plate was used as an adjustable load and plugged into the AC connection of the fuel cell system (see Figure 4.4). For calculation of degrees of efficiency the power was measured at three different points of the fuel cell system (see Figure 4.3).

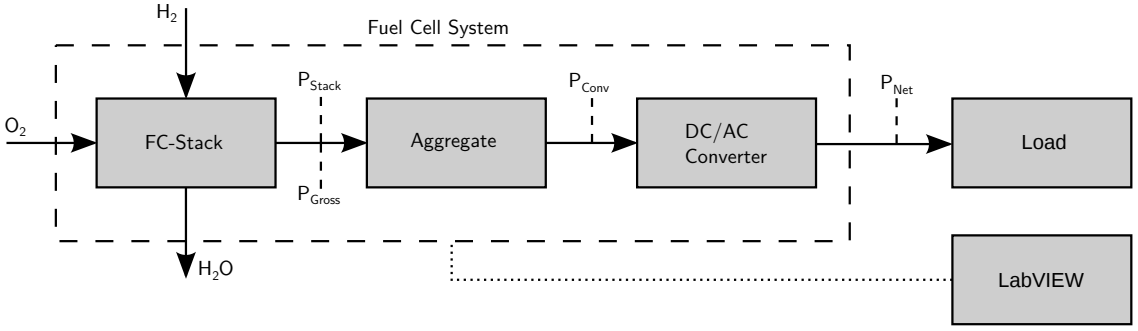

Figure 4.3: Mobixane^{TM} PEM fuel cell measurement setup

For operation with BioH$_2$, the fuel cell was started with pure Alphagaz 1^{TM} H$_2$. Then, after a few minutes and adjusting the suitable load, the feed gas was slowly switched from Alphagaz 1^{TM} to BioH$_2$. Before the shutdown down of the PEM fuel cell the same procedure was done in the opposite direction.

This PEM fuel cell system has a water management that causes power and H$_2$ flow rate peaks during operation which can be seen in Figure 5.13. During these peaks the proton exchange membrane is flushed with hydrogen in order to keep the humidity of the membrane at a certain level.

Figure 4.4: Mobixane^{TM} fuel cell system

To consider the higher power output and higher hydrogen volumetric flow rate of the stack during the hydrogen flushing, the stack power was quantified in two different ways. First of all P_{Gross} (see Equation 4.1) which did not consider the power peaks next to mean value calculation and second P_{Stack} (see Equation 4.2) which did consider the higher power next to mean value calculation. The mean values of the hydrogen flow rate were calculated in the same way.

Two additional powers were measured. On the one hand P_{Conv} for the power before the DC/AC converter and on the other hand P_{Net} which was equal to the power of the heating plate.

The lower heating value (LHV) of hydrogen was taken into consideration for means of comparison with already established combustion engines and condensing boilers. The higher heating value (HHV) would have been a better physical meaning because of the low temperature of the fuel cell and therefore water formation in liquid state.

With this setup four different degrees of efficiency could be calculated:

$$\eta_{Gross} = \frac{P_{Gross}}{\dot{V}_{H_2,Gross} \cdot LHV_{H_2} \cdot 22.41 \frac{m^3}{kmol}} \tag{4.1}$$

$$\eta_{Stack} = \frac{P_{Stack}}{\dot{V}_{H_2,Stack} \cdot LHV_{H_2} \cdot 22.41 \frac{m^3}{kmol}} \tag{4.2}$$

$$\eta_{Conv} = \frac{P_{Conv}}{\dot{V}_{H_2,Stack} \cdot LHV_{H_2} \cdot 22.41 \frac{m^3}{kmol}} \tag{4.3}$$

$$\eta_{Net} = \frac{P_{Net}}{\dot{V}_{H_2,Stack} \cdot LHV_{H_2} \cdot 22.41 \frac{m^3}{kmol}}. \tag{4.4}$$

Chapter 5

Experimental Results

This chapter presents an overview of the results of the $BioH_2$ process chain operation. Details can be found in the papers in Appendix C of this work.

The results of the PEM fuel cell operations with two different hydrogen qualities ($BioH_2$ and Alphagaz 1^{TM} H_2) are described in detail within this chapter.

5.1 $BioH_2$ Process Chain

During the 223 hours experimental run for $BioH_2$ production, chemical analysis of the main gas components and trace components (sulfur, C_xH_y and ammonia) were carried out. In addition a parameter study was performed in order to find the optimal operation parameters of each operation unit. No components, which would have critical negative influence on the performance of the PEM fuel cell have been measured in the generated $BioH_2$. The only detectable impurities in the fuel cell feed were 0.02 $vol.\%_{db.}$ of O_2 and 0.01 $vol.\%_{db.}$ of N_2. Furthermore, a hydrogen recovery calculated according Equation 5.1 of 131 %, based on the hydrogen amount in the biomass feed, was achieved.

$$Recovery = \frac{\text{Molar amount of } H_2 \text{ in the outlet}}{\text{Molar amount of } H_2 \text{ in the inlet}} \tag{5.1}$$

During the studied period, the hydrogen composition made a flawless fuel cell operation possbile. Furthermore, the achieved hydrogen recovery was higher than in former experimental approaches for producing fuel cell suitable hydrogen ([8] [18]) which were carried out within the last years. Figure 5.1 provides an overview of the main results of the $BioH_2$ process chain.

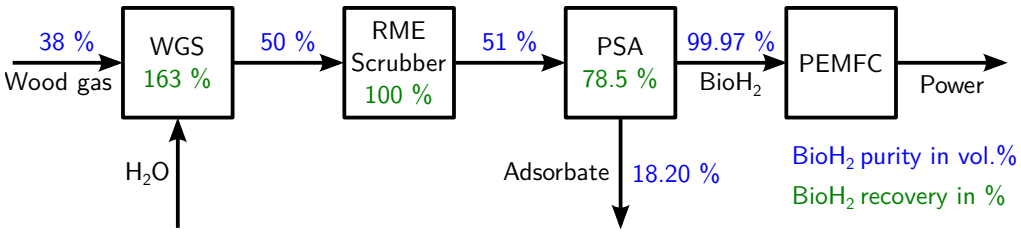

Figure 5.1: BioH$_2$ production chain summary

5.2 Fuel Cell Operation with BioH$_2$

In order to demonstrate the high purity of the PSA raffinate, respectively the generated BioH$_2$, it was fed into a PEM fuel cell (Mobixane^{TM}) for three hours after the process chain itself was already operated for 220 hours. Figure 5.2 shows the BioH$_2$ operation of the PEM fuel cell with arrows indicating the start and the end of the PEM fuel cell operation with BioH$_2$. Before the start and after the end of the test run with BioH$_2$ the PEM fuel cell was operated with Alphagaz 1^{TM} H$_2$. During the transition from Alphagaz 1^{TM} H$_2$ to BioH$_2$, the fuel cell was operated with a mixture of both gases.

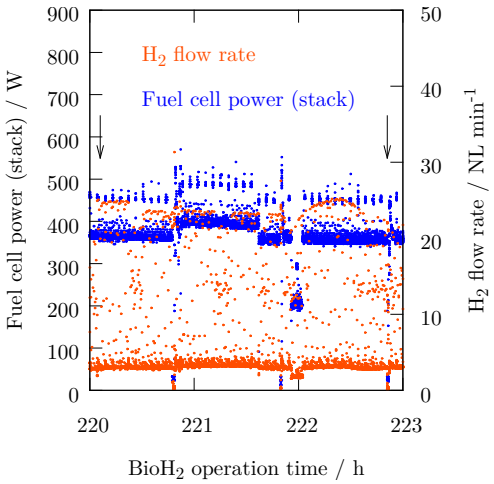

Figure 5.2: Mobixane^{TM} PEM fuel cell operation with BioH$_2$, 17.01.2014

The comparison of the operation data with the generated BioH$_2$ and Alphagaz 1^{TM} H$_2$ is shown in Table 5.1. The high standard deviation of the electrical power and the H$_2$ volumetric flow rate is likely due to the water management system of the fuel cell. In order to keep the water content in the membrane at an optimum level, it is periodically purged with H$_2$, depending on the power consumption of the fuel cell. Higher power results in higher repetition of the purge process. As the fuel cell power is directly proportional to the H$_2$ flow rate, the fuel cell power was increased as well.

Table 5.1: Comparison of PEM fuel cell (Mobixane^{TM}) performance and operating conditions with BioH$_2$ respectively Alphagaz 1^{TM} H$_2$ as feedstock, 17.01.2014.

Parameter	Unit	BioH$_2$			Alphagaz 1^{TM} H$_2$		
Current	A	4.2	±	0.3	4.3	±	0.3
Voltage	V	87.6	±	0.5	86.2	±	0.4
Electrical power	W	369	±	25	367	±	27
H$_2$ partial pressure	mbara	1268	±	27	1245	±	24
H$_2$ flow rate	$\frac{NL}{min}$	3.8	±	3.5	3.8	±	3.2
Fuel cell temperature	°C	40.5	±	1.5	36.8	±	0.9

Table 5.2: Comparison of the electrical degree of efficiency between operation with BioH$_2$ respectively Alphagaz 1^{TM} H$_2$.

	Unit	BioH$_2$	Alphagaz 1^{TM} H$_2$
η_{Gross}	-	0.67 ± 0.14	0.66 ± 0.15
η_{Stack}	-	0.55 ± 0.14	0.54 ± 0.15
η_{Conv}	-	0.30 ± 0.09	0.29 ± 0.09
η_{Net}	-	0.22 ± 0.05	0.22 ± 0.06

It could be demonstrated that there was no significant difference in the fuel cell performance regarding operation with BioH$_2$ and the operation with Alphagaz 1^{TM} H$_2$ during the investigated period, as Figure 5.3 and 5.4 and Table 5.2 indicates.

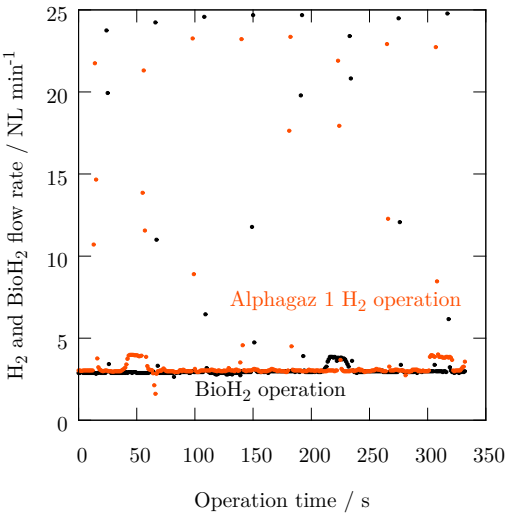

Figure 5.3: Comparison of PEM fuel cell H$_2$ flow rate operated with Alphagaz 1^{TM} H$_2$ and BioH$_2$, 17.01.2014.

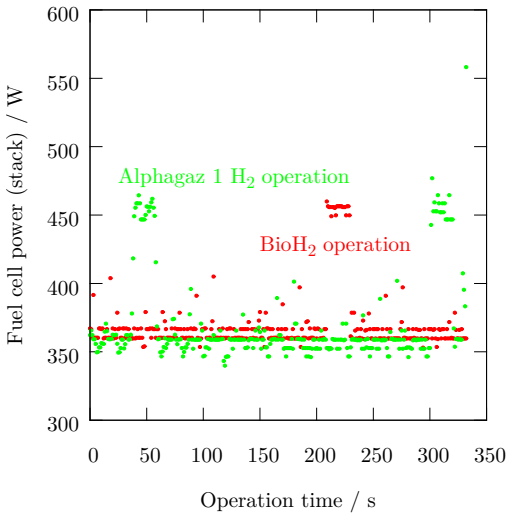

Figure 5.4: Comparison of PEM fuel cell power operated with Alphagaz 1^{TM} H$_2$ and BioH$_2$, 17.01.2014.

In the past, another BioH$_2$ PEM fuel cell operation was done within this workgroup. There the BioH$_2$ was generated by a process which also included a membrane separation step. The WGS unit was removed and the membrane unit was placed between the RME gas

scrubber and the PSA unit. There was also no difference in performance between operation with Alphagaz 1^{TM} H_2 and $BioH_2$ generated by the process chain. Detailed results of this operation can be found in [8] and [18].

5.3 Fuel Cell Operations with Alphagaz 1^{TM} H_2

The PEM fuel cell was operated periodically (see Table B.1 in Appendix B) with Alphagaz 1^{TM} H_2 (purity > 99.999 %) for keeping the membrane (PEM) in the fuel cell humid as well as for observing if its performance changes over time. Therefore, this section provides an overview of some operation results.

5.3.1 1st Alphagaz^{TM} Operation

This operation was a pretest in order to find out if the fuel cell is still working properly before starting with experimental test runs with $BioH_2$ operation after an operation break of about 6 months. Figure 5.5 shows the power consumption and the related hydrogen flow. Notable seems that the ratio of the peaks due to the water management is much higher at the hydrogen flow than at the fuel cell power. The degree of efficiency in Figure 5.6 is very low at low power consumption. The reason for this could be the operation of the fuel cell below its minimum power consumption, see Table 4.2. The overall high degree of effciency compared to earlier results, see [18] and below, could be explained by the long operation break of the fuel cell from summer 2013 to January 2014. According to Axane^{TM}, the manufacturer of the PEM fuel cell, the effect of higher efficiency can occur after a long operation break. Another result is that the fuel cell's nominal operation temperature of 65 °C (see Figure 5.7) is reached at its minimal power consumption of about 500 W. The voltage-current trend in Figure 5.8 is likely due to the power and hydrogen flow behaviour at the power of 1087 W in Figure 5.5. It seems that a steady state at this power consumption is not reached until an operation time of about 5 hours.

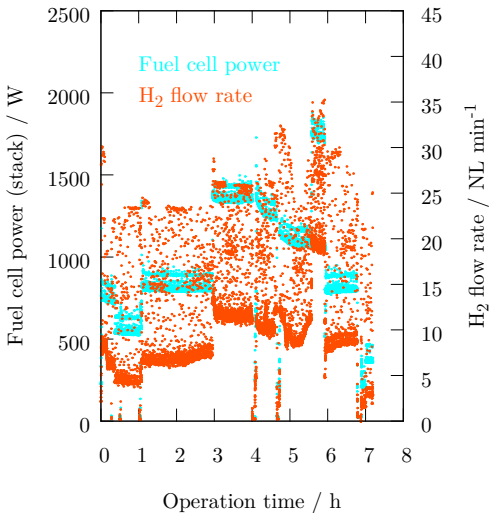

Figure 5.5: Electrical efficiency of the PEM fuel cell operated with Alphagaz 1^{TM} H_2, 17.01.2014.

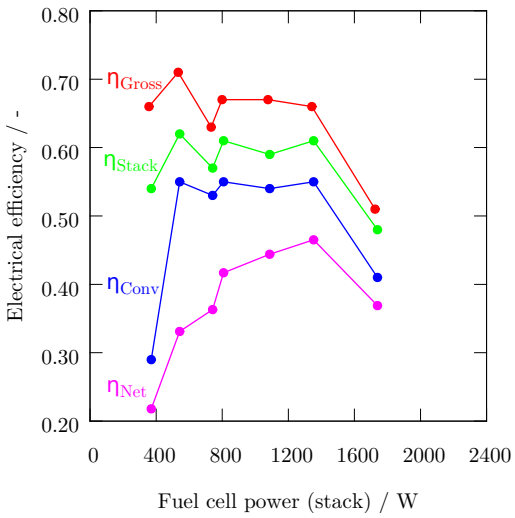

Figure 5.6: PEM fuel cell operation with Alphagaz 1^{TM}, 17.01.2014.

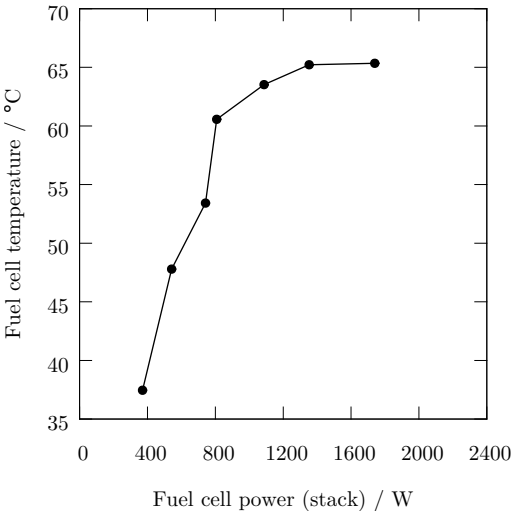

Figure 5.7: PEM fuel cell temperature over stack power with Alphagaz 1^{TM} H_2, 17.01.2014.

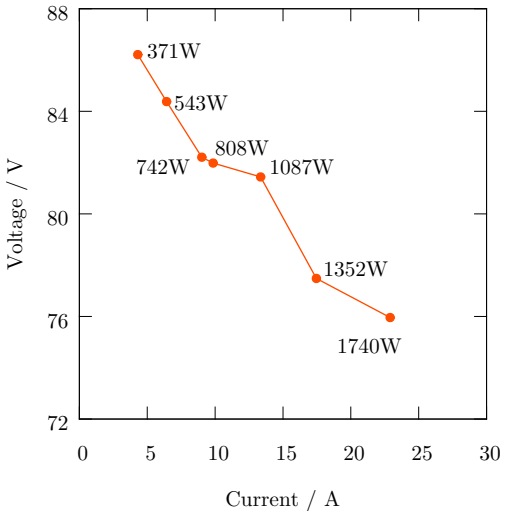

Figure 5.8: PEM fuel cell voltage over current with Alphagaz 1^{TM} H_2, 17.01.2014.

5.3.2 2nd Alphagaz™ Operation

After a warm up period, different powers were adjusted starting with the highest to the lowest (see Figure 5.9). The degree of efficiency chart in Figure 5.10 shows again a very high efficiency at medium powers. The temperature profile in 5.11 is quite the same as it is in 5.7. The voltage current diagram in Figure 5.12 shows a higher voltage for all powers compared to 5.8, especially for 524 W and 612 W.

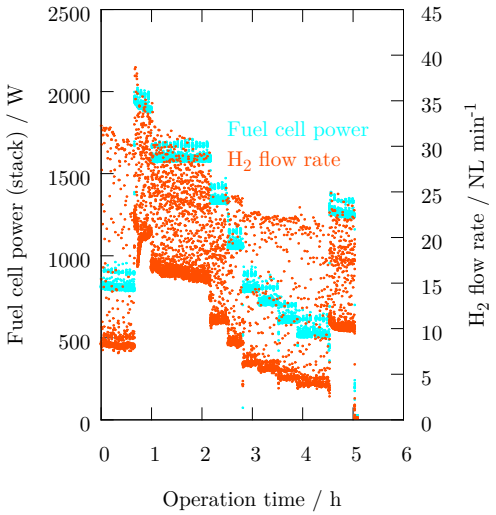

Figure 5.9: Electrical efficiency of the PEM fuel cell operated with Alphagaz 1™ H_2, 06.02.2014.

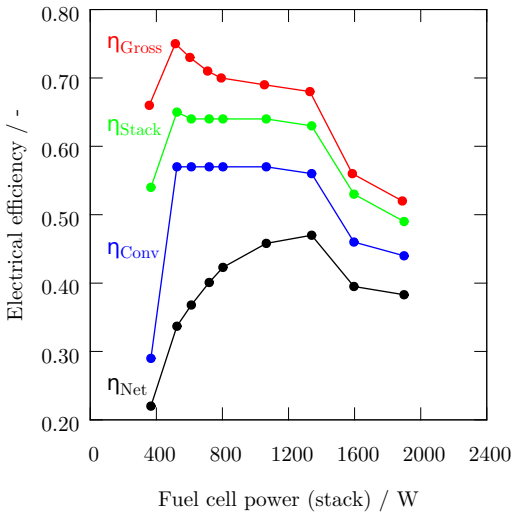

Figure 5.10: PEM fuel cell operation with Alphagaz 1™ H_2, 06.02.2014.

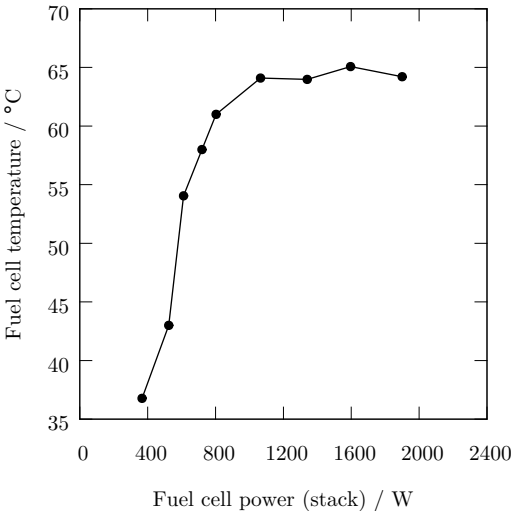

Figure 5.11: PEM fuel cell temperature over stack power with Alphagaz 1™ H_2, 06.02.2014.

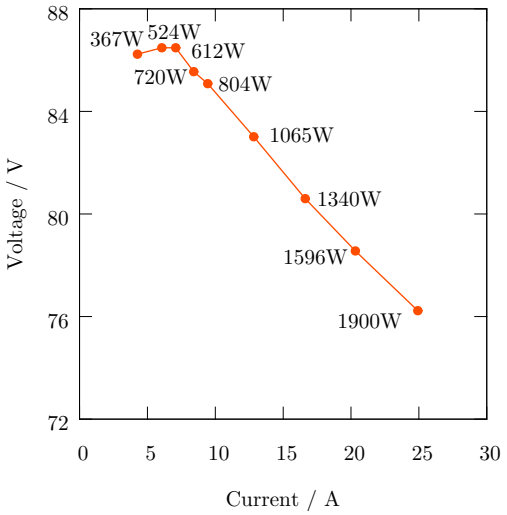

Figure 5.12: PEM fuel cell voltage over current with Alphagaz 1™ H_2, 06.02.2014.

5.3.3 3rd Alphagaz™ Operation

The test from 27.02.2014 showed that electrical degree of efficiency was in the same range as in the past operations from 28.02.2011 and 07.05.2013 (see [18]). As mentioned before, this behaviour often happens after a long operational break. Then the fuel cell needs a certain amount of operation hours to recover. The voltage-current diagram shows a very linear profile as described in literature [20].

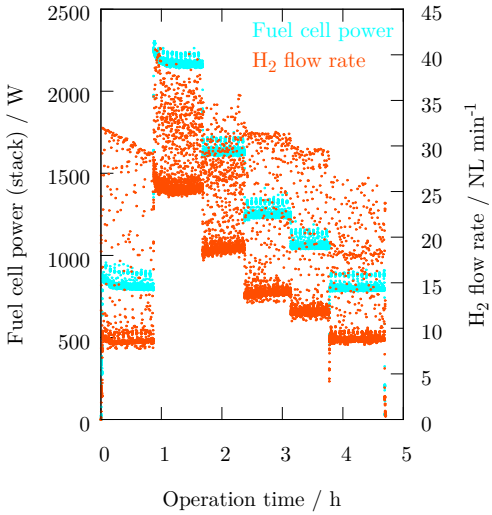

Figure 5.13: Electrical efficiency of the PEM fuel cell operated with Alphagaz 1™ H_2, 27.02.2014.

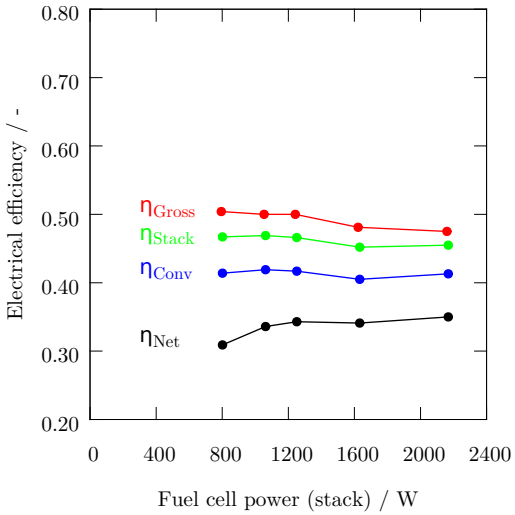

Figure 5.14: PEM fuel cell operation with Alphagaz 1™, 27.02.2014.

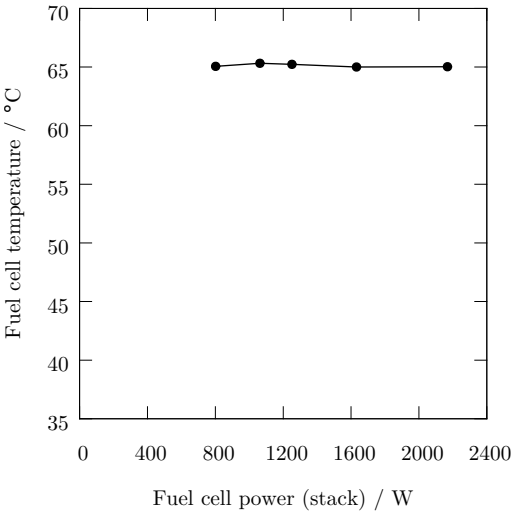

Figure 5.15: PEM fuel cell temperature over stack power with Alphagaz 1™ H_2, 27.02.2014.

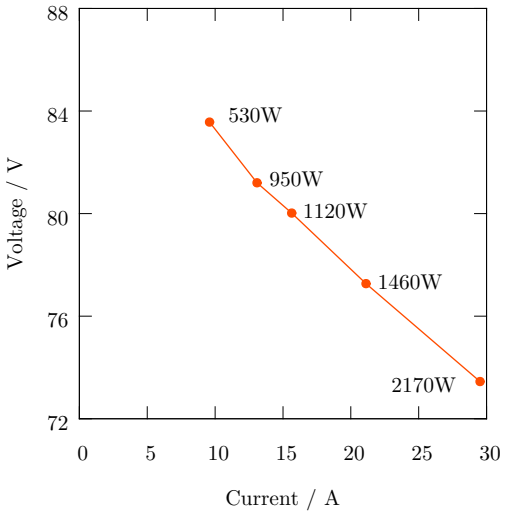

Figure 5.16: PEM fuel cell voltage over current with Alphagaz 1™ H_2, 27.02.2014.

The PEM fuel cell (Mobixane^{TM}) showed very unconventional behaviour in some experiments which did not fit to data given in literature, for example [34]. It is possible that these characteristics were due to the long operation break between summer 2013 and January 2014. According to Axane^{TM}, the fuel cell PEM membrane's humidity is decreasing during a long operation break and so several ageing effects occur. These ageing effects do not necessarily affect performance in a negative way. It is shown that these effects can also have positive influence on the performance of a PEM fuel cell. Unfortunately, these effects are not permanent and after a few hours of operation the fuel cell gets back to its design performance (see Figures 5.13 to 5.16 and [18]).

Chapter 6

Applications of Fuel Cells and $BioH_2$

For hydrogen usage a proper technological and economical storage technology is necessary. Afterwards an overview of possible applications for $BioH_2$ with focus on applications with fuel cells is given. Also usage in metal and chemical industry is covered because those two divisions are consuming most of today's produced hydrogen. The possibility of hydrogen usage in existing natural gas networks is discussed and in this context material compatibility. Also hydrogen and fuel cell applications in vehicles are covered as well as fuel cell usage in households in order to satisfy heat and electricity demand.

6.1 Hydrogen Storage

Four methods for hydrogen storage are presented in this thesis. These are storage in gaseous and liquid state, storage by physisorption and storage in form of metal hydrids. The specific energy of hydrogen of 120 $MJ \cdot kg^{-1}$ outreaches all fossil fuels in contrast to the low volumetric energy of 10 $MJ \cdot Nm^{-3}$. The upper and lower explosion limit is 4.0 respectivly 75.6 vol.% H_2 in air at 20 °C. Above 40 % humidity hydrogen detonates and above 60 % it does not inflame any more. The ignition energy with 0.02 mJ lies about ten times lower than for natural gas. The ignition temperature of 585 °C is higher than that for gasoline and natural gas [34, p. 21-232].

6.1.1 Gaseous Storage of Hydrogen

Above the critical point at -240 °C and 1.3 MPa, hydrogen cannot be liquefied anymore. At ambient conditions hydrogen well complies the ideal gas equation meaning that the compressibility factor Z is close to 1.

$$Z = \frac{p \cdot v}{R_{H_2} \cdot T} \tag{6.1}$$

The process which requires the least work for compression is the isothermal compression. For a compression from 1 to 900 bar at ambient temperature a specific work of $w_{H_2} = 8777\ \mathrm{kJ \cdot kg^{-1}}$ is needed in case of real gas behaviour. This means that the compression step needs an energy input of about 7.5 % of the calorific value of hydrogen. If the efficiency of a compressor is taken into account with about 50 % the compression to 900 bar needs about 15 % of the calorific value. Compression of gases usually lead to a temperature increase while expansion leads to a decrease. The change in state of a real gas during an expansion can be described by the Joule-Thomson effect and its coefficient

$$\mu_{JT} = \left(\frac{\partial T}{\partial p}\right)_h, \tag{6.2}$$

which can occur during filling of a pressure vessel from a reservoir. A positive value for μ_{JT} means that a decrease in pressure results in a temperature decrease. A negative value means that a decrease in pressure results in a temperature increase. The effect is only valid for real gases during an isenthalpic change of state, in case of an ideal gas the Joule-Thomson coefficient is equal to 0. Within the relevant range of pressures, hydrogen shows a negative Joule-Thomson coefficient meaning expansion causes a rise in temperature, e.g. an expansion from 1000 to 13 bar results in a temperature increase of 50 K [26, p. 1-10].

For storage of hydrogen in compressed state, pressure vessel with pressures up to 700 bar and higher have been realized and are commercially available. Due to its high diffusion coefficient and its tendency for adsorbing and dissociating at surfaces, materials have to be suitable for hydrogen. Commercial available pressure tanks are usually made of steel but they are slowly replaced by composite pressure tanks in order to reduce weight with the side effect of a higher price. With adequate materials and dimensioning, hydrogen storage in gaseous state takes place in a closed system. Therefore it can be stored without loss for extended periods of time [26, p. 13]. At 700 bar, an energy density of 1.3 $\mathrm{kWh \cdot L^{-1}}$ is possible which is about 10 % of the energy density of one litre of gasoline [34, p. 230].

6.1.2 Liquid Storage of Hydrogen

Industrial applications for liquefaction of hydrogen consumes about 20 to 30 % of the hydrogen's calorific value. First step in this process is the compression of gaseous hydrogen to about 30 bar. Then the gas is cooled with liquid nitrogen to about 80 K. Between 80 and 30 K the hydrogen is cooled by compression cooling and expanding in turbines. The last step which involves a cool down to 20 K is achieved by Joule-Thomson valves. At this temperature level the Joule-Thomson coefficient (see Equation 6.2) is positive and, therefore, the gas is cooled [26, p. 15-17].

A problem of liquid hydrogen storage is the boil off. There is always a gaseous phase over a liquid phase. The pressure of this vapor increases with rising temperature. Therefore,

tanks for liquid hydrogen need a proper pressure release system. The leaking hydrogen is then either burned or led into the ambient [21, p. 111-127] [33].

The first large scale hydrogen liquefaction plants were built during the Apollo program of NASA. Today's worldwide installed capacity for hydrogen liquefaction is 270 t/d. The largest single plant produces about 60 t/d at an energy consumption of 40 $\mathrm{MJ \cdot kg^{-1}}$ [21, p. 103]. Current R&D tasks are the development of more efficient liquefaction processes, improving of container insulation and development of systems which automatically capture boil off and re-liquefy the fuel [48]. The energy densitiy of liquefied hydrogen is about 2.1 $\mathrm{kWh \cdot L^{-1}}$ at 26 K and 4 bar [34, p. 230].

6.1.3 Storage by Physisorption

According to Section 2.2.4, hydrogen can be stored via adsorption on solids. Because of the weak interaction of hydrogen molecules with common adsorbents, high storage capacity is only reached at low temperatures of about 77 K. For a long period, zeolites and activated carbon were the best materials for physisorbtion of hydrogen. Recently, new classes of crystalline metal organic materials and novel porous carbon have been developed which can store a higher amount. At present, up to 7 wt.% hydrogen can be stored with the best materials at 77 K absolute temperature which equals about 2.3 $\frac{\mathrm{kWh}}{\mathrm{kg_{Ads}}}$ [26, p. 39-58] [34, p. 230].

6.1.4 Storage as Metal Hydrid

Binary bondings of hydrogen with more electropositive elements are called hydrids. Three different groups are defined:

- Saline hydrids which are formed by alkali and earth alkali metals, e.g. LiH and CaH_2.
- Covalent hydrids are formed with metals from III. to VI. main group (e.g. SnH_4 or InH_3).
- Metal hydrids are formed by transition metals including the rare earth and actinide series (e.g. NiH). In these hydrides, hydrogen acts as a metal and forms a metallic bond. Metal hydrids have high thermal and electrical conductivity and are brittle compared to metals.

Metal hydrids are promising and important candidates for many stationary and mobile hydrogen storage applications. The most common use of metal hydrides is as anode material in nickel-metal-hydrids (Ni-MH) rechargeable batteries. The storage technology offers a hydrogen volumetric density of about 1.05 $\mathrm{kWh \cdot L^{-1}}$ as well as easy adsorbing and desorbing due to a small change of pressure at levels from 1 to 60 bar and temperatures up to 300 °C. Metal hydrids are very promising storage devices for fuel cells because impurities can be adsorbed at the surface of the metal. A huge disadvantage are the high costs and the high weight at

storage densities of about 2 to 3 wt.% in case of low pressure hydrids and 6 to 8 wt.% in case of high pressure hydrids. Traces of H_2S, CO and SO_2 can cause a decrease in storage performance due to lowering the kinetics of the hydrid formation. Hydrogen atoms use places in the metal lattice and increase anisotropically, therefore, the volume of the storage up to 20 %. If hydrogen is in contact with the metal it is dissociated. Hydrogen atoms diffuse into the material and become a part of the crystal structure. Most hydrids have a standard formation enthalpy of 20 $MJ \cdot kmol^{-1}$. The hydrogen adsorption and hydrid formation is exothermic, therefore, in case of desorption heat must be provided. Safety aspects take into account that if in case of a failure of the heat or pressure supply the hydrid storage is deactivated [12, p. 13] [26, p. 81-110].

An application for metal hydrid storage is the German submarine class 212 A. It uses 120 kW PEM fuel cell systems powered by hydrogen from a metal hydrid storage and pressurized oxygen. With this configuration the submarine can operate up to four weeks under water. Conventional batteries would only last two days for non stop under water operation [34, p. 107].

6.2 Material Issues and Compatibility

Usually a hydrogen system consists of several parts and, therefore, of different materials. In order to assure safe handling and operation of hydrogen, appropriate data for the selection of materials must be available. The following properties need to be considered:
Properties suitable for the design and operating conditions; compatibility with the operating environment; availability of selected material and appropriate test data for it; corrosion resistance; ease of fabrication, assembly and inspection; consequence of material failure; toxicity; hydrogen embrittlement; potential for exposure to high temperature from a hydrogen fire; cold embrittlement; thermal contraction; property changes that occur at cryogenic temperatures.

If hydrogen is in contact with materials it can diffuse inside them and influence their properties. Molecular hydrogen dissociates and can cause embrittlement and tension in the material. Whether steels are suitable for the application with hydrogen depends on the alloy elements as well as on the structural conditions. Under hydrogen atmosphere a decreasing ductility, stability and fracture toughness is observed. These effects are depending on the hydrogen pressure and the temperature. If this behaviour is considered a save operation is possible [21, p. 271-273] [37].

Slush hydrogen (SLH_2) is a combination of liquid hydrogen and solid hydrogen at the triple point with a lower temperature and a higher density than liquid hydrogen. It is formed by bringing liquid hydrogen down to nearly its melting point (14.01 K) which consequently increases density up to 20 % as compared to liquid hydrogen [2].

According to [43] aluminium and its alloys, copper and its alloys (brass, bronze and copper-nickel) and titan and its alloys are all suitable for GH_2, LH_2 and SLH_2 as well as Austenitic steels with > 7 % nickel (such as 304, 304L, 308, 316, 321 and 347)[1]. Plastics like Teflon® and Kel-F® can also be used with hydrogen in all states. Only appropriate for GH_2 are materials like carbon steels, low alloy steels, Neoprene®, Dacron®, Viron®, Mylar®, Buna-N® and Nylon® because they are reported to be too brittle for cryogenic service. Nickel and its alloys (Inconel® and Monel®) are just suitable for LH_2 and SLH_2 because they are susceptible to hydrogen embrittlement. Nickel steels (such as 2.25, 3.5, 5 and 9 % Ni) and grey, ductile or cast iron show no compatibility with hydrogen at all.

6.3 Hydrogen in Natural Gas Grids

According to the Austrian law (ÖVGW-Richtlinie G31) it is allowed to add up to 4 mol.% hydrogen to the natural gas grid. With a natural gas fuel station nearby it is just 2 mol.%. In this range the gas key parameters (heating value, Wobbe index and density) show no significant differences compared to natural gas [41].

The capacity of the Austrian natural gas grid and storages is about 40 TWh which equates about 50 % of the yearly electricity demand in Austria [50].

Hydrogen-methane mixtures with a hydrogen fraction up to 21 vol.% (≈ 3 wt.%) are called Hythanes®. Mixtures with > 21 vol.% to 50 vol.% are tagged as HCNG. In the following, all hydrogen-methane mixtures are referred to as H_2NGxx whereas xx indicates the volumetric hydrogen fraction. Table 6.1 shows a selection of the lower heating values and other key data for different mixtures of hydrogen and methane.

Table 6.1: Partial pressure, mass and lower heating value of different CH_4-H_2 mixtures (H_2NGxx) in a storage vessel at 350 bar and 25 °C and a volume of 100 L considering ideal and real gas behaviour [21, p. 193].

	Unit	CH_4	H_2NG10	H_2NG15	H_2NG30	H_2NG50	H_2NG80	H_2
vol.% H_2	-	0	10	15	30	50	80	100
p_{H_2}	bar	0	35	52.5	105	175	280	350
p_{CH_4}	bar	350	315	297.5	245	175	70	0
$m_{H_2,ideal}$	kg	0.00	0.28	0.43	0.85	1.42	2.28	2.85
$m_{CH_4,ideal}$	kg	22.65	20.38	19.25	15.85	11.32	4.53	0.00
LHV_{ideal}	MJ/kg	50.0	51.0	51.5	53.6	57.8	73.4	120
$m_{H_2,real}$	kg	0.00	0.22	0.33	0.66	1.11	1.75	2.19
$m_{CH_4,real}$	kg	20.94	18.85	17.80	14.66	10.47	4.19	0.00
LHV_{real}	MJ/kg	1047	969	929	812	655	420	263

[1] Notation according to American Iron and Steel Institute

Table 6.2: Volumetric HHV and Wobbe index (based on HHV) for methane, Austrian natural gas regulations, different H_2NGxx mixtures and hydrogen at T=0 °C, p=1.013 bar and ρ_{Air}=1.2929 kg/m^3 [21, p. 195].

	Unit	CH_4	NG in A	H_2NG15	H_2NG30	H_2NG50	H_2NG80	H_2
HHV	MJ/Nm^3	39.91	39.86	35.38	31.76	26.33	18.18	12.75
W_o	MJ/Nm^3	54.00	53.01	52.01	50.02	47.48	44.87	48.66

Under standard conditions both gases can be mixed in every ratio and, therefore, be stored in a pressure vessel. Materials which are suitable for hydrogen operations can also be used for methane operations. Methane allows to compensate the low volumetric energy density of hydrogen up to a certain degree.

The energy throughput of a gas through a cross section is defined according to DIN 51857 by the Wobbe index

$$W_o = \frac{\mathrm{HHV}_{vol.}}{\sqrt{\frac{\rho_{Gas}}{\rho_{Air}}}}. \tag{6.3}$$

It is calculated using the volumetric heating value (either lower or higher heating value) and the density ratio of the fuel gas and air at same conditions. The Wobbe index is used to compare the combustion energy output of different fuel gases in an appliance (burner, cooker, etc.). If two fuel gases have the same Wobbe indices the energy output will also be identical for given pressure and valve settings. Table 6.2 shows the higher Wobbe index for methane, natural gas according the Austrian law, hydrogen-methane mixtures and pure hydrogen at certain conditions. The Wobbe index as a function of the volumetric percentage of hydrogen in the mixture (xx) shows a minimum at about 80 vol.%.

Due to the similarity of the Wobbe index of hydrogen and methane it would be possible to use hydrogen instead of methane in, for example, natural gas powered cars without need to change the injectors. The only factor which has to be considered is the material compatibility (see Section 6.2) [21, p. 187-201].

6.4 Hydrogen Fueling Station

In order to apply fuel cell powered cars and hydrogen powered combustion engines, hydrogen fueling stations are necessary. These are explained using the example of two hydrogen fueling stations. One from the USA and the other one from Austria.

6.4.1 UCI Hydrogen Fueling Station, USA

The UCI hydrogen fueling station was deployed in Irvine, California, in 2003. After several modifications the UCI station has now a 35 and 70 MPa dual dispensing capacity for fueling cars. In 2011, about 8000 kg hydrogen during 2700 hydrogen filling operations were dispensed. Figure 6.1 shows a simple flowchart of the UCI hydrogen fueling station.

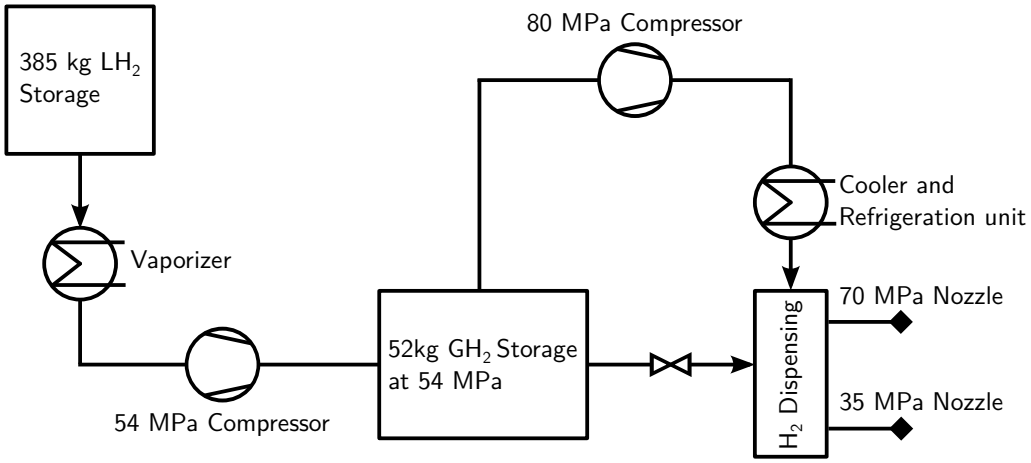

Figure 6.1: Flowchart of UCI hydrogen fueling station in Irvine, California [13]

Hydrogen is delivered to the UCI fueling station in liquid state and is stored onsite in a 385 kg insulated liquid storage vessel. As needed, the liquid is vaporized and compressed by the main compressor to 54 MPa and stored in three equally sized storage tubes capable of holding combined 52 kg of hydrogen at 54 MPa. Hydrogen vehicles are equipped with onboard storage tanks pressurized to either 35 MPa or 70 MPa, depending on the vintage and the manufacturer [13].

When a 35 MPa vehicle refuels, hydrogen is taken directly from the 54 MPa storage tubes to the vehicle's tank. Hydrogen is drawn from the lowest pressure storage tube first. As the vehicle tank pressure nears parity with the first station tube, the second storage tube is activated. If this pressure is insufficient to completely fill the vehicle, the third tube is used. Two additional steps are required to fill a 70 MPa vehicle. The stored 54 MPa hydrogen is further compressed by means of a piston compressor up to a final pressure of nearly 80 MPa. However, the extra compression and high pressure require that the fuel is cooled substantially in order to accomplish quick vehicle refueling without overheating the vehicle's tank. Therefore, high pressure hydrogen passes through a heat exchanger (cooling block) which cools the gas just before it enters the vehicle. The cooling block is cooled by an onsite refrigeration unit. The station has a nominal daily maximum fueling capacity of 25 kg which is limited by the 54 MPa compressor capable of compressing roughly 2 kg hydrogen per hour, with a 50 % duty cycle [13].

The bottleneck to more hydrogen dispensation at the UCI Hydrogen Station varies depending on the type, rate and timing of fueling events. Two bottlenecks are possible for 35 MPa vehicle fueling. The first is simply due to waiting in line when other vehicles are fueled at one dispenser. The second bottleneck occurs when onsite storage is consumed so quickly by multiple filling events that the pressure in the high pressure tank drops below 35

MPa. Vehicle refuelings with 70 MPa hydrogen can experience the same two bottlenecks that impact 35 MPa vehicles, plus an additional constraint due to the necessary precooling of the 70 MPa fueling operation. If the precooler temperature rises above a set threshold due to a combination of ambient temperature and hydrogen throughput, safety protocol prevents further 70 MPa refueling until the temperature drops back to the predetermined level. This is a frequent issue, particularly in the warmer summer months, with waiting times as long as 1 h for the cooling block temperature to drop so the next fueling can begin. There was no single safety incident in any of the 8976 refueling operations performed at the UCI station [13].

6.4.2 Hycent Hydrogen Fueling Station, Austria

The Hycent fueling station can store about 1060 kg liquefied hydrogen at 5 bar in a 17600 L tank. It consists of an inner tank made of Cr-Ni steel and an outer tank made of construction steel. Between these layers a vacuum insulation is applied. Through the insulation the daily evaporation rate is about 0.9 % of the tank's content. If no hydrogen is extracted the pressure increases and at a certain pressure level hydrogen is blown off to the ambient. Extraction of hydrogen takes place at the top of the tank were hydrogen is in gaseous state. If a higher amount is needed there are also two ambient air evaporators onsite with an evaporation power of 150 $Nm^3 \cdot h^{-1}$. Afterwards hydrogen is compressed by means of a piston compressor up to 480 bar where it can be used for fueling cars. In order to refill the LH_2 storage tank its pressure is reduced to enable a filling due to pressure difference of a trailer with liquid hydrogen [3] [21, p. 124-150].

Figure 6.2: Hycent Hydrogen Center, Austria [3]

Figure 6.3: Fuel dispenser at Hycent Hydrogen Center, Austria [3]

6.5 H_2 Application in Cars and Public Transport

Vehicles in private and public transportation can utilize hydrogen in two ways. First in a fuel cell and second in an ordinary combustion engine which is optimized for operation with hydrogen. This section gives an overview of both possibilities and reveals advantages and disadvantages of both concepts.

6.5.1 Fuel Cell Vehicles

Fuel cell powered vehicles consist in most cases of a hydrogen storage, a rechargeable battery, an electric motor and the fuel cell. Due to the electric motor usually no gear box is necessary. The high torque at low rotation speed allows an even higher acceleration than combustion engine vehicles with the same power [34, p. 110-116].

In Austria, Hyundai Motor Cooperation offers a PEM fuel cell powered electric vehicle, the ix35 FCEV (fuel cell electric vehicle). It has a power of 100 kW and a 700 bar hydrogen pressure tank with a capacity of 5.64 kg hydrogen which enables a range of 594 km according to the NEFZ. For energy recovery and storage a rechargeable battery is used. The car can operate at temperatures levels till -20 °C. The whole car's weight inclusive hydrogen is 1846 kg. Crashtests were carried out in order to test the integrity of the fuel system according to Federal Motor Vehicle Safety Standard (FMVSS) 301 and in order to test the car for hybrid hydrogen car safety according to FMVSS 305EV. Figure 6.4 shows the principle of the ix35 FCEV.

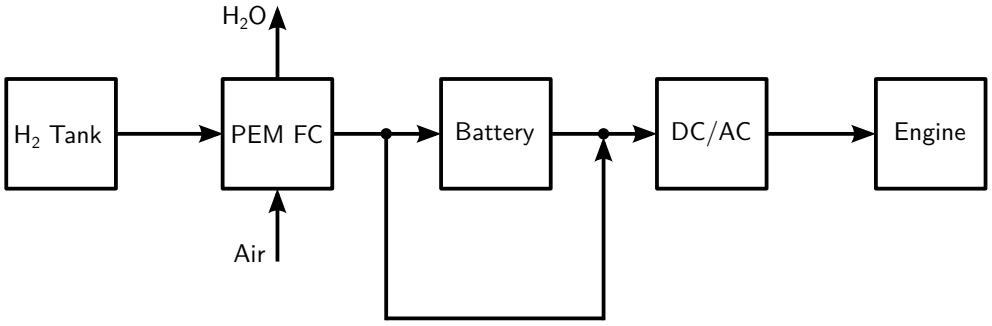

Figure 6.4: Simplified flowchart of the Hyundai ix35 FCEV [30]

The PEMFC is fed by hydrogen from the hydrogen storage tank. At the same time ambient air is used to generate electricity by means of the electro-chemical reaction. The only emission is water. The current flows into the battery and from there to a DC/AC converter and finally to the electric motor. If the battery is fully charged the fuel cell is able to send the current directly to the converter and subsequently to the electric motor [30].

Despite all the positive aspects of a fuel cell powered car there are still problems, for example, [53] reports that fuel cell cars have higher total costs than conventional hybrid cars even if the price of the fuel cell units would decrease about 90 %.

A lot of other car manufacturers like Daimler, Honda, Toyota and Mazda, General Motors and Ford support the application of fuel cells in vehicles and see the fuel cell as a future source for locomotion [51].

6.5.2 Hydrogen as Fuel for Combustion Engines

The idea of hydrogen utilization in combustion engines came up in the 30s of the twentieth century. Researchers achieved remarkable success in increasing the degree of efficiency by mixing hydrogen to ordinary fuel. Hydrogen powered combustion engines show a relative high power density, are, compared to fuel cells, cheap in production and well proven. They can also be operated with fuel mixtures like H_2NGxx and could be established quite fast in the market. In theory it is possible to operate hydrogen combustion engines up to an air ratio of λ=10 due to the wide ignition limits of hydrogen. Because of the high laminar flame speed, short burning periods can be realized which would increase the degree of efficiency. If the engine is powered with pure hydrogen there would be no carbon dioxide emissions except those caused by the engine lubricant, which are considered below detection limit. But NO_x emission still have to be considered. Of course a disadvantage would be the lower range of these cars because of the lower volumetric energy density which is in case of gaseous hydrogen about 10 and in case of liquid hydrogen about 4 times lower compared to gasoline. Overall, hydrogen is very suitable for the utilization in combustion engines. Different combustion concepts can be realized with very differences in complexity [21, p. 151-178].

In 2000 BMW presented a hydrogen powered combustion engine car. It had a LH_2 tank with a capacity of 140 L and an operation pressure up to 4 bar. With this amount of hydrogen a range of about 300 km was possible. Instead of a battery for powering the onboard electronics a PEMFC was used [34, p. 235].

Since 1996, MAN operates busses with hydrogen combustion engines. They collected about 500000 km mileage. The best degree of efficiency of 42 % was achieved by a charged engine with 150 kW power. Pressure tanks at the roof of the bus with 350 bar allowed a range of about 200 km. Due to the utilization of hydrogen as fuel nearly no carbon dioxide emissions can be detected. NO_x emission are reduced by an proper combustion operation [21, p. 179-180].

6.6 State of the Art Household Energy Supply

This section presents the heat and electricity demand of a typical household in Austria and state of the art technology for providing this energy.

6.6.1 Energy Demand and Supply of a Typical Household

In 2006, according to VDEW, the typical electricity demand of a single person household was 1790 kWh/a. For a two, three and four person household it was 3030, 3380, and 4430 kWh/a. During a whole day the highest electricity demands occurred in the morning with 130 to 150 W, at noon with 200 to 230 W and in the evening with 150 to 200 W. Load peaks were flattened due to their rapid behaviour. Figure 6.5 shows the electrical load profile of a typical household.

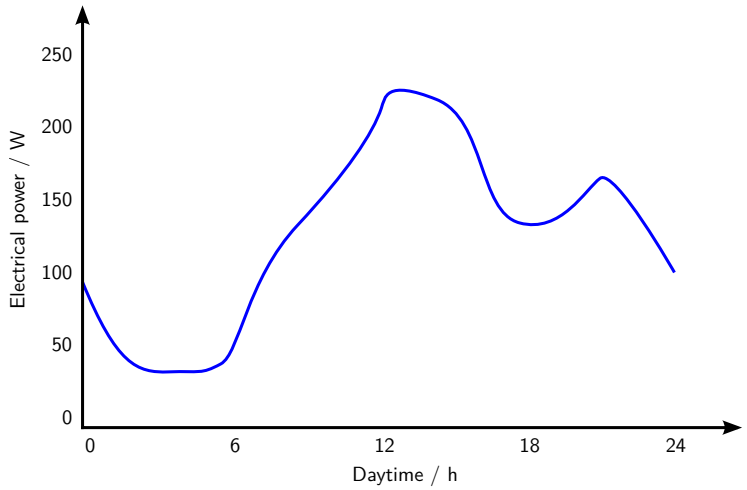

Figure 6.5: Scheme of an electrical load profile of a typical household [19, p. 56].

Heat demand in order to prepare hot water and for room heating strongly depends on the age of a house. Table 6.3 gives the average heat demand for a one family house (200 m^2) according to EnEV .

Table 6.3: Yearly average heat demand for different one family houses with an area of 200 m^2 [22]

Type of building	Heat demand per area and year	Heat demand per year
Year of construction before 1977	200 kWh/a m^2	40000 kWh/a
Year of construction until 2002	100 kWh/a m^2	20000 kWh/a
Efficiency house 70	60 kWh/a m^2	12000 kWh/a
Passive house	15 kWh/a m^2	3000 kWh/a

The qualitative trend of the heat demand profile (see Figure 6.6) shows peaks in the morning and in the evening. In those two periods hot water usage sets the heat demand. The

trend shows nearly the same profile in summer and wintertime with the difference that in wintertime the whole profile is shifted toward higher relative heat demand because of higher basic load caused by room heating.

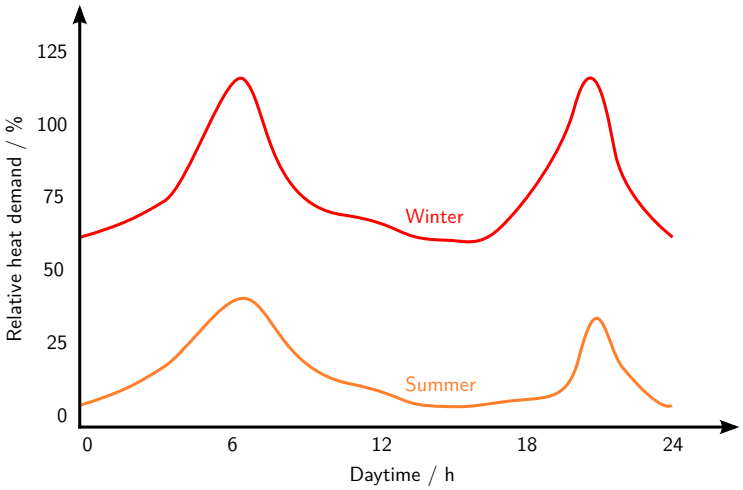

Figure 6.6: Scheme of a relative heat load profile of a typical household in winter and summer time over a day [19, p. 54-56].

Assuming an average electricity demand of 3000 kWh/a and an average heat demand of about 12000 kWh/a the heat demand is about four times higher than the electricity demand. Furthermore, it is assumed that the energy can just be delivered by fuels like coal or gas. With this data one can compare the energy and electricity supply of a household how it is done today and how it could be possible with an onsite PEM fuel cell based on [19, p. 44] in Section 6.7.

Figure 6.7 shows the situation in most households nowadays. Assuming a demand of 25 fictitious energy units for electricity and 100 units for heat based on data above. Heat can be allocated by means of a condensation boiler which can reach a theoretical degree of efficiency of about 100 %. Electricity is provided by a conventional thermal power plant, utilizing natural gas, assuming a degree of efficiency of 40 %. This configuration results in a total energy demand of 162.5 energy units for satisfying the whole energy demand of one household.

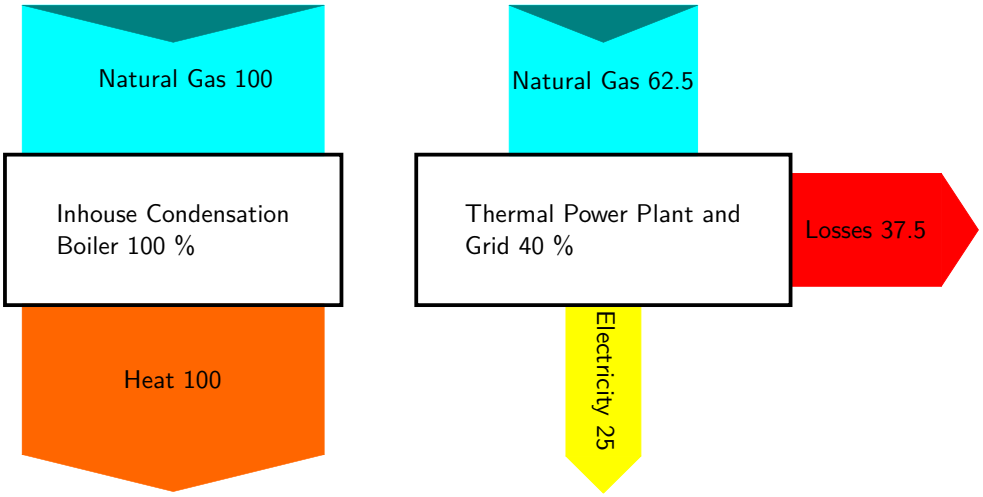

Figure 6.7: Heat and electricity supply with a condensation boiler in the house and a large centralized thermal power plant for electricity supply showing theoretical degrees of efficiency and fictitious energy units
[19, p. 44].

Figure 6.8 shows a way of providing heat and electricity by a combined heat and power plant based on the biomass gasification plant Oberwart, Austria. There, biomass is converted into district heat and electricity with an overall efficiency of 78 % (see Table 4.1).

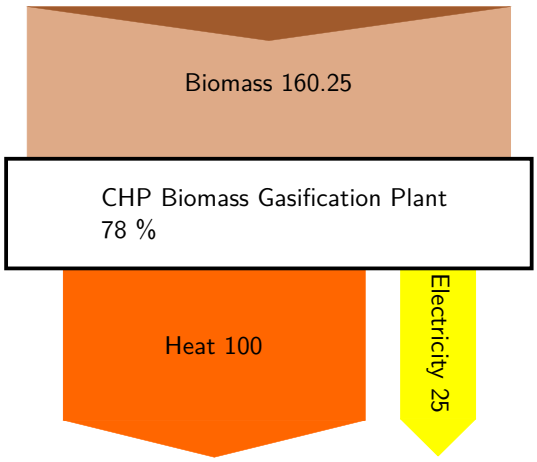

Figure 6.8: Heat and electricity supply with a biomass gasification plant producing district heat and electricity showing the degree of efficiency and fictitious energy units.

6.6.2 Condensation Boilers

The condensation boiler is a technology which allows to utilize heat of condensing water in the flue gas in addition to the heat acquired by combustion based on the lower calorific value. In theory degrees of efficiencies up to 108 % can be reached. This physically incorrect representation is due to the definition of the degree of efficiency. In practice this value is not

reached because of different reasons [19, p. 65]. A detailed thermodynamical analysis of this technology is presented in [4, p. 584-586].

6.6.3 Wood Pellet Boilers

Modern wood pellet boilers show improved emission technology and efficiencies. The degree of efficiency can reach up to 90 %. A disadvantage of this kind of heating are the heat losses to the ambient [19, p. 66]. Detailed information can be reviewed in [31, p. 497-501].

6.6.4 Heat Pumps

Within the last years the application of heat pumps for household heating increased. Heat pumps increase a certain lower heat level due to additional work to a usable heat level. A detailed technical explanation can be seen in [4, p. 586-588]. Performance of heat pumps is indicated by the coefficient of performance (COP). It is the ratio between energy output to energy input. For bad systems the value is about 2.5. Well designed systems can reach 3.9 to 4.2. If hot water preparation is also part of the system the COP decreases significant because of the high heat capacity of water [19, p. 66-68].

6.6.5 Thermal Solar Panels

Thermal solar panels use the direct sun radiation for hot water preparation. A typical panel with an area of about 6 m^2 can cover up to 60 % of the hot water demand of a household over a year. In summer it's 100 % and in winter it's lower than 60 % and so an additional heating device is necessary. For utilization of possible excess heat in summer different approaches like heat storage or regeneration of heat sources for heat pumps exist [19, p. 68].

6.7 Fuel Cells and Virtual Power Plants for Household Heating

Fuel cells are assumed as an efficient and environmental friendly possibility for satisfying heat and electricity demand in households. Coupling of several fuel cells in different households would result in a so called "Virtual Power Plant". A "Virtual Power Plant" is a network consisting of several small decentralized power plants which are connected and able to replace a larger centralized power plant [19, p. 6]. Due to the parallel electricity and heat generation in a fuel cell, losses could be minimized and the fuel utilization could be improved as Figure 6.9 indicates.

According to above it is assumed that a household needs 125 fictitious energy units in order to satisfy heat and electricity demand. In theory, a PEM fuel cell would be able to convert 125 energy units of hydrogen into heat and electricity without losses. Hydrogen is generated by a steam reforming process using natural gas as feedstock. The reformer efficiency

is assumed to be 80 % [49]. The result is an overall energy demand of 156.25 energy units which is slightly lower than the energy demand in case of conventional energy supply with a condensation boiler and a thermal power plant (see Figure 6.7 and 6.8). If a hydrogen grid is assumed the steam reforming step could be neglected and the energy unit demand would just be 125 in order to satisfy heat and electricity demand of a household.

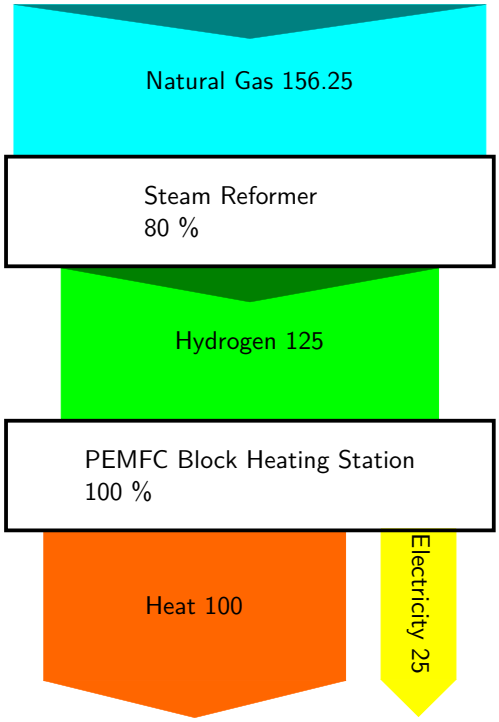

Figure 6.9: Heat and electricity supply with a PEM fuel cell in a household showing energy units and theoretical degrees of efficiency [19, p. 44].

6.7.1 Location Possibilities for Fuel Cell Household Energy Supply

Depending on the power of the applied fuel cells different concepts for the location of the fuel cell can be realized [19, p. 53]:

Energy supply for one household The fuel cell design is matched to one household providing its heat and electricity demand. In order to cover electrical load peaks electricity supply is realized with other households and fuel cells together.

Settlement supply In this case a fuel cell with higher power would supply a whole settlement with heat and electricity. Heat and electricity loads would be homogenized and, therefore, the power per household would be lower. Again, covering of load peaks would be realized with several fuel cells in a network.

Isolated operation It is comparable to the settlement supply. The difference is that there is no interconnection to other fuel cells and the electrical grid. This means that heat and electricity can only be supplied by the fuel cell of this settlement.

6.7.2 Design Considerations for Fuel Cells used for Household Energy Supply

In order to design a fuel cell to meet the above described requirements two possible ways are available [19, p. 58]:

Thermal design To enable a continuous operation of the fuel cell it is recommended to adapt the power according to the heat demand for hot water supply. The reason is that hot water supply does not strongly oscillate over a year because hot water demand is quite the same in summertime and in wintertime. To cover thermal peaks a peak load boiler would be necessary. This could be, for example, a heat pump, or a boiler. The generated electricity could be used directly by the household or it can be fed back to the grid. Figure 6.10 shows a basic layout for a fuel cell in a household which can satisfy energy demand for hot water preparation.

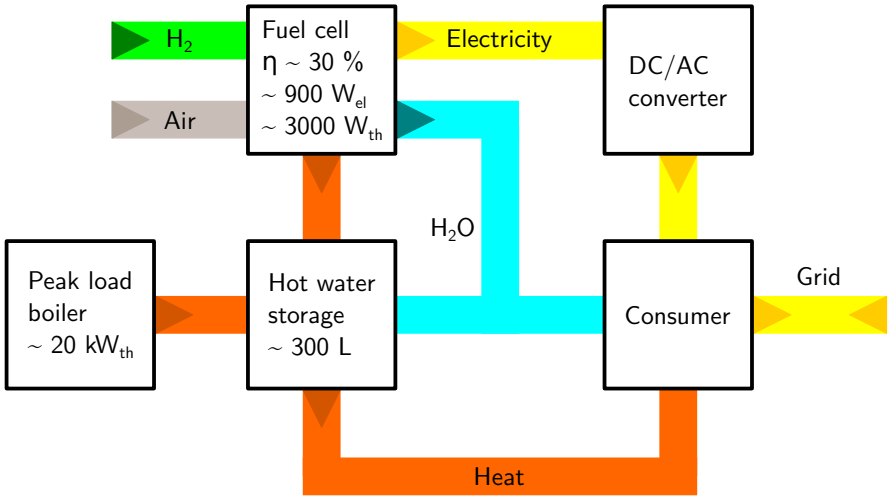

Figure 6.10: Design principle of a fuel cell in a household for providing heat for hot water preparation. Data was gathered from measurements in this thesis and from a single household (140 m^2), Trofaiach, Austria, 04.06.2014. Thickness of flows is not in scale with the amount of energy or other values.

If the design parameters equal the heat demand for room heating, there would be a lot of excess electricity in wintertime. In summertime electricity demand would have to be supplied from somewhere else. This layout is unfavourable because of lower yearly run time of the fuel cell.

Electrical design If the fuel cell is designed in order to satisfy the electricity demand it is useful to design it to cover the basic electrical load according to Figure 6.11. Electrical peak loads would be covered by the grid. In case of thermal peaks, an additional heating device would be necessary (heat pump, condensation boiler, solar systems etc.). In addition, it has also to be considered that if the fuel cell generates electricity it generates heat as well. Therefore, a heat sink must be provided which would be able to grab the excess heat which can be used, for example, for recovering a heat pump source or for preparing hot water. Figure 6.11 shows a basic layout for a fuel cell in a household which can satisfy basic electrical energy demand. In this configuration the fuel cell could achieve a very high run

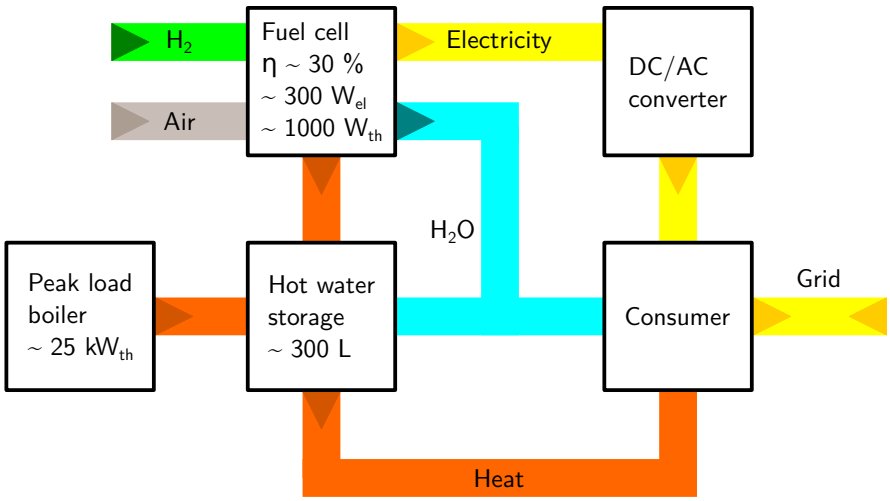

Figure 6.11: Design principle of a fuel cell in a household for providing basic electrical load. Data was gathered from measurements in this thesis and from a single household (140 m^2), Trofaiach, Austria, 04.06.2014. Thickness of flows is not in scale with the amount of energy or other values.

time over a year because electricity demand needs to be satisfied over a whole day without major differences in summer and winter time. A possible problem of this layout could be too much excess heat of the fuel cell. In the worst case, this excess heat needs to be released into the ambient if no heat sink is able to collect this additional heat.

Due to their modular layout fuel cells can provide electrical energy in different dimensions. They have fast start up and shut down periods and can easily follow load changes. In order to utilize the generated heat of a fuel cell its temperature level should be around 70 °C [19, p. 58-59].

6.7.3 The Hydrogen House, USA

There are also combinations of fuel cells and other renewable power sources like solar energy possible. An example for such a combination is the Hydrogen House in the USA. The Hydrogen House is a solar-hydrogen powered residence. It operates by collecting solar energy from a 21 kW array of solar panels. The gathered energy is collected in a small battery and

used to operate a low pressure electrolyzer. The produced hydrogen is stored in low pressure storage tanks. From there it can be used for cooking similar to natural gas or it can be utilized in a fuel cell for electricity generation. The whole system's emission are medical pure oxygen and water. An additional geothermal heat system can provide heat if it is needed. Furthermore, the owner of the house is able to fill the tank of his fuel cell vehicle by means of a compressor [1].

6.8 Industrial Applications for $BioH_2$

One of the most important hydrogen applications is the Haber-Bosch synthesis which is used to generate ammonia (NH_3). In 2007, about 130 million tons of hydrogen were consumed by this process which is about the half of the overall hydrogen production.

$$N_2 + 3H_2 \leftrightharpoons 2NH_3 \quad \Delta H_R^0 = -92 \ \frac{\text{kJ}}{\text{mol}} \tag{6.4}$$

The reaction takes place at a temperature level of about 500 °C and a pressure level of about 450 bar. The presence of an iron oxide / aluminium oxide catalyst accelerates the reaction's kinetics. The nitrogen to hydrogen ratio is 3 to 1 (excess nitrogen). A modern ammonia production facility for about 1350 tons of NH_3 needs about 72000 Nm^3 natural gas for the hydrogen production by means of steam reforming described in Chapter 1.2 [21, p. 259-261] [35, p. 34] [40, p. 428].

Refineries are also a large hydrogen consumer. Hydrogen is needed for hydrofining and hydrocracking. During hydrofining middle distillates like gasoline and diesel are desulfurized at temperatures about 350 °C and pressures up to 50 bar in presence of a platinum catalyst. Sulfur forms H_2S with hydrogen which is processed in a Claus process to elementary sulfur. Hydrocracking forms shorter hydrocarbons from longer hydrocarbons at the presence of a Ni/Mo catalyst at temperatures from 300 to 500 °C and pressures between 80 and 200 bar [21, p. 256-259] [40, p. 351].

In metal industry hydrogen is an important reduction agent, e.g. for copper production according

$$CuO + H_2 \rightarrow Cu + H_2O \quad \Delta H_R^0 = -128.5 \ \frac{\text{kJ}}{\text{mol}}. \tag{6.5}$$

Another application related with metals is the utilization of hydrogen as cover gas in welding processes. Hydrogen is also used in cutting operations for metals due to the hot hydrogen-oxygen flame [21, p. 265-267] [35, p. 34] [40, p. 382].

Food industry uses hydrogen for formation of hard fats from liquid oils, e.g. for production of margarine. Another food related application is the usage as preserving agent where hydrogen is referred to as E 949. Hydrogen is also used for water cleaning in order to remove NO_3^- which otherwise would be transformed to the toxic NO_2^- in the human body. Semiconductor industry uses hydrogen for contamination [21, p. 263-264] [40, p. 598].

Chapter 7

Conclusion and Outlook

Hydrogen is an energy carrier which would be able to reduce the carbon dioxide emissions and to establish a renewable energy supply. There are several possibilities to generate hydrogen in a sustainable and environmental friendly way. Especially the generation by means of electrolyzers powered by renewable electricity and wood gasification needs to be taken into account. Both technologies are able to produce hydrogen in a carbon dioxide neutral way. Fuel cells are a promising technology for converting hydrogen into electricity and heat. Several types exist with their certain advantages depending on the application. It was proven that hydrogen generated by wood gasification is suitable for a PEM fuel cell and enabled its operation for several hours without any flaws. The operation with BioH_2 showed no differences compared to the operation with Alphagaz 1^{TM} H_2. Operation with Alphagaz 1^{TM} H_2 revealed that long operation breaks of the PEM fuel cell causes a certain performance increase which is decreasing after a few hours of operation. Former experiments can be reviewed in [8] [18] as well as in Appendix C of this work. Material issues of hydrogen play an important role. Considering these it seems to be possible to add hydrogen to the natural gas grid without problems which could help to lower the natural gas imports. Despite the use of hydrogen in the energy sector, it is an educt which is necessary in a lot of industrial fields. This makes a sustainable hydrogen production even more interesting.

Research and development tasks need to be and still are carried out in order to make a sustainable hydrogen supply possible. Especially the wood gasification will be a topic for future work. SER gasification of biomass seems to be a promising way in order to increase the hydrogen content in wood gas. Also fuel cells are still under development in order to increase their efficiency, power and long term stability. A sustainable hydrogen production could be used for household energy supply with fuel cells which would be able to provide heat and electricity. Furthermore, many car manufacturers see fuel cell application in cars as one possible future for locomotion.

Nomenclature

Abbreviations & Acronyms

A	Austria
AC	Alternating current
AFC	Alkaline fuel cell
$BioH_2$	Hydrogen generated from biomass
Cermet	Ceramic and metal
CHP	Combined heat and power
DMFC	Direct methanol fuel cell
EnEV	Energie Einspar Verordnung
FC	Fuel cell
FMVSS	Federal motor vehicle safety standard
GH_2	Gaseous hydrogen
GHSV	Gas hourly space velocity
H_2NGxx	Hydrogen-methane mixture with xx vol.% hydrogen
HCNG	Hydrogen enriched compressed natural gas
HT-PEMFC	High temperature PEM fuel cell
LH_2	Liquid hydrogen
LT-PEMFC	Low temperature PEM fuel cell
MCFC	Molten carbonate fuel cell
mol.	Molar

NASA	National aeronautics and space administration
NEFZ	Neuer europäischer Fahrzyklus
NG	Natural gas
NO_x	Nitric oxides
ORC	Organic rankine cycle
PAFC	Phosphoric acid fuel cell
PBI	Polybenzimidazole
PC	Personal computer
PEM	Proton exchange membrane
PSA	Pressure swing adsorption
R&D	Research and development
RME	Rapeseed methyl ester
SLH_2	Slush hydrogen
SOEC	Solid oxide electrolyzer cell
SOFC	Solid oxide fuel cell
SO_x	Sulfur oxides
VDEW	Verband der Elektrizitätswirtschaft
vol.	Volumetric
WGS	Water gas shift
wt.	Weight
YSZ	Yttrium stabilized zirconium

Indices

Ads	Adsorbent
Conv	Value acquired directly before the DC/AC converter of the PEM fuel cell
db.	Dry basis
el	Electrical

Gross	Value which does not take peaks into account next to mean value calculation
h	Enthalpy
ideal	Ideal gas behaviour
Net	Value acquired directly before the load of the PEM fuel cell
real	Real gas behaviour
Stack	Value which takes peaks into account next to mean value calculation
th	Thermal
x	Molar amount of carbon in a hydrocarbon
y	Molar amount of hydrogen in a hydrocarbon

Symbols

a_i	Activity of component i in Pa
COP	Coefficient of performance in -
ΔG	Gibbs energy difference in J
ΔH	Enthalpy difference in J
ΔH_f^0	Standard formation enthalpy in kJ/mol
ΔS	Entropy difference in J/K
Δx	Difference in length in m
D_{ij}	Diffusion coefficient in m^2/s
E_0	Potential according to electrochemical series in V
E	Theoretical cell electrical potential in V
E_{Load}	Actual fuel cell potential in V
η	Degree of efficiency in -
η_E	Degree of efficiency of an electrolysis process in -
$\eta_{FC_{H_2}}$	Theoretical degree of efficiency of a fuel cell powered by hydrogen in -
$\eta_{FC,Load}$	Actual degree of efficiency of a fuel cell with current flow in -

F	Faraday constant in C/mol
HHV	Higher heating value in kJ/kmol
H_{ij}	Henry coefficient of component i and solvent j in Pa
J_i	Specific areic mass flow of component i in m/s
K_{WGS}	Equilibrium constant for the WGS reaction in -
λ	Air ratio for a combustion engine in -
LHV	Lower heating value in kJ/kmol
μ_{JT}	Joule-Thomson coefficient in K/Pa
n_i	Molar amount of component i in mol
p_i	Partial pressure of component i in Pa
P	Power in W
p^s	Saturation pressure in Pa
Q	Electrical charge in C
$\dot{Q}_{H_2}$	Chemical energy in the generated hydrogen in W
R	Gas constant in J/mol K
R_{H_2}	Specific gas constant of hydrogen in J/kg K
ρ_i	Density of component i in kg/m^3
T	Absolute temperature in K
$\dot{V}$	Volumtric flowrate in m^3/s
v	Specific volume in m^3/kg
w_{H_2}	Specific work for compression of hydrogen in kJ/kg
W_o	Wobbe index in MJ/Nm^3
x_i	Molar fraction of component i in -
Z	Compressibility factor of a gas in -
z	Number of charge carriers in -

Bibliography

[1] The Hydrogen House, April 2014. http://hydrogenhouseproject.org.

[2] Encyclopedia Astronautica. Slush H_2, April 2014. http://www.astronautix.com/props/airshlh2.htm.

[3] HycentA Hydrogen Center Austria, April 2014. http://hycenta.tugraz.at.

[4] H. D. Baehr. *Thermodynamik - Grundlagen und technische Anwendungen.* Springer, 2009.

[5] A. Behr. *Einführung in die technische Chemie.* Spektrum Akademischer Verlag, 2005.

[6] R. Benesch and T. Jacksier. Hydrogen and material quality issues for PEM fuel cells. In *Vehicle Power and Propulsion, 2005 IEEE Conference*, pages 646–651, 2005.

[7] K. Bennaceur, B. Clark, F. M. Orr, T. S. Ramakrishnan, C. Roulet, and E. Stout. Hydrogen: A Future Energy Carrier ?, 2005.

[8] I. Bergamo. Hydrogen separation and electricity production from product gas generated by biomass gasification. Master's thesis, Politecnico di Milano, 2013.

[9] B. M. Besancon, V. Hasanov, R. Imbault-Lastapis, R. Benesch, M. Barrio, and M. J. Molnvik. Hydrogen quality from decarbonized fossil fuels to fuel cells. *International Journal of Hydrogen Energy*, 34(5):2350 – 2360, 2009.

[10] I. Blessing, C. Gardner, and M. Ternan. Separation of hydrogen from a hydrogen/methane mixture using a PEM fuel cell. *International Journal of Hydrogen Energy*, 32(32):908–914, 2007.

[11] K. Bosch. Biomasse-KWK auf Basis der Wirbelschicht-Dampfvergasung mit integriertem ORC Prozess - bisherige Betriebserfahrungen. In *Central European Biomass Conference*, 2011.

[12] H. Briehl. *Chemie der Werkstoffe.* Teubner, 2008.

[13] T. Brown, S. Stephens-Romero, and S. Samuelson. Quantitative analysis of a successful public hydrogen station. *Hydrogen*, 37:12731–12740, 2012.

[14] Freedom Car and Fuel Partnership. Hydrogen production overview of technology options, 2009.

[15] ChemgaPedia. Grundlagen der Adsorption, March 2014. `http://www.chemgapedia.de/vsengine/vlu/vsc/de/ch/10/adsorption/grundlagen/grundlagen_der_adsorption.vlu/Page/vsc/de/ch/10/adsorption/grundlagen/adsorptionsgleichgewichte/klassifizierung_von_sorptionsisothermen.vscml.html`.

[16] X. Cheng, Z. Shi, N. Glass, L. Zhang, J. Zhang, D. Song, Z. S. Liu, H. Wang, and J. Shen. A review of PEM hydrogen fuel cell contamination: Impacts, mechanisms, and mitigation. *Journal of Power Sources*, 165(2):739–756, 2007.

[17] C. Czeslik, H. Seemann, and R. Winter. *Basiswissen Physikalische Chemie*. Vieweg & Teubner, 2010.

[18] N. Diaz. *Hydrogen Separation from Producer Gas Generated by Biomass Steam Gasification*. PhD thesis, Vienna University of Technology, 2013.

[19] B. Droste-Franke, H. Berg, A. Kötter, J. Krüger, K. Mause, J. C. Pielow, I. Romey, and T. Ziesemer. *Brennstoffzellen und Virtuelle Kraftwerke*. Springer, 2009.

[20] Inc. EG & G Technical Services. *Fuel Cell Handbook*. US Department of Energy, 2004.

[21] H. Eichlseder. *Wasserstoff in der Fahrzeugtechnik*. Springer Vieweg, 2012.

[22] Energieheld. Durchschnittlicher Stromverbrauch und Energieverbrauch im Einfamilienhaus, April 2014. `http://www.energieheld.de/blog/energieverbrauch-eines-wohnhauses`.

[23] J. C. Ganley. High temperature and pressure alkaline electrolysis. *Hydrogen Energy*, 34(34):3604–3611, 2009.

[24] R. Halseid, J. S. V. Preben, and T. Reidar. Effect of ammonia on the performance of polymer electrolyte membrane fuel cells. *Journal of Power Sources*, 154(154):343–350, 2006.

[25] A. Hauch. Durability of Solid Oxide Electrolysis Cells for Hydrogen Production. In *Energy Solutions for Sustainable Development Energy Solutions for Risoe International Energy Conference*, 327-338, 2007.

[26] K. Hirose. *Handbook of Hydrogen Storage: New Materials for Future Energy Storage*. Wiley-VCH, 2010.

[27] H. Hofbauer, R. Rauch, and K. Bosch. Zwischenbericht Wäscher. Report for Renewable Energy Network Austria 12, Technische Universität Wien, Insitut für Verfahrens-, Brennstoff- und Umwelttechnik, 2000.

[28] H. Hofbauer, R. Rauch, K. Bosch, R. Koch., and C. Aicherning. *Biomass CHP Plant Güssing A Success Story*. CPL Press, 2003.

[29] J.D. Holladay, J. Hu, D.L. King, and Y. Wang. An overview of hydrogen production technologies. *Catalysis Today*, 139(4):244–260, 2009.

[30] Austria Hyundai Import Gesellschaft m.b.H. ix 35 fcev, April 2014. `http://www.hyundai.at`.

[31] M. Kaltschmitt, H. Hartmann, and H. Hofbauer. *Energie aus Biomasse*. Springer Verlag, 2009.

[32] S. Koppatz, C. Pfeifer, R. Rauch, H. Hofbauer, T. Marquard-Moellenstedt, and M. Specht. H_2 rich product gas by steam gasification of biomass with in situ CO_2 absorption in a dual fluidized bed system of 8MW fuel input. *Fuel Processing Technology*, 90:914–921, 2009.

[33] B. Kruse, S. Grinna, and C. Buch. Hydrogen - status og muligneter. Technical report, Bellona, 2002.

[34] P. Kurzweil. *Brennstoffzellentechnik*. Springer Vieweg, 2013.

[35] H. P. Latscha. *Chemie der Elemente*. Springer, 2011.

[36] K. Liu, C. Song, and V. Subramani. *Hydrogen and Syngas Production and Purification Technologies*. Wiley, 2010.

[37] V. Madina and I. Azkarate. Compatibility of materials with hydrogen. particular case: Hydrogen embrittlement of titanium alloys. *International Journal of Hydrogen Energy*, 34(14):5976 – 5980, 2009. 2nd International Conference on Hydrogen Safety 2nd International Conference on Hydrogen Safety.

[38] T. Melin. *Membranverfahren - Grundlagen der Modul - und Anlagenauslegung*. Springer, 2007.

[39] A. Mersmann. *Thermische Verfahrenstechnik - Grundlagen und Methoden*. Springer Berlin Heidelberg, 2005.

[40] C. E. Mortimer. *Chemie*. Thieme, 2010.

[41] G. Müller. Erarbeitung von Basisinformationen zur Positionierung des Energieträgers Erdgas im zukünftigen Energiemix in Österreich. Technical report, Österreichische Vereinigung für das Gas- und Wasserfach, 2012.

[42] S. Müller. *Hydrogen from Biomass for Industry - Industrial Application of Hydrogen Production Based on Dual Fluid Gasification.* PhD thesis, Vienna University of Technology, 2013.

[43] NASA. Safety Standard for Hydrogen and Hydrogen Systems, 2005.

[44] N. W. Ockwig and T. M. Nenoff. Membranes for hydrogen separation. *Chemical Reviews*, 107(10):4078–4110, 2007.

[45] R. et al. Perry. *Perry's Chemical Engineers Handbook.* McGraw - Hill, 1997.

[46] C. Pfeifer, B. Puchner, and H. Hofbauer. Comparison of dual fluidized bed steam gasification of biomass with and without selective transport of CO_2. *Chemical Engineering Science*, 64(23):5073–5083, 2009.

[47] T. Pröll and H. Hofbauer. H_2 rich syngas by selective CO_2 removal from biomass gasification in a dual fluidized bed system - process modelling approach. *Fuel Processing Technology*, 89:1207–1217, 2008.

[48] T. Riis, E. F. Hagen, P. J. S. Vie, and O. Ulleberg. Hydrogen Production and Storage - R&D Priorities and Gaps. Technical report, IEA, 2006.

[49] G. Simbolotti. Hydrogen production and distribution. Technical report, IEA, 2007.

[50] G. Syring Müller. Smart Gas Grids in Österreich. Technical report, Österreichische Vereinigung für das Gas- und Wasserfach, 2011.

[51] Fuel Cell today. Fuel cell electric vehicles: The road ahead, 2013.

[52] Fuel Cell today. Water electrolysis and renewable energy systems, 2013.

[53] O. P. R. Van Vliet, T. Kruithof, W. C. Turkenburg, and A. P. C. Faaij. Techno-economic comparison of series hybrod, plug-in hybrid, fuel cell and regular cars. *Journal of Power Sources*, 195:6570–6585, 2010.

Appendix A

Starting Procedure of the PEM Fuel Cell (Mobixane^{TM})

For starting the Mobixane^{TM} fuel cell system, several steps need to be taken into account. As a first step it would be useful to make sure that the water storage of the fuel cell is empty to avoid spillage. Then the starting key needed to be plugged in. Before connecting the hydrogen hose it was flushed in order to remove impurities which possibly accumulated over time. The next step involved the connection to the PC and to start the LabVIEW^{TM} program in order to view and record operation data. Data was visible after pressing the ON button of the fuel cell which just started the measurement and control systems. The fuel cell stack itself was not work in that moment. The next step was to adjust the required hydrogen pressure of about 250 mbarg either by observing the fuel cell display or the LabVIEW^{TM} measurement program. After adjustment of the correct pressure, the Mobixane^{TM} fuel cell system could be started by pressing the START button. Then loads could be connected in order to achieve the fuel cell's minimum power of 500 W, which accorded to the power value visible at the applied wattmeter before the load. For shutting down the fuel cell the steps which are described above need to be done reversely.

Appendix B

PEM Fuel Cell (Mobixane^{TM}) Operation Table

Table B.1: Overall operation periods and characteristics of the PEM fuel cell (Mobixane^{TM}).

No.	Date (dd.mm.yyyy)		Time (hh:mm)		Operation hours		Gas type
	From	To	From	To	From	To	
1	01.07.2011	01.07.2011	17:23	17:44	82	82	Alphagaz 1^{TM} H_2
2	06.07.2011	06.07.2011	10:43	12:45	82	84	Alphagaz 1^{TM} H_2
3	07.07.2011	07.07.2011	14:05	15:36	84	86	Alphagaz 1^{TM} H_2
4	28.07.2011	28.07.2011	10:24	13:49	86	89	BioH_2
5	21.04.2012	21.04.2012	12:08	15:11	91	94	BioH_2
6	07.05.2013	12.05.2013	11:26	22:04	102	210	BioH_2 & Alphagaz 1^{TM}
7	26.11.2013	26.11.2013	17:30	18:36	212	213	Alphagaz 1^{TM} H_2
8	13.01.2014	13.01.2014	12:58	19:05	213	219	Alphagaz 1^{TM} H_2
9	16.01.2014	16.01.2014	21:42	22:19	220	220	Alphagaz 1^{TM} H_2
10	17.01.2014	17.01.2014	11:16	13:25	220	222	Alphagaz 1^{TM} H_2
11	17.01.2014	17.01.2014	15:23	19:23	222	227	BioH_2 & Alphagaz 1^{TM}
12	06.02.2014	06.02.2014	11:40	16:46	227	231	Alphagaz 1^{TM} H_2
13	27.02.2014	27.02.2014	09:27	14:09	231	236	Alphagaz 1^{TM} H_2

The PEM fuel cell (Mobixane^{TM}) was already delivered with 82 operation hours at its internal counter.

Appendix C

Papers of the Process Chain for $BioH_2$ Production: Part I and II

This chapter provides the two papers written during the period this master thesis was carried out. Both give extensive information about the experimental pilot plant for $BioH_2$ production at the CHP Oberwart, Austria, considering a process chain consisting of a WGS unit, RME scrubber, PSA unit and a PEM fuel cell. Both versions are from 25^{th} of April 2014 and haven't been released yet (10^{th} of June 2014).

Wood Gas Processing to Generate Hydrogen Suitable for PEM Fuel Cells - Part 1: Design and Overall Performance

S. Fail[a,*], F. Benedikt[a], M. Kraussler[a], J. Hinteregger[a], N. Diaz[b], K. Bosch[d], M. Hackel[c], R. Rauch[a,b] and H. Hofbauer[a,b]

[a] *Vienna University of Technology, Institute of Chemical Engineering, Vienna, Austria.*

[b] *Bioenergy 2020+ GmbH, Güssing, Austria.*

[c] *Air Liquide^{TM} Forschung und Entwicklung GmbH, Frankfurt Research and Technology Center (FRTC), Germany.*

[d] *Energie Burgenland^{TM} AG, Eisenstadt, Austria.*

Abstract

A test campaign was carried out generating renewable hydrogen based on wood gas derived from the commercial biomass steam gasification plant in Oberwart, Austria. The implemented process consisted of four operation units: (I) catalysed water gas shift (WGS) reaction, (II) gas drying and cleaning in a scrubber, (III) hydrogen purification by pressure swing adsorption and (IV) use of biohydrogen ($BioH_2$) in a proton exchange membrane (PEM) fuel cell. The aim was to demonstrate reliable operation and to carry out an extensive chemical analysis.

Part 1 of this paper describes the design and basic overall performance of the process. For almost 250 hours, the pilot plant was operated continuously. 560 $\frac{NL_{db.}}{h}$[1] of wood gas were extracted to produce 280 $\frac{NL_{db.}}{h}$ of $BioH_2$ with a purity of 99.97 $vol.\%_{db.}$. The catalyzed WGS reaction enabled an overall hydrogen recovery of 131% $\frac{\dot{n}_{BioH_2}}{\dot{n}_{H_2,\text{wood gas}}}$. A detailed chemical analysis along the process

*Vienna University of Technology, Institute of Chemical Engineering
Getreidemarkt 9/166, 1060 Vienna
silvester.fail@tuwien.ac.at

[1] db. = dry basis

will be presented in Part 2 [1].

Keywords: Hydrogen, Wood Gas, Water Gas Shift, Pressure Swing Adsorption, PEM Fuel Cell

1. Introduction

Hydrogen is required chiefly for the synthesis of ammonia and methanol as well as various applications in refineries. In 2007, the world's installed capacity of production was about 65 million tonnes of hydrogen. 96% of this is directly based on fossil fuels, mainly natural gas (49%) [2].

Considerable research has been carried out in the field of renewable hydrogen production. Thermochemical, electrochemical and biological approaches can be distinguished [3]. This article deals with hydrogen production via the thermochemical processing of biomass, which is assumed to be less costly than other renewable production technologies, e.g. electrolysis of water using electricity [4].

The discussed process chain for $BioH_2$ production was operated with wood gas from the commercial biomass gasification plant in Oberwart, Austria (Figure 1). The design of this combined heat and power (CHP) plant is based on the well documented plant in Güssing, Austria [5]. Both plants employ dual fluidized bed (DFB) steam gasification technology. Wood gas is generated, cooled down, cleaned by means of a baghouse filter and a scrubber, and subsequently burned in gas engines generating electricity and district heat. Unlike the plant in Güssing, a biomass dryer and an organic rankine cycle (ORC) are employed in the CHP plant Oberwart. The pilot plant was operated with a partial flow of wood gas extracted after its gas cleaning units. Therefore particles were removed in a baghouse filter and the majority of the tar was already separated in a gas scrubber operated with rapeseed methyl ester (RME).

The presented process for hydrogen generation involves carbon monoxide conversion via (I) sulfur tolerant catalysis of the water gas shift (WGS) reaction, (II) gas drying and cleaning in a scrubber, and (III) hydrogen purification via

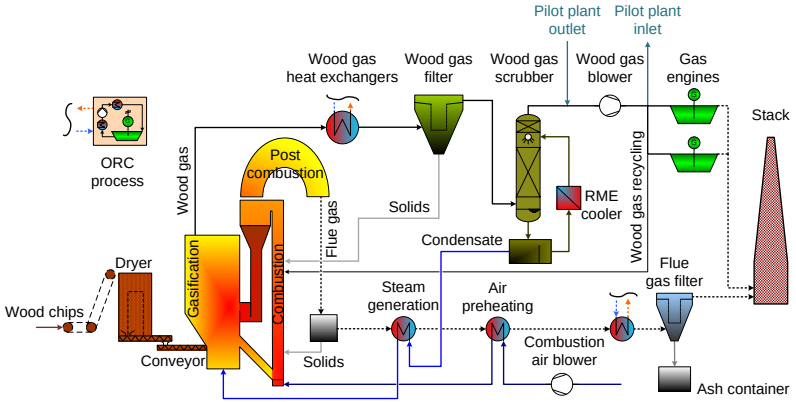

Figure 1: Flowchart of the biomass gasification plant Oberwart and sampling point of wood gas of the investigated pilot plant for $BioH_2$ production.

pressure swing adsorption (PSA).

I. Catalysis of the WGS reaction (Equation 1) is a state of the art technology. A two stage system with different catalysts is industrially applied in order to produce additional hydrogen by the conversion of carbon monoxide with steam [6].

$$CO + H_2O \rightleftharpoons H_2 + CO_2 \quad \Delta H_R^0 = -41.1 \ \frac{\text{kJ}}{\text{mol}} \tag{1}$$

II. Wood gas contains traces of ammonia; sulfur components; benzene, toluene, ethylbenzene, and xylene (BTEX); as well as condensable organic compounds (tar). A highly effective approach towards the removal of the tar is its absorption in organic solvents (e.g. RME). In parallel, condensing water enables a removal of the ammonia and hydrogen sulfide [7].

III. The PSA process is based on the physical binding of gas molecules to a solid adsorbent material. The interaction between the gas and the adsorbent depends mainly on the gas component, its partial pressure, the type of adsorbent, and the temperature. Hydrogen is a highly volatile compound with a low polarity and its adsorption capacity in activated carbon is very low [8].

2. Concept and Methodology

The studied process chain shown in Figure 2 is the third configuration for $BioH_2$ production which has been tested experimentally at Oberwart. A series of test campaigns which included a membrane separation unit were carried out in 2013: its results have been already published [9] [10]. The current configuration

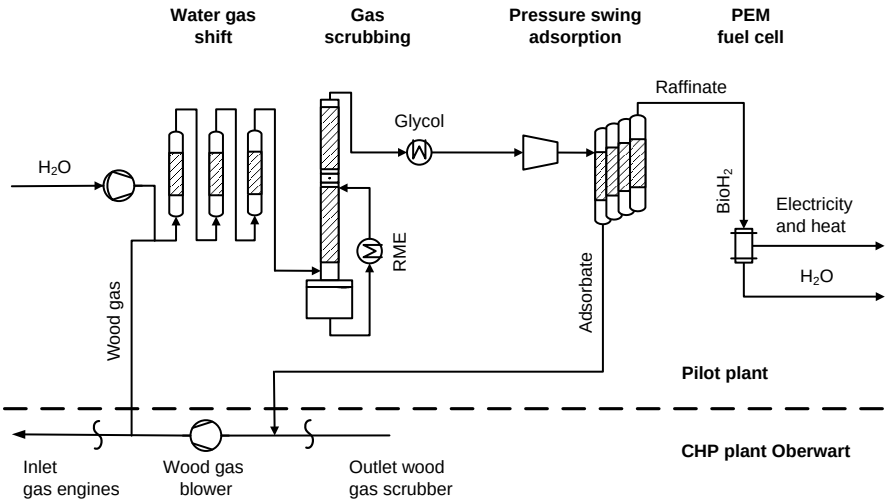

Figure 2: Flowchart of the investigated pilot plant for $BioH_2$ production.

can be seen as a polygeneration concept, aiming at the simultaneous production of H_2, electricity, and district heat. The complexity and the costs of investment should be kept low, with high overall efficiencies and an acceptable H_2 recovery calculated according to Equation 2.

$$H_{2,recovery} = \frac{\dot{n}_{H_2,out}}{\dot{n}_{H_2,in}} \tag{2}$$

2.1. Water Gas Shift Unit

A commercial Fe_2O_3/CrO_3 based catalyst was applied for heterogeneous fixed bed catalysis of the WGS reaction. Prior to the operation of the process chain, the catalyst had initially been reduced according to Equation 3 in order to form the catalytically active magnetite (Fe_3O_4). Subsequently, the catalyst had been conditioned by processing real wood gas for almost 400 hours. Thereby FeS

had been formed according to Equation 4 which is reported to exhibit an activity reduced by 50% compared to magnetite [6]. It could therefore be assumed, that by the beginning of the reported long term experiment, the catalyst was not in its induction period any more.

$$Fe_2O_3 + H_2 \rightleftharpoons 2Fe_3O_4 + H_2O \quad \Delta H_R^0 = -16.3\ \frac{\text{kJ}}{\text{mol}} \tag{3}$$

$$Fe_3O_4 + 3H_2S + H_2 \rightleftharpoons 3FeS + 4H_2O \quad \Delta H_R^0 = -75.0\ \frac{\text{kJ}}{\text{mol}} \tag{4}$$

WGS catalysis was realized in three fixed bed reactors connected in series. The Figure 3 shows a picture of the experimental setup of the employed test rig for catalysis of the WGS reaction. Steam was added to the wood gas in order to

Figure 3: Picture of the WGS unit employed for fixed bed catalysis of the WGS reaction in wood gas.

enhance the water gas shift reaction and to prevent coking on the surface of the catalyst [11]. The wood gas flow rate over the WGS unit was set with the compressor of the PSA unit. The gas at the inlet of each reactor was electrically heated and the temperature was monitored every 10 cm along the fixed bed. A temperature profile along the three reactors was set, attempting to optimize

the overall CO conversion rate. Equilibrium calculations of the WGS reaction have been accomplished using the software HSC^{TM}. Table 1 summarizes the operating conditions of the WGS unit. In the following, ± denotes the standard deviation of the measured values. The CO conversion rate (X_{CO}) in Equation 5

Table 1: Operating conditions of the WGS unit

	Value	Unit
Wood gas in	0.56 ± 0.02	$\frac{\mathrm{Nm^3_{db.}}}{\mathrm{h}}$
Water addition	0.55 ± 0.02	$\frac{\mathrm{kg}}{\mathrm{h}}$
T_{in} reactor 1	403 ± 5	°C
T_{in} reactor 2	358 ± 3	°C
T_{in} reactor 3	309 ± 3	°C
Pressure	76 ± 7	mbarg
GHSV_{wet}	170 ± 5	h^{-1}
$\frac{\mathrm{H_2O}}{\mathrm{CO}}$ molar ratio	5 ± 0.2	-

was used to describe the performance of the WGS catalysis. The gas hourly space velocity (GHSV) was calculated using Equation 6.

$$X_{CO} = \frac{\dot{n}_{CO,in} - \dot{n}_{CO,out}}{\dot{n}_{CO,in}} \tag{5}$$

$$GHSV = \frac{\dot{V}_{gas}}{V_{catalyst}} \tag{6}$$

2.2. Scrubber Unit

The water gas shifted gas subsequently entered a scrubbing unit in order to be cleaned and dried for PSA operation. A counter current flow of wood gas and organic solvent (RME) was realized over a structured packed column. The RME was cooled with a plate heat exchanger provided with cold ethylene glycol from an external chiller. In order to assure complete gas drying, a gas washing bottle filled with glycol cooled to 0 °C was implemented afterwards. The operating conditions of the scrubbing unit can be seen in Table 2.

Table 2: Operation conditions of the scrubber unit

	Solvent	Value	Unit
T_{in} gas	RME	48.3 ± 2.4	°C
T_{out} gas	RME	5.1 ± 0.2	°C
Pressure	RME	58.5 ± 5.8	mbarg
RME circulation	RME	700	$\frac{L}{h}$
Fresh RME addition	RME	0.5	$\frac{L}{h}$
T_{out} gas	Glycol	0	°C

2.3. Pressure Swing Adsorption Unit

The cleaned gas was further processed in a PSA unit for H_2 purification. The unit consisted of four vessels with a capacity of 4.72 L each. Every reactor was filled with 2.5 kg of activated carbon as adsorption agent. The volumetric flow rates of PSA feed and raffinate were quantified with diaphragm gas meters enabling a complete mass balance of the PSA unit. The adsorption pressure was built up with a gas compressor and the desired desorption pressure was achieved using a diaphragm vacuum pump. A picture of the experimental setup for H_2 purification is given in Figure 4. A detailed description of the PSA unit can be found in [9]. The applied adsorption time and pressure equalization for the long term experiment were estimated in a previous parameter study. During this parameter study the adsorption time per column was varied between 400 and 800 s, and the pressure equalization was set to the values 4.0 and 4.5 bara. Table 3 summarizes the basic operating conditions of the PSA unit.

2.4. Fuel Cell Unit

A proton exchange membrane (PEM) fuel cell from AXANE^{TM} was operated with the generated BioH_2 to demonstrate its quality. A picture of this unit can be seen on the left hand side of Figure 4. As a benchmark the PEM fuel cell was also operated with Alphagaz 1^{TM} (H_2 purity > 99.999 vol.%). Key data of the PEM fuel cell are shown in Table 4 provided by [12]. The principles of a PEM fuel cell are reviewed in [13].

Figure 4: Right: PSA unit employed for H_2 purification in the preconditioned wood gas; Left: PEM fuel cell for the demonstration of the quality of the generated BioH_2.

Table 3: Operating conditions of the PSA unit

	Value	Unit
Adsorption pressure	6.5	bara
Desorption pressure	0.1	bara
Purge/feed time ratio	$5 \cdot 10^{-3}$	-
Feed flow rate	0.7 ± 0.04	$\frac{\mathrm{Nm}^3_{\mathrm{db.}}}{\mathrm{h}}$
Feed pressure	1000 ± 17	mbara
Adsorption time per column	650	s
Equalization pressure	4.5	bara

Table 4: Key data of the PEM fuel cell unit

	Value	Unit
Nominal voltage DC	48	V
Nominal voltage AC	230	V
Minimum power	500	W
Maximum power	2500	W
H_2 quality (ISO 14687)	99.99	vol.%
H_2 operating pressure	250 ± 30	mbarg
H_2 consumption at maximum power	35.1	$\frac{\mathrm{NL}}{\mathrm{min}}$

3. Results and Discussion

During the presented long term experiment the CHP plant Oberwart was constantly generating an average of 2100 $\frac{\mathrm{Nm}^3}{\mathrm{h}}$ of wood gas, whereas 350 $\frac{\mathrm{Nm}^3}{\mathrm{h}}$ where recycled back into the combustion zone of the DFB reactor. The outlet temperature of the CHP plant scrubber from where the gas was taken was 35 ± 6 °C. Assuming a relative humidity of 100% at the outlet of this scrubber, a humidity of about 6 mol.% could be calculated in the feed gas of the experimental setup [7].

The pilot plant for H_2 production was successfully operated continuously for almost 250 hours. This section gives an overview of the performance of each operation unit. A detailed chemical analysis of the entire process chain can be found in [1].

3.1. Water Gas Shift Unit

The performance of the WGS unit is illustrated in Figure 5, summarizing all three reactors. The measured gas compositions are plotted on a logarithmic scale and can be compared with the WGS equilibrium at the corresponding outlet temperature of each reactor. Due to the exothermic reaction, within the first 10 cm of the catalyst bed in the first reactor, the temperature increased by about 60 °C starting from the inlet temperature of approximately 403 °C. Subsequently,

the temperature along the bed height decreased due to heat losses. The inlet temperature of reactors 2 and 3 was steadily lowered in order to harness lower equilibrium CO contents. At the outlet of the WGS unit the CO content could

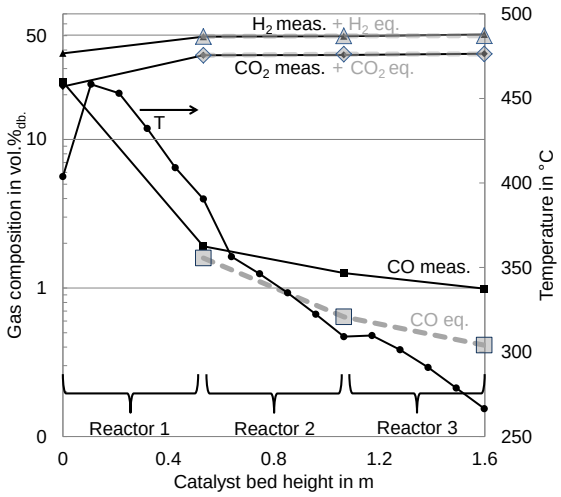

Figure 5: Results of the WGS unit, measured (meas.) and equilibrium (eq.) gas composition as well as temperature along the bed height.

be reduced to < 1 vol.%$_{db.}$, representing a CO conversion rate of 95% and a H_2 recovery of 163% within this unit. The volumetric flow rate was increased from 0.56 $\frac{\mathrm{Nm^3_{db.}}}{\mathrm{h}}$ to 0.70 $\frac{\mathrm{Nm^3_{db.}}}{\mathrm{h}}$ while the H_2O content was lowered from 56 to 45 mol.%. Low GHSV, low sulfur loads in the feed gas [1] and the approach of temperature optimization enabled high overall conversion rates. In order to enhance the CO conversion in reactor 2 and 3, the temperature could have been set slightly higher.

3.2. Scrubber Unit

The scrubber unit was capable of cooling the shifted gas to 0 °C. Hence, it could be assumed that there was a negligible amount of H_2O present at the inlet of the PSA unit. A generated condensate flow rate of 0.32 $\frac{L}{h}$ was estimated at the end of the experiment, which was in good agreement with the overall water balance of the process chain. The performance of the scrubber in terms of tar

separation and removal of other undesired gas components can be found in Part 2 of this article [1].

3.3. Pressure Swing Adsorption Unit

A parameter study was carried out previous to the long term experiment at steady state operation. The operation parameters adsorption time and pressure equalization were varied, revealing a trade-off between the purity of the product and the H_2 recovery. An increase in adsorption time and pressure equalization boosted the H_2 recoveries but decreased the purity of the product. The effect of a variation in adsorption time on the content of the impurities is shown in Figure 6. During this investigation, the equalization pressure was adjusted to 4.5 bara. Similar results were achieved at a pressure equalization of 4.0 bara. The influence of varying pressure equalization as well as adsorption time on the H_2 recovery is shown in Figure 7.

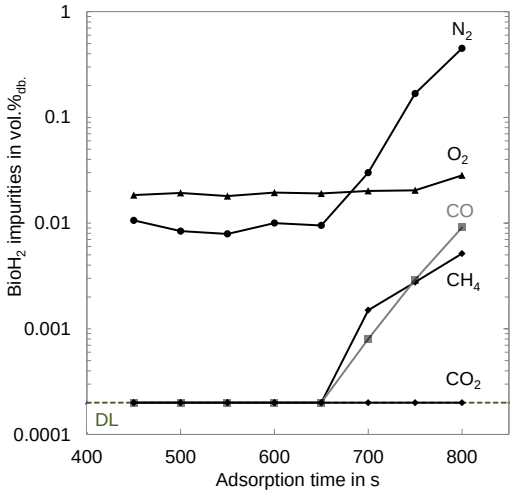

Figure 6: Results of PSA parameter study: $BioH_2$ impurities over adsorption time at a pressure equalization of 4.5 bara, DL = Detection Limit = 2 vol.ppm.

The aim of the study was to optimize the H_2 recovery provided that the components CO, CO_2 and CH_4 were reduced below the detection limit (2 vol.ppm$_{db.}$). As a result, the parameters in Table 3 were chosen for steady state operation.

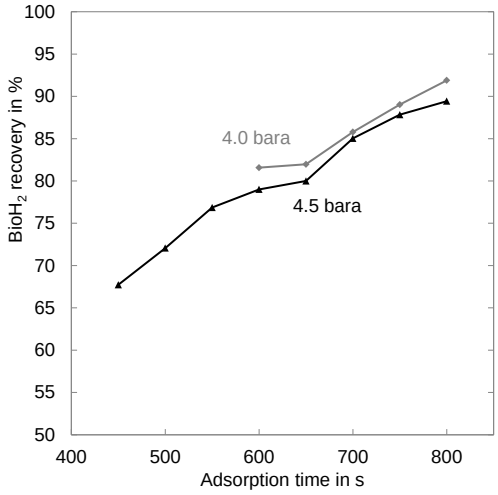

Figure 7: Results of PSA parameter study: $BioH_2$ recovery over adsorption time at a pressure equalization of 4.0 and 4.5 bara.

Under these conditions, an H_2 purity of 99.97 vol.%$_{db.}$ as well as an H_2 recovery of 78.5% were reached. These results are within the range of similiar reported PSA systems obtaining H_2 purities up to 99.99 vol.%$_{db.}$ and H_2 recoveries between 70% and 85% [14, 15, 16, 17]. The feed volumetric flow rate of 0.70 $\frac{\mathrm{Nm^3_{db.}}}{\mathrm{h}}$ was split into an adsorbate fraction of 0.42 $\frac{\mathrm{Nm^3_{db.}}}{\mathrm{h}}$ and a raffinate fraction ($BioH_2$) of 0.28 $\frac{\mathrm{Nm^3_{db.}}}{\mathrm{h}}$. As shown in [1], the only detected impurities in the PSA raffinate were O_2 with 0.02 vol.%$_{db.}$ and N_2 with 0.01 vol.%$_{db.}$.

3.4. Fuel Cell Unit

To demonstrate the high purity of the PSA raffinate, the generated H_2 was fed into a PEM fuel cell (Mobixane$^{\mathrm{TM}}$ from AXANE$^{\mathrm{TM}}$). The unit was operated flawlessly for over three hours. The comparison between its operation with the produced $BioH_2$ and Alphagaz 1$^{\mathrm{TM}}$ H_2 is shown in Table 5. The high standard deviation of the electric power and the H_2 volumetric flow rate could be explained by the water management system of the fuel cell. In order to keep the water content in the membrane at an optimum level, it is purged with H_2 in controlled time intervals.

Table 5: Comparison of the PEM fuel cell performance with $BioH_2$ and Alphagaz 1^{TM}.

	$BioH_2$	Alphagaz 1^{TM}	Unit
Current	4.2 ± 0.3	4.3 ± 0.3	A
Voltage	87.6 ± 0.5	86.2 ± 0.4	V
Electric power	369 ± 25	367 ± 27	W
H_2 partial pressure	1268 ± 27	1245 ± 24	mbara
H_2 flow rate	3.8 ± 3.5	3.8 ± 3.2	$\frac{\mathrm{NL}}{\mathrm{min}}$
Fuel cell temperature	40.5 ± 1.5	36.8 ± 0.9	°C

It could be demonstrated that there was no significant difference in the fuel cell performance regarding operation with $BioH_2$ and the operation with Alphagaz 1^{TM} in the investigated period.

4. Conclusion and Outlook

Continuous $BioH_2$ production from wood gas was achieved in a process based on catalysis of the WGS reaction, gas scrubbing and PSA. The aim of this polygeneration approach was to minimize its complexity at acceptable H_2 recoveries. The process used one single compression step and worked flawlessly for 250 hours. The WGS unit decreased the CO content in the PSA feed from about 24 to below 1 vol.%$_{db.}$. An overall H_2 recovery of 131% $\frac{\dot{n}_{\mathrm{BioH_2}}}{\dot{n}_{\mathrm{H_2 wood\ gas}}}$ was achieved. The only detectable impurities in the PSA raffinate were O_2 (0.02 vol.%$_{db.}$) and N_2 (0.01 vol.%$_{db.}$). This gas composition enabled the operation of a PEM fuel cell. An extensive chemical analysis along the process chain will be provided in a sequel to this publication, Part 2 of this paper [1].

Future work will cover an upscale of the process to a capacity of 100 $\frac{\mathrm{Nm^3}}{\mathrm{h}}$ $BioH_2$. Simulation work will be carried out in order to optimize the presented process for its integration into the CHP plant. In order to reduce the heat demand for steam production, a first step of optimization should include a feed extraction upstream of the wood gas scrubber of the power plant. A water content of already 35 mol.% can be estimated at this point of the process. In

that case, the catalyst of the WGS unit would also have to face a considerably higher load of impurities. Ongoing work is being carried out on the long term stability of the catalyst in combination with this tar rich wood gas.

5. Acknowledgements

The authors would like to thank the project partners: Energie Burgenland, Air Liquide^{TM}, Binder Industrieanlagenbau and cts. The company Clariant© is gratefully acknowledged for providing the WGS catalyst. Especially the CHP plant Oberwart should be thanked for providing a unique working environment and a stable supply of wood gas. The long term conditioning of the WGS catalyst could only be achieved with the help of Matthias Binder. Nicolas Diaz received financial support from Conicyt-Becas Chile. Several research projects collaborated to realize the presented process chain: "Polygeneration 2" (Bioenergy2020+), "Green H_2" (FFG) and "Simple SNG" (FFG). Bioenergy2020+ is funded within the Austrian COMET program managed by the Austrian Research Promotion Agency (FFG). The financial support of the funding association FFG and the Austrian Climate and Energy Fund is gratefully acknowledged.

6. References

[1] S. Fail, M. Kraussler, F. Benedikt, J. Hinteregger, N. Diaz, K. Bosch, M. Hackel, R. Rauch, H. Hofbauer, Wood Gas Processing to Generate Hydrogen Suitable for PEM Fuel Cells - Part 2: Chemical Analysis, Article, 2014.

[2] IEA, Hydrogen production and distribution, international energy agency - energy technology essentials, 2007.

[3] R. Chaubey, S. Sahu, O. O. James, S. Maity, Renewable and Sustainable Energy Reviews 23 (2013) 443 – 462. doi:10.1016/j.rser.2013.02.019.

[4] A. Züttel, A. Borgschulte, L. Schlapbach, Hydrogen as a Future Energy Carrier, Wiley, 2008.

[5] H. Hofbauer, R. Rauch, K. Bosch, R. Koch., C. Aicherning, Biomass CHP Plant Güssing A Success Story, CPL Press, 2003.

[6] M. V. Twigg, Catalyst Handbook-Chapter 6: The Water-Gas Shift Reaction, Manson Publishing, 1989.

[7] T. Pröll, I. G. Siefert, A. Friedl, H. Hofbauer, Industrial & Engineering Chemistry Research 44 (2005) 1576–1584. doi:10.1021/ie049669v.

[8] D. M. Ruthven, Pressure Swing Adsorption, VCH, 1994.

[9] N. Diaz, Hydrogen Separation from Producer Gas Generated by Biomass Steam Gasification, Ph.D. thesis, Vienna University of Technology, 2013.

[10] S. Fail, N. Diaz, D. Konlechner, M. Hackel, E. Sanders, R. Rauch, M. Harasek, K. Bosch, F. Schwenninger, P. Zapletal, Z. Schee, H. Hofbauer, in: H. Hofbauer, M. Fuchs (Eds.), Proceedings of the ICPS 2013, Vienna University of Technology, Getreidemarkt 9/166 A1060 Vienna, pp. 109–126.

[11] Y. Shiratori, T. Ijichi, T. Oshima, K. Sasaki, International Journal of Hydrogen Energy 35 (2010) 7905 – 7912.

[12] S. Moine, Mobixane operation manual, Axane Fuel Cell Systems, 2009.

[13] I. EG & G Technical Services, Fuel Cell Handbook, US Department of Energy, 2004.

[14] J. Yang, S. Hana, C. Chob, C.-H. Lee, H. Lee, Separations Technology 5 (1995) 239–249.

[15] A. M. Ribeiro, C. A. Grande, F. V. Lopes, J. M. Loureiro, A. E. Rodrigues, Chemical Engineering Science 63 (2008) 5258–5273. doi:10.1016/j.ces.2008.07.017.

[16] J.-H. Park, J.-N. Kim, S.-H. Cho, AIChE Journal 46 (2000) 790–802. doi:10.1002/aic.690460413.

[17] S. Ahn, Y.-W. You, D.-G. Lee, K.-H. Kimb, M. Oh, C.-H. Lee, Chemical Engineering Science 68 (2012) 413–423.

Wood Gas Processing to Generate Hydrogen Suitable for PEM Fuel Cells - Part 2: Chemical Analysis

S. Fail[a,*], M. Kraussler[a], F. Benedikt[a], J. Hinteregger[a], N. Diaz[b], K. Bosch[d], M. Hackel[c], R. Rauch[a,b] and H. Hofbauer[a,b]

[a] *Vienna University of Technology, Institute of Chemical Engineering, Vienna, Austria.*

[b] *Bioenergy 2020+ GmbH, Güssing, Austria.*

[c] *Air Liquide^{TM} Forschung und Entwicklung GmbH, Frankfurt Research and Technology Center (FRTC), Germany.*

[d] *Energie Burgenland^{TM} AG, Eisenstadt, Austria.*

Abstract

A test campaign was carried out generating renewable hydrogen based on wood gas derived from the commercial biomass steam gasification plant in Oberwart, Austria. The implemented process consisted of four operation units: (I) catalysed water gas shift (WGS) reaction, (II) gas drying and cleaning in a scrubber, (III) hydrogen purification by pressure swing adsorption and (IV) use of the bio hydrogen ($BioH_2$) in a proton exchange membrane (PEM) fuel cell. The aim was to demonstrate reliable operation and to carry out an extensive chemical analysis.

Part 2 of this publication provides the gas analysis along the process chain as well as a short literature study of the effects of various wood gas components on a PEM fuel cell. A chemical analysis of the main gas components and trace components (sulfur, C_xH_y and ammonia) was carried out. No PEM fuel cell poisons were measured in the generated $BioH_2$. The only detectable hydrogen impurities were 0.02 vol.$\%_{db.}$ of O_2 and 0.01 vol.$\%_{db.}$ of N_2. A detailed description of the implemented process chain was presented in Part 1 [1].

*Vienna University of Technology, Institute of Chemical Engineering
Getreidemarkt 9/166, 1060 Vienna
silvester.fail@tuwien.ac.at

Keywords: Hydrogen, PEM Fuel Cell, Water Gas Shift, Pressure Swing Adsorption, Wood Gas

1. Introduction

Since the beginning of the industrial revolution, the predominantly used energy carriers have changed with respect to their molar hydrogen/carbon ratio. In the second half of the twentieth century, the previously dominant coal, with a ratio of about 1/2, was surpassed by liquid hydrocarbons with a ratio of about 2/1. Nowadays natural gas with a ratio of 4/1 enjoys great popularity, also because of its low carbon dioxide emissions per energy output. Some authors consider a global hydrogen economy as the logical consequence of this historical decarbonization. With this outlook, the use of hydrogen in fuel cells is more and more in the spotlight [2]. Especially, the proton exchange membrane (PEM) fuel cell technology requiring hydrogen with a high purity is desired by certain car manufacturers to power their vehicles. [3].

An increasing number of power-to-gas concepts are being realized to use the excess electricity from wind power and photovoltaics. Besides the electrolysis of water using renewable electricity, the thermal processing of lignocellulosic biomass can also be used for sustainable hydrogen production [4]. In this context, it is useful to rely on the established technology of large scale hydrogen production [5].

The investigated process was designed in the style of the well-proven industrial approach, but replacing the fossil feedstock with wood chips. Therefore, the different structure of the lignocellulosic biomass as well as its very different elemental composition had to be taken into consideration.

The feed of the studied process was wood gas from the commercial biomass steam gasification plant in Oberwart, Austria. Analogous to hydrogen production based on steam methane reforming, the employed biomass gasifier is also operated with steam as a gasification agent. A more detailed description of the power plant, including a process flowchart, can be found in the first part of this

paper [1]. The subsequently applied unit operations for wood gas conditioning were the sulfur tolerant catalysis of the water gas shift (WGS) reaction for hydrogen enrichment, gas cleaning in a scrubber operated with rapeseed methyl ester (RME), and pressure swing adsorption (PSA) for hydrogen purification. A flowchart of the employed pilot plant is shown in Figure 1. As a demonstration of the high quality of the product, its use in a PEM fuel cell was chosen. In order to meet the requirements of this fuel cell type, care had to be taken to avoid the presence of a series of wood gas components in the $BioH_2$ product. In the following, the influence of the different wood gas components on a PEM fuel cell are described.

Carbon monoxide (CO). The performance of PEM fuel cells is greatly influenced by CO. This includes dilution effects, but is mostly because of the poisoning of the platinum catalyst: CO is adsorbed on the active surface of the catalyst and reduces the available area for hydrogen oxidation. Concentrations as low as 0.5 to 4.5 vol.ppm have been reported to cause performance losses due to a voltage drop which is directly proportional to the CO concentration [6]. On the surface of the platinum catalyst, CO can be converted to CO_2 employing the water gas shift reaction. The adsorption of CO_2 is inferior to the adsorption of CO, leading to an equilibrium voltage drop after achieving steady state operation. Higher amounts of CO in the feed lead to a complete deactivation of the anode because CO is adsorbed faster than the CO_2 can be desorbed. CO poisoning is reversible if the fuel cell is flushed with pure hydrogen [7].

Carbon dioxide (CO_2). The performance loss caused by CO_2 seems to be higher than that from inert components like N_2. The reason seems to be the formation of CO, either through the reverse WGS reaction or an electrochemical reduction reaction. Severe performance loss by these effects has been reported for CO_2 concentrations of about 20% and higher [7].

Hydrogen sulfide (H_2S). H_2S affects the catalyst the same way CO does. It is adsorbed on the catalyst surface and reduces the area for H_2 oxidation. This

mechanism is even observed at concentrations as low as 0.25 vol.ppm. In contrast to CO poisoning, the adsorption of H_2S seems to be irreversible [7]. Also COS is reported to reduce the active surface of the catalyst [8].

Methane (CH_4). According to [9], even high amounts of CH_4 in the feed gas have no negative effects on the performance of a PEM fuel cell.

Ammonia (NH_3). NH_3 is oxidized to NH_4^+ ions, reducing the proton concentration at the catalyst layer, leading to a reduction in the performance of the anode. After long exposure times, NH_4^+ ions migrate into the proton exchange membrane, resulting in a conductivity loss. These effects have already been observed at ammonia concentrations as low as 1 vol.ppm. Recovery of the catalyst with H_2 seems to be possible but is reported to be time consuming [7].

Air (N_2 and O_2). The inert N_2 reduces the partial pressure of the H_2, which leads to a potential loss according to the Nernst equation. The O_2 content in the $BioH_2$ needs to be as low as possible in order to avoid the direct formation of water at the anode [7].

2. Concept and Methodology

The employed operation units for WGS catalysis, gas scrubbing and PSA were described in detail in the Part 1 of this article. The generated $BioH_2$ was fed into a PEM fuel cell (Mobixane^{TM}) from Axane^{TM}, which was also described in [1]. This section focuses on the adopted methods of chemical analysis. Figure 1 illustrates the investigated process chain as well as the selected sampling points. Table 1 provides a matrix of the analyzed components at the available sampling points. Extensive analysis of main gas components, sulfur components, tar, water, BTEX (benzene, toluene, ethylbenzene, xylene) and ammonia was carried out. The water containing sampling streams of the WGS unit had to be dried before gas analysis. Therefore the wet gas was introduced into the bottom path of sampling shown in Figure 2.

Figure 1: Flowchart of the investigated pilot plant for $BioH_2$ production including the applied sampling points (1–6) for chemical analysis.

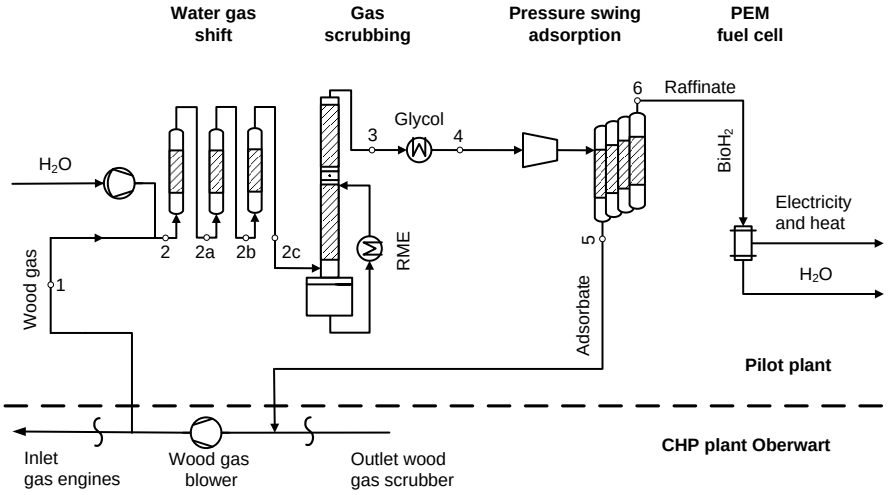

Table 1: Matrix of sampling points and the corresponding chemical analysis. The volumetric flow rates of the PSA feed and the raffinate were determined.

Analysis	Sampling point								
	1	2	2a	2b	2c	3	4	5	6
Main gas components	✓		✓	✓	✓		✓	✓	✓
Sulfur components	✓		✓	✓	✓		✓	✓	✓
Tar	✓				✓	✓			
Water	✓	✓	✓	✓	✓	✓	✓		
BTEX	✓				✓		✓	✓	✓
Ammonia	✓				✓	✓	✓		
Flow rate							✓		✓

Figure 2: Flowchart of the experimental setup for chemical analysis of the main gas components, sulfur, tar and water.

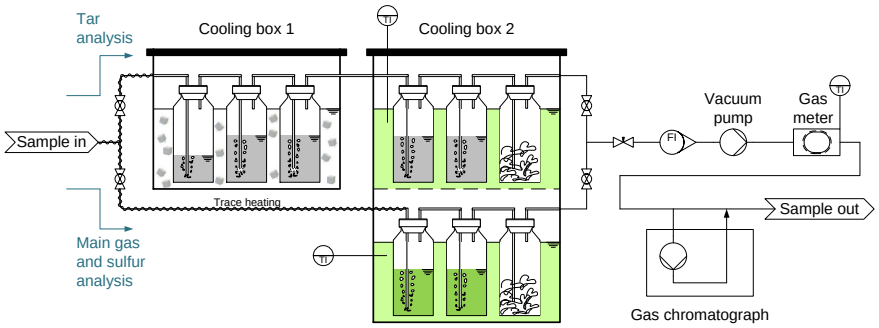

Prior to GC injection, the gas was dried in a temperature controlled cooling box at -3 °C over two gas washing bottles filled with ethylene glycol which were connected in series. The flow was controlled with a needle valve upstream to a vacuum pump. A gas meter from Kromschröder (BKG2,5T) was used to quantify the volumetric flow rate of the dry sampling gas at ambient pressure. A corresponding increase in weight of the ethylene glycole filled flasks enabled a parallel estimation of the water content.

The main gas components (CO_2, N_2, CO, O_2, CH_4, C_2H_6, C_2H_4 and C_2H_2) were separated in a combination of two different columns (7' HayeSep N, 60/80 1/8" SF and 9' Molecular Sieve 13x 45/60, 1/8" SF) in a gas chromatograph (GC - Clarus 500^{TM}) from Perkin Elmer^{TM}. A thermal conductivity detector (TCD) was used for quantification. The sulfur components (H_2S, COS, C_4H_4S, CH_3CH_2SH and CH_3SH) were separated in a different column (Rt-XL Sulfur 1 m.x 0.95 mm OD) and quantified by a flame photometric detector (FPD).

Tar sampling was performed over the upper path of Figure 2. A combination of 2 cooling boxes was applied. Scrubbing bottles filled with 50 mL or 100 mL of toluene were applied to dissolve tar components. Three gas washing bottles were placed in an ice bath at 0 °C and two additional impingers where placed in the temperature controlled cooling box at -8 °C. For each tar analysis a

sampling stream of 2 $\frac{\mathrm{NL}}{\mathrm{min}}$ was taken over a period of 8 hours. For detection of the tar components a gas chromatograph from Perkin Elmer$^{\mathrm{TM}}$ (XL GC$^{\mathrm{TM}}$) coupled with a mass spectrometer from Perkin Elmer$^{\mathrm{TM}}$ (Turbo Mass MS$^{\mathrm{TM}}$) was used. A detailed description of the applied method for tar analysis can be found in [11].

Benzene, toluene, ethylbenzene and xylene (BTEX) were measured by gas chromatography - mass spectrometry (GC-MS, Shimadzu QP2010 Plus$^{\mathrm{TM}}$) at Vienna University of Technology. 6 samples of each relevant point of the process were taken by means of gas sampling bags. For the quantification of NH_3 an absorption method was used. A sample of 1 $\frac{\mathrm{NL}}{\mathrm{min}}$ was extracted from the process for three hours and passed through three gas washing bottles connected in series in a cooling bath at 0 °C. The bottles were filled with 0.05 M H_2SO_4, which solves NH_3 in the form of NH_4^+ ions. NH_4^+ ions were quantified by ion chromatography (Dionex ICS 5000$^{\mathrm{TM}}$).

The H_2 content was determined via mass balance. The volumetric flow rates of the PSA feed and raffinate were quantified with diaphragm gas meters. The adsorbate flow rate was calculated via mass balance. The flow rate of the wood gas at the inlet of the WGS unit was calculated via mass balance based on the feed flow rate of the PSA and the change of the gas composition according to the WGS reaction. Standard reaction enthalpies were calculated based on the standard formation enthalpies in [12].

3. Results and Discussion

The overall performance of the process in terms of H_2 recovery was discussed in Part 1 of this article [1]. 0.56 $\frac{\mathrm{Nm}^3}{\mathrm{h}}$ of dry wood gas was extracted after the CHP plant scrubber. Catalysis of the WGS reaction caused an increase in the dry volumetric feed flow rate of the PSA to 0.70 $\frac{\mathrm{Nm}^3}{\mathrm{h}}$. In the PSA unit the feed was split into 0.42 $\frac{\mathrm{Nm}^3}{\mathrm{h}}$ of adsorbate and 0.28 $\frac{\mathrm{Nm}^3}{\mathrm{h}}$ of raffinate, respectively BioH$_2$. The raw wood gas from the CHP plant was extracted with a water content of 6 mol.%. Because of the water addition at the inlet of WGS unit the

steam content of the feed was increased up to 65 mol.%. Due to the catalysis of the WGS reaction the water content was reduced to 45.6 mol.% at the outlet of the WGS unit forming additional H_2 from the conversion of CO. The scrubber unit was capable of cooling down the shifted gas mixture to below 0 °C. Hence it could be expected that there was only a negligible amount of water present at the inlet of the PSA unit.

In this chapter the evolution of the dry gas composition along the process chain is presented. All results are measured gas compositions, except for the adsorbate composition which was calculated via mass balance. Table 2 depicts the evolution of the main gas components on a dry base, detected with the TCD detector of the GC.

Table 2: Results of the analysis of the main gas components; BDL = Below Detection Limit, DL = 2 vol.ppm$_{db.}$, the adsorbate composition (5) was calculated via mass balance

Sampling point	Unit	CO_2	C_2H_4	C_2H_6	C_2H_2	O_2	N_2	CH_4	CO	H_2
1	vol.%$_{db.}$	22.7±0.8	2.3±0.3	0.17±0.03	0.15±0.02	0.1±0.02	2.3±0.4	10.0±0.3	24±1	38.0±1.2
2a	vol.%$_{db.}$	36.9±0.8	1.8±0.1	0.17±0.02	0.001±0.001	0.06±0.01	1.8±0.1	8.2±0.1	1.9±0.3	49.2±0.9
2b	vol.%$_{db.}$	37.0±0.8	1.8±0.1	0.17±0.03	BDL	0.08±0.04	2±0.1	8.1±0.2	1.3±0.2	49.5±0.9
2c	vol.%$_{db.}$	37.1±0.9	1.9±0.2	0.18±0.02	BDL	0.07±0.06	1.9±0.3	8.2±0.2	1.0±0.1	49.6±0.9
4	vol.%$_{db.}$	36.9±0.2	1.6±0.3	0.14±0.03	BDL	0.03±0.01	1.5±0.1	8.0±0.2	0.98±0.04	50.9±0.4
5	vol.%$_{db.}$	61.4	2.6	0.23	BDL	0.03	2.6	13.3	1.63	18.2
6	vol.%$_{db.}$	BDL	BDL	BDL	BDL	0.02±0.0003	0.01±0.004	BDL	BDL	99.97±0.004

The WGS unit with an overall CO conversion rate of about 95% increased the H_2 content from 38 vol.%$_{db.}$ to about 50 vol.%$_{db.}$. The simultaneous increase in the dry gas flow rate by 25% led to a general dilution effect. C_2H_2 was totally hydrogenated to C_2H_4 and could not be detected at the outlet of the WGS unit. C_2H_4 was assumed to be partly hydrogenated to C_2H_6. The overall mass balance of the C_2H_y components was approaching 98%. The slightly higher content of H_2 in the PSA feed (4) compared to the outlet of the WGS unit (2c) could be explained by the low solubility of hydrogen in water as well as by the removal of a series of gas components in the scrubber unit (e.g. benzene and ammonia). It is also seen that O_2 and N_2 were the only detectable impurities that were fed into the fuel cell. O_2 is reported to be tolerated up to 500 vol.ppm and N_2 has only dilution effects on the PEM fuel cell [7].

The evolution of the sulfur components along the process is provided in Table 3. The low sulfur load in the wood gas presented a good precondition

Table 3: Results of the analysis of the sulfur components; DL = 0.3 vol.ppm$_{db.}$

Sampling point	Unit	H_2S	COS	C_4H_4S
1	vol.ppm$_{db.}$	59±10	1.0±0.1	7.2±3.1
2a	vol.ppm$_{db.}$	49±4	BDL	2.0±0.7
2b	vol.ppm$_{db.}$	50±3	BDL	1.0±0.5
2c	vol.ppm$_{db.}$	4±1	BDL	1.0±0.6
4	vol.ppm$_{db.}$	2.5±0.3	BDL	0.3±0.01
5	vol.ppm$_{db.}$	0.4±0.3	BDL	0.5±0.3
6	vol.ppm$_{db.}$	BDL	BDL	BDL

for high catalyst activities in the WGS unit [13]. As proved by constant H_2S concentrations, the catalyst sulfidation was completed in the first two reactors, where the main CO conversion took place. Anyway, only 4 vol.ppm$_{db.}$ of H_2S were measured after the third reactor, assuming an incomplete sulfidation of this stage during the presented study. COS was not detected at the outlet of the WGS unit, which could be explained by the reactions shown in Equations

1 and 2. The decrease in thiophene (C_4H_4S) along the WGS unit is suggested to be due to the reaction of thiophene hydrogenolysis in Equation 3 [13]. Less C_4H_4S and H_2S could be detected after gas scrubbing. The organic C_4H_4S was assumed to dissolve in the RME whereas the H_2S dissolved in the condensate. Table 3 also indicates that a fraction of the H_2S present in the feed was captured in the PSA unit. As small amounts of O_2 were present in the PSA feed, this is explained by the formation of elementary sulfur according to Equation 4 [14].

$$H_2 + COS \rightleftharpoons H_2S + CO \quad \Delta H_R^0 = 10.9 \ \frac{\text{kJ}}{\text{mol}} \tag{1}$$

$$H_2O + COS \rightleftharpoons H_2S + CO_2 \quad \Delta H_R^0 = -30.3 \ \frac{\text{kJ}}{\text{mol}} \tag{2}$$

$$C_4H_4S + 4H_2 \rightleftharpoons C_4H_{10}S + H_2S \quad \Delta H_R^0 = -261.2 \ \frac{\text{kJ}}{\text{mol}} \tag{3}$$

$$2H_2S + O_2 \rightleftharpoons \frac{1}{4}S_8 + 2H_2O \quad \Delta H_R^0 = -444.0 \ \frac{\text{kJ}}{\text{mol}} \tag{4}$$

The analysis of the benzene, toluene, ethylbenzene and xylene (BTEX) is shown in Table 4. In the WGS unit, no significant change in the BTX composition could be observed, apart from a dilution effect due to an increased volumetric gas flow rate. The hydrogenation of styrene (see Table 5) was assumed to be responsible for the formation of the ethylbenzene as a side reaction in the WGS unit. The scrubber unit removed the majority of the BTEX compounds. Only benzene and toluene could be detected at the inlet of the PSA unit. Analysis of the PSA raffinate and adsorbate suggests a complete adsorption and subsequent desorption of these compounds from the activated carbon.

The results of the tar analysis in Table 5 are based on one continuous long-term sample. Therefore no standard deviations can be given. As a side reaction in the WGS unit, styrene and indene were probably hydrogenated to form ethylbenzene (see Table 4) and indane (not analyzed). Furthermore, a hydrogenation of phenylacetylene to ethylbenzene as well as a hydrogenation of acenaphthylene to acenaphthene could be assumed. Besides the frequently observed dilution effect, naphthalene as the predominant tar component was probably not affected in the WGS unit. In the scrubbing unit, all tar components except naphthalene

Table 4: Results of the analysis of BTEX; DL = 1 vol.ppm$_{db.}$

Sampling point	Unit	Benzene	Toluene	Ethylbenzene	Xylene
1	vol.ppm$_{db.}$	3296±36	201±5	1.3±0.6	1.1±0.6
2c	vol.ppm$_{db.}$	2850±54	176±6	33±12	2.2±0.9
4	vol.ppm$_{db.}$	536±5	17±2	BDL	1.2±0.6
5	vol.ppm$_{db.}$	641±13	21±1	BDL	BDL
6	vol.ppm$_{db.}$	BDL	BDL	BDL	BDL

could be removed to below the detection limit.

The results of the NH_3 analysis in Table 6 are based on one continuous sample. Therefore no standard deviations can be given. Apart from the dilution effect in the WGS unit, no influence of the catalyst on the NH_3 was observed. In the scrubbing unit, the amount of NH_3 was reduced below the detection limit. There was no NH_3 present at the inlet of the PSA unit.

4. Conclusion and Outlook

Continuous BioH_2 production from wood gas was achieved in a process based on catalysis of the WGS reaction, gas scrubbing and PSA. The aim of this polygeneration approach was to minimize its complexity at acceptable H_2 recoveries. The process used one single compression step and worked flawlessly for 250 hours. A detailed description of the pilot plant and the overall process performance was provided in Part 1.

Wood gas components can affect a PEM fuel cell in many ways. A process chain for wood gas conditioning that provides a suitable feed flow is required in order to prevent catalyst poisoning of the electrodes. In this context, CO, CO_2, H_2S, NH_3 and C_xH_y should not be present in the feed flow of a PEM fuel cell. The investigated process chain was capable of providing BioH_2 free from these components. The only detected impurities in the PSA raffinate were O_2 (0.02 vol.%$_{db.}$) and N_2 (0.01 vol.%$_{db.}$), which enabled a flawless operation of a PEM fuel cell (Mobixane^{TM}) from Axane^{TM}.

Table 5: Results of the analysis of tar components (one continuous sample); DL = 1 $\frac{\text{mg}}{\text{Nm}^3_{db.}}$

Component	Unit	1	2c	3
Naphthalene	$\frac{\text{mg}}{\text{Nm}^3_{db.}}$	1139	824	2
Styrene	$\frac{\text{mg}}{\text{Nm}^3_{db.}}$	247	BDL	BDL
Indene	$\frac{\text{mg}}{\text{Nm}^3_{db.}}$	191	9	BDL
Phenylacetylene	$\frac{\text{mg}}{\text{Nm}^3_{db.}}$	25	BDL	BDL
Mesitylene	$\frac{\text{mg}}{\text{Nm}^3_{db.}}$	BDL	4	BDL
Benzofuran	$\frac{\text{mg}}{\text{Nm}^3_{db.}}$	2	BDL	BDL
1-Benzothiophene	$\frac{\text{mg}}{\text{Nm}^3_{db.}}$	2	BDL	BDL
2-Methylnaphthalene	$\frac{\text{mg}}{\text{Nm}^3_{db.}}$	5	4	BDL
1-Methylnaphthalene	$\frac{\text{mg}}{\text{Nm}^3_{db.}}$	3	2	BDL
Biphenyl	$\frac{\text{mg}}{\text{Nm}^3_{db.}}$	1	BDL	BDL
Acenaphthylene	$\frac{\text{mg}}{\text{Nm}^3_{db.}}$	13	BDL	BDL
Acenaphthene	$\frac{\text{mg}}{\text{Nm}^3_{db.}}$	2	7	BDL
Anthracene	$\frac{\text{mg}}{\text{Nm}^3_{db.}}$	2	4	BDL
Flouranthene	$\frac{\text{mg}}{\text{Nm}^3_{db.}}$	1	3	BDL
Pyrene	$\frac{\text{mg}}{\text{Nm}^3_{db.}}$	1	3	BDL

Table 6: Results of the analysis of NH_3 (one continuous sample); DL = 1 vol.ppm$_{db.}$

Sampling point	Unit	NH_3
1	vol.ppm$_{db.}$	954
2c	vol.ppm$_{db.}$	740
3	vol.ppm$_{db.}$	1
4	vol.ppm$_{db.}$	BDL

Future work has to focus on the behaviour of certain components along the process chain. Especially the behaviour of higher sulfur loads in the PSA unit will be studied. In order to reduce the detection limit of impurities in the $BioH_2$, an adsorption tube will be installed in the feed of the fuel cell. Prior to the planned scale-up of the process, the long term stability of the PEM fuel cell operated with $BioH_2$ will also be demonstrated.

5. Acknowledgements

The authors would like to thank the project partners: Energie Burgenland™, Air Liquide™, Binder Industrieanlagenbau™ and cts™. The company Clariant© is gratefully acknowledged for providing the WGS catalyst. Especially the CHP plant Oberwart should be thanked for providing a unique working environment and a stable supply of product gas. Also the work from Christian Jordan on aromatic compounds analytics is greatly appreciated. Nicolas Diaz received financial support from Conicyt-Becas Chile. Bioenergy2020+ is funded within the Austrian COMET program managed by the Austrian Research Promotion Agency (FFG). The financial support of the funding association FFG and the Austrian Climate and Energy Fund is gratefully acknowledged.

6. References

[1] S. Fail, M. Kraussler, F. Benedikt, J. Hinteregger, N. Diaz, K. Bosch, M. Hackel, R. Rauch, H. Hofbauer, Wood Gas Processing to Generate Hydrogen Suitable for PEM Fuel Cells - Part 1: Design and Overall Performance, Article, 2014.

[2] S. Dunn, Hydrogen futures: toward a sustainable energy system, International Journal of Hydrogen Energy 27 (2002) 235–264.

[3] F. C. today, Fuel cell electric vehicles: The road ahead, 2013.

[4] G. Gahleitner, Hydrogen from renewable electricity: An international review of power-to-gas pilot plants for stationary applications, International Journal of Hydrogen Energy 38 (2013) 2039 – 2061.

[5] K. Liu, C. Song, V. Subramani, Hydrogen and Syngas Production and Purification Technologies, Wiley, 2010.

[6] R. Benesch, T. Jacksier, Hydrogen and material quality issues for PEM fuel cells, in: Vehicle Power and Propulsion, 2005 IEEE Conference, 2005, pp. 646–651. doi:10.1109/VPPC.2005.1554601.

[7] B. M. Besancon, V. Hasanov, R. Imbault-Lastapis, R. Benesch, M. Barrio, M. J. Mlnvik, Hydrogen quality from decarbonized fossil fuels to fuel cells, International Journal of Hydrogen Energy 34 (2009) 2350–2360.

[8] P. Kurzweil, Brennstoffzellentechnik, Springer Vieweg, 2013.

[9] I. Blessing, C. Gardner, M. Ternan, Separation of hydrogen from a hydrogen / methane mixture using a PEM fuel cell, International Journal of Hydrogen Energy 32 (2007) 908–914.

[10] N. Diaz, Hydrogen Separation from Producer Gas Generated by Biomass Steam Gasification, Ph.D. thesis, Vienna University of Technology, 2013.

[11] U. Wolfesberger, I. Aigner, H. Hofbauer, Tar content and composition in producer gas of fluidized bed gasification of wood-influence of temperature and pressure, Environmental Progress & Sustainable Energy 28 (2009) 372–379.

[12] D. R. Lide, CRC Handbook of Chemistry and Physics, Internet Version 2005, CRC Press, 2005.

[13] M. V. Twigg, Catalyst Handbook-Chapter 6: The Water-Gas Shift Reaction, Manson Publishing, 1989.

[14] M. Brune, Verfahren zur Entschwefelung von flüssigen handelsüblichen Brennstoffen, 27-29, Scientific Publishing, 2009.